Development of Metal Sulfide Based Nanocomposite for High Performance Sodium-ion Batteries

By

Ahmed Abdul Qayyum

Reg no# 00000207024

Session 2017-19

Supervised by

Dr. Zuhair S. Khan

A thesis submitted to the U.S.-Pakistan Center for Advanced Studies in Energy in partial fulfillment of the requirements for the degree of

MASTER of SCIENCE in

ENERGY SYSTEMS ENGINEERING

U.S.-Pakistan Center for Advanced Studies in Energy (USPCAS-E)

National University of Sciences and Technology (NUST)

H-12, Islamabad 44000, Pakistan

October 2020

THESIS ACCEPTANCE CERTIFICATE

Certified that final copy of MS/MPhil thesis written by Mr. Ahmed Abdul Qayyum, (Registration # 00000207024) of U.S.-Pakistan Center for Advanced Studies in Energy (USPCAS-E), NUST, has been vetted by undersigned, found complete in all respects as per NUST Statues/Regulations, is within the similarity indices limit and mistakes and is accepted as partial fulfillment for award of MS/MPhil degree. It is further certified that necessary amendments as pointed out by GEC members of the scholar have also been incorporated in the said thesis.

Signature: _____

Name of Supervisor: Dr. Zuhair S. Khan

Date: _____

Signature (HoD): _____

Date: _____

Signature (Dean/Principal): _____

Date: _____

CERTIFICATE

This is to certify that the work in this thesis has been carried out by **Mr. Ahmed Abdul Qayyum** and completed under my supervision in Advanced Energy Materials & Systems Laboratory, U.S.-Pakistan Center for Advanced Studies in Energy, National University of Sciences and Technology, H-12, Islamabad, Pakistan.

Supervisor: _____

Dr. Zuhair S. Khan
USPCAS-E
NUST, Islamabad

GEC member 1: _____

Dr. Naseem Iqbal
USPCAS-E
NUST, Islamabad

GEC member 2: _____

Dr. Nadia Shahzad
USPCAS-E
NUST, Islamabad

GEC member 3: _____

Dr. Sehar Shakir
SCME
NUST, Islamabad

HOD-ESE: _____

Dr. Naseem Iqbal
USPCAS-E
NUST, Islamabad

Principal: _____

Dr. Adeel Waqas
USPCAS-E
NUST, Islamabad

DEDICATION

Firstly, all praise to Allah Almighty who has provided me with appropriate skills, guidance, strength, perseverance, power of mind and for uncountable blessings that allowed me to complete this study.

I would like to dedicate this study to my beloved parents who have always act a source of inspiration for me and gave me hope again and again, when it was required. I would also like to dedicate this thesis my supervisor Prof. Dr. Zuhair S. Khan, who allowed me to a be part of his research group at Advanced Energy Materials Lab, USPCAS-E, NUST. It's the blend of his patience, persistence, guidance and motivation that made me accomplish my research aims in due time. He polished my research skills and I have learned a lot under his supervision and guidance. Furthermore, I want to dedicate this research thesis to my GEC committee members Dr. Naseem Iqbal, Dr. Nadia Shahzad and Dr. Sehar Shakir for guiding me in completing this study. I would also like to pay gratitude and dedicate this book to Dr. Ghulam Ali and lab engineers for their unmatchable support during the whole research work.

ABSTRACT

Over the past few decades lithium-ion batteries (LIBs) were commercialized and had dominated the market as a small-large scale energy store device but recently, rapid increase in lithium prices was observed because of its high demand and low resource ratio. Ultimately, this makes lithium highly unfeasible for large scale applications and to meet those requirements, alternate electrochemical energy storage systems have to be looked at. Considering this, Sodium has the potential to fill the gap left by LIBs owing to the fact that sodium ion batteries (NIBs) follows the same electrochemistry mechanism as LIBs and more importantly, highly resource availability thus, making a cheaper alternative. However, because of large sodium ion radii than lithium ion and low electrochemical reduction potential than lithium, NIB electrodes face serious amount of volume expansion during cycling and also fail to deliver same volumetric and gravimetric energy density as LIBs.

Among different available anode materials, metal chalcogenides have piqued interest because of its high theoretical capacity however, since it undergoes partial alloying-conversion reaction phenomena during cycling, it also experiences large volume expansion which reduces its cyclic life and capacity retention. One such materials is tin sulfide-based anode materials and many approaches have been devised so far to improve its cyclic life, capacity retention and initial coulombic efficiency of NIB anode such as by adding a matrix material like graphene, carbon black or by tuning its morphology etc. Here in this work, via solvothermal route, doped carbon nanotubes were added SnS which created a network with SnS and enhanced its electrochemical performance. XRD, SEM revealed its amorphous nature and cauliflower like morphology while TGA gave us an estimated amount of CNTs that were used to create this amorphous framework. Galvanostatic charge/discharge analysis revealed that this nanocomposite shows better initial coulombic efficiency and also delivers good cyclic life with enhanced capacity retention. CV confirmed partial alloying/conversion reaction mechanism that it follows and EIS revealed reduction to Na^+ diffusion resistance was observed. This enhanced electrochemical performance in nanocomposite can be ascribed to heteroatom dopants forcing nanocomposite to develop an amorphous structure thus, providing sufficient space, which act as a buffer to volume expansion.

Keywords: Sodium ion batteries, metal sulfide, electrochemical performance, CNTs, SnS, anode, capacity retention, coulomb efficiency

TABLE OF CONTENTS

TABLE OF FIGURES

LIST OF TABLES

LIST OF ABBREVIATIONS/ NOMENCLATURE

LIBs	Lithium ion batteries
NIBs	Sodium ion batteries
CNTs	Carbon nanotubes
NS-CNTs	Nitrogen and sulfur co-doped CNTs
NS-SnS/CNTs	Nitrogen and sulfur co-doped nanocomposite
XRD	X-ray diffraction
SEM	Scanning electron microscopy
TEM	Transmission electron microscopy
TGA	Thermogravimetric analysis
FTIR	Fourier transform infrared spectroscopy
CV	Cyclic voltammetry
EIS	Electrochemical impedance spectroscopy
CVD	Chemical vapor deposition

LIST OF JOURNAL PAPERS PUBLISHED

Amorphous codoped SnS/CNTs nanocomposite with improved capacity retention as an advanced sodium- ion battery anode, A.A. Qayyum, Z.S. Khan, S. Ashraf, N. Ahmed, Journal of Materials Science: Materials in Electronics, July 2020

CHAPTER 1: Introduction

During the course of last few decades electrochemical energy storage devices have gained alot of importance for applications ranging from small, portable electronic systems to electric vehicles and stationary systems (such as grids, solar panels). For small to medium range storage systems, lithium ion batteries (LIBs) have dominated the market owing to its high energy density and small size but they are proving to be too costly large-scale energy storage systems which is also fueled by low abundance of lithium in the earth crust (0.0065%) [1]. Moreover, due to ever increasing demand of sustainable energy storage sources to mitigate the effect of global warming, renewable energy sources including biomass, tidal, solar etc. are being tapped in abundance since last decade [2]. These sources require large size storage devices to store electrochemical energy which can be converted into electrical energy when required as a power backup [3]. Therefore, sodium ion batteries (NIBs) as an alternative to LIBs have caught the eye of scientists and world leaders particularly due to its high abundance in the earth crust (2.75%) [4]. The research on NIBs have also gained substantial pace due to the fact that it exhibits same charge storage mechanism as is shown by LIBs, which led researchers toward using similar electrode materials as they were previously being used for li-ion chemistry. However, this tactic didn't yield similar performance efficiency as it did in LIBs simply because of large Na^+ radius as compared to Li^+ (1.02 Aº vs 0.76 Aº) [5]. Furthermore, sodium ion is three times as heavier as lithium ion and this difference along with its large ionic radii causes NIBs to behave poorly during cyclic performance, giving low charge/discharge capacity as the electrodes that are involved in it undergoes large volume expansion when an ion insertion/extraction phenomenon takes place [3,5]. NIBs so far have also failed in delivering same gravimetric and volumetric energy density as that can be achieved by LIBs due to higher standard reduction potential of Na in the electrochemical series (-2.71 vs -3.04 for Li) [6].

Thus, In the field of NIBs, to enhance capacity and cyclic life, many different areas of research have gained importance including novel anodes, cathodes, separator and electrolyte materials. Among different novel electrode materials, metallic and bimetallic sulfides are considered to be the most promising among them owing to their high theoretical capacity [7]. These metallic sulfides can be used as an anode material for NIBs when they are undergone through treatments and modifications to create a necessary structure design [7]. In this study, by tuning

crystallinity, metallic sulfide nanocomposite electrode with a unique morphology was synthesized which delivered enhanced electrochemical performance in NIBs.

1.1. Lithium-ion Batteries

LIBs are currently dominating the market as a storage device for portable mobile electronics such as tablets, smartphones, computer etc. and also for electric vehicles. LIBs main components comprise of anode (negative electrode), cathode (positive electrode), separator and an electrolyte [8]. In a typical commercialized LIBs, the material of these components consists of $LiCoO_2$ as a positive, graphite as a negative electrode. Both of these electrodes are separated by a porous separator of either a Teflon sheet or polyethylene sheet meanwhile the ion transport in them is facilitated through an electrolyte such a $LiPF_6$ [9]. When a secondary battery such as LIBs are discharged, Li ion moves from anode to cathode and the corresponding active material anode oxidizes and reduces at cathode. Similarly, during charge, Li ion get transported from cathode to anode and the reverse oxidation/reduction phenomenon occurs. Hence, the electrons which are generated through an electrochemical reaction need to travel between electrodes and deliver energy which can be utilized to power tools etc., and to achieve that current collectors like aluminum foil and copper foil is used at cathode and anode respectively. Figure 1.1 below outlines the schematic of working principle in lithium ion batteries.

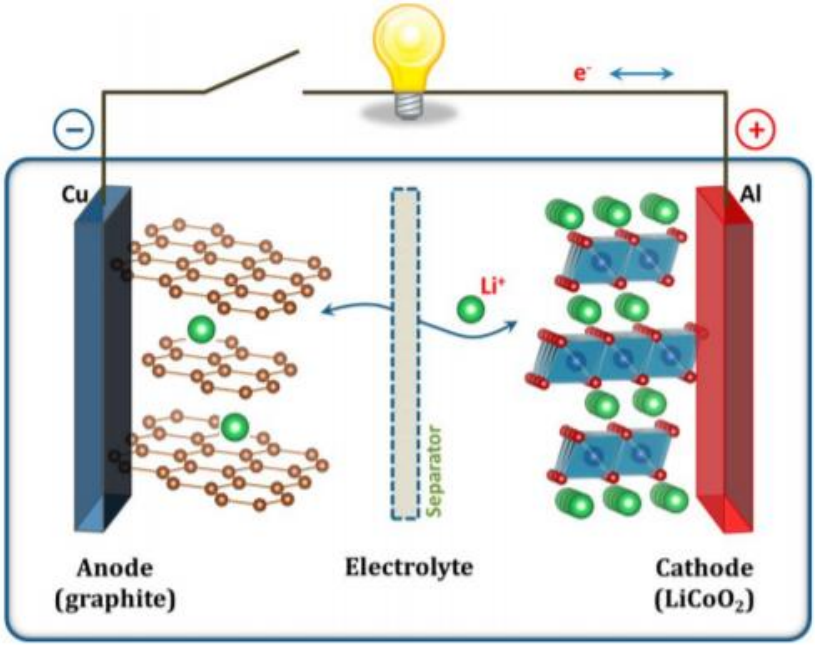

Figure 1.1 Schematic of working principle in LIBs

However, with the ever-growing versatility of applications for LIBs, extending from small portable electronics to large scale smart grid energy storage systems increases the price of raw

materials that are being used majorly lithium. This combined with the fact that over 70% of lithium reserves can be found in the region of South America, this enforces political and geological limitations [10]. Thus, to overcome these limitations, we have to look for an alternative to LIBs and with respect to that, sodium ion batteries have attracted attention owing to the low cost of sodium reserve and its evenly distribution in the earth crust. Furthermore, the chemistry followed by NIBs is similar to LIBs and thus this removes most of the hurdles that these batteries face towards commercialization except for a few [11].

1.2. Sodium-ion Batteries

Sodium ion insertion and extraction chemistry was discovered in 1980s and at the same time, LIBs intercalation chemistry was also investigated which halted further research in NIBs. That was because of exponential growth in consumer electronic devices which required storage devices and LIBs technology was an ideal choice for them owing to their high energy density [12]. However, over the past decade, NIBs technology was revisited again particularly due to low cost of sodium as compared to lithium as shown in figure 1.2. Since then many efforts made to achieve the same energy density, capacity and cyclic life as that is being delivered by LIBs which is intrinsically difficult to achieve due to higher reduction potential of sodium than lithium and because of its large ionic radii [13,14,15].

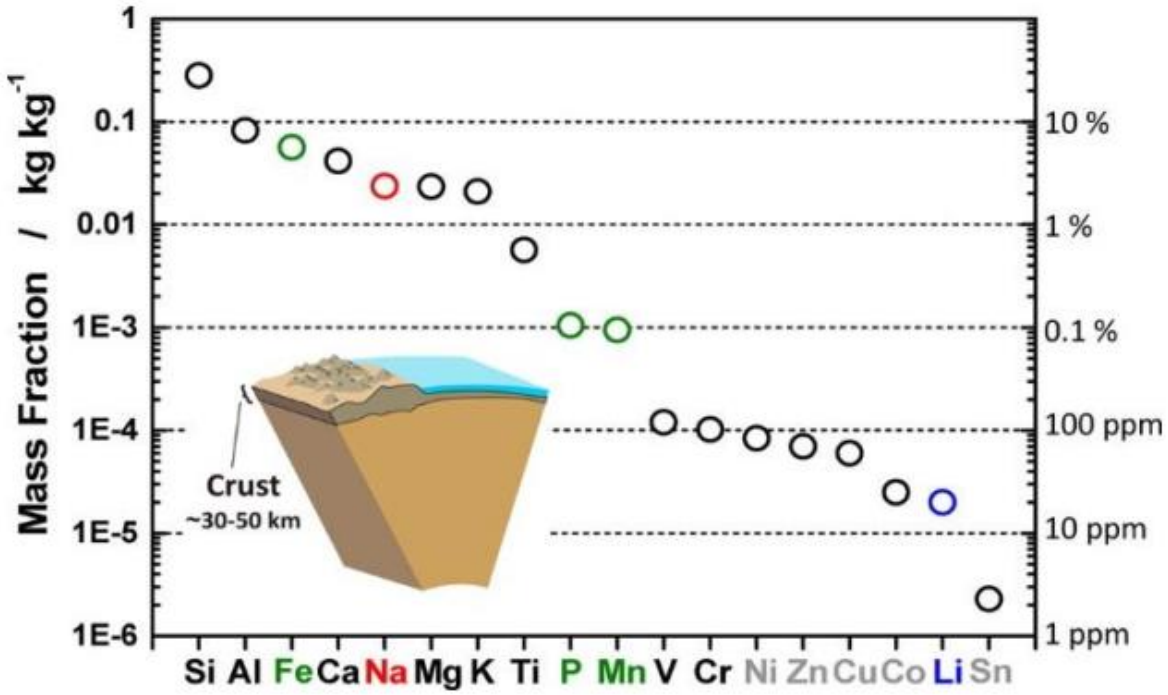

Figure 1.2 Concentration of sodium in earth crust [13]

Table 1.1 Comparison of sodium and lithium properties [14,15]

Properties	**Lithium**	**Sodium**
Distribution	70% in South America	Everywhere
Cost	~$5000/ ton	~ $150/ ton
Abundance in earth crust	20 mg/kg	(2.36~2.84) × 10^4 mg/kg
Abundance in sea water	0.18 mg/l	1.1 × 10^4 mg/l
Standard reduction potential	-3.04	-2.7
Ionic radius	0.69 Å	0.98 Å
Specific capacity	3829 mAh/g	1165 mAh/g
Melting point	180.5 º C	97.7 º C
Molar mass	6.9 g/mol	23 g/mol
density	0.53 g/cm^3	0.9 g/cm^3

Further sodium and lithium properties are compared in table 1.1. Analyzing this table gives indication that price of sodium can be further reduced with improved mining techniques and considering its toxic free nature, the price of NIBs can be decreased significantly. Although, large sodium ion ionic radius poses some problems but they can be countered by designing new active materials having lattice spacing large enough to accommodate Na^+ during ion insertion and extraction mechanism [16]. Moreover, these active materials that are designed for NIBs also have to over thermodynamic and kinetic barriers to store sodium ions during discharge/charge phenomenon. Additionally, due to higher weight of sodium than lithium (sodium ion is 3 times heavier than lithium ion) and due to higher standard reduction potential, the energy density given by NIBs is less than LIBs. So, novel approaches are required to design electrode materials to develop sodium ion battery storage device which is capable of delivering

high power with high rate capability when required for applications like grids, solar energy and wind energy [17].

1.3. Basic Mechanism of Sodium-ion Batteries

NIBs typically behave in a same manner as LIBs. Briefly, a NIB device consists of disorderd carbon anode and layered cathode material to accept Na ions. Both of these electrodes are separated by a glass fiber or any other polymeric sheet having enough porosity to allow sodium ions to travel from anode to cathode in a non-aqueous electrolyte ($NaPF_6$) [18]. The basic purpose of this polymeric separator is to prevent cell from short circuiting by preventing anode and cathode from coming in contact with each other. During discharge, sodium ions move from anode to cathode and intercalate there and the reverse phenomenon occurs during charge process. The capacity shown by any active materials depends on how many ions can be stored by them during charge/discharge mechanism. Figure 1.3 below shows the schematic of basic operating mechanism in NIBs [19].

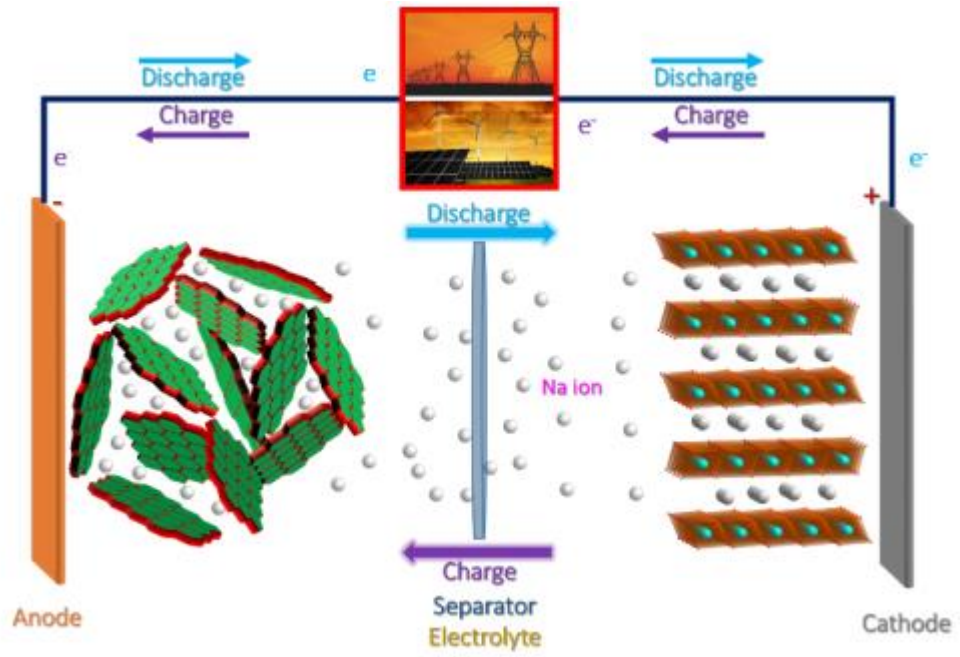

Figure 1.3 schematic of NIBs operating mechanism [19]

1.4. Challenges of Sodium ion Batteries

For NIBs, the intercalation chemistry is not as simple as it seems but infact, it is much more complex than LIBs particularly because of large cation size (1.02 Å) of sodium and they generally prefer to remain at octahedral position [20]. This poses limitations to type of

crystalline materials that can be used as electrodes to fabricate a stable NIB device. Figure 1.4 below depicts the type of different electrodes material that can be used cathode and anode. For cathode materials, the ideal choice of materials is those which at a high voltage for example $Na_3V_2(PO4)_3$, and $NaFePO_4F$, while for anode, they should operate at a low working potential i-e below 1 V which mostly comprises different form of carbon materials [21]. These restriction to choices is owed to (1) different sodium ion chemistry as compared to lithium ion because of size difference (2) due to large sodium ion size, kinetics of Na^+ is different than lithium ion (high charge transfer resistance) (3) initial capacity loss due to solid electrolyte interphase (SEI) formation. This SEI development at electrodes mainly occur because of electrolyte which are not stable at low operating voltage i-e below 1 V [22]. This layer increases the diffusion resistance for sodium ions to move from one electrode to another which leads to sodium loss and eventually decreases cyclic life. (4) During cyclic process, active anode materials undergo large volume expansion and this phenomenon is more prominent in electrode materials which store sodium ions through alloying, conversion or partial alloying/conversion reaction mechanism. One such material includes different compounds of tin (oxides and sulfides) in which large volume changes occur during ion insertion and extraction process due to pulverization of particles thus, capacity fading [23]. These are the few limitations which provide hinderance in borrowing electrode materials from lithium ion batteries.

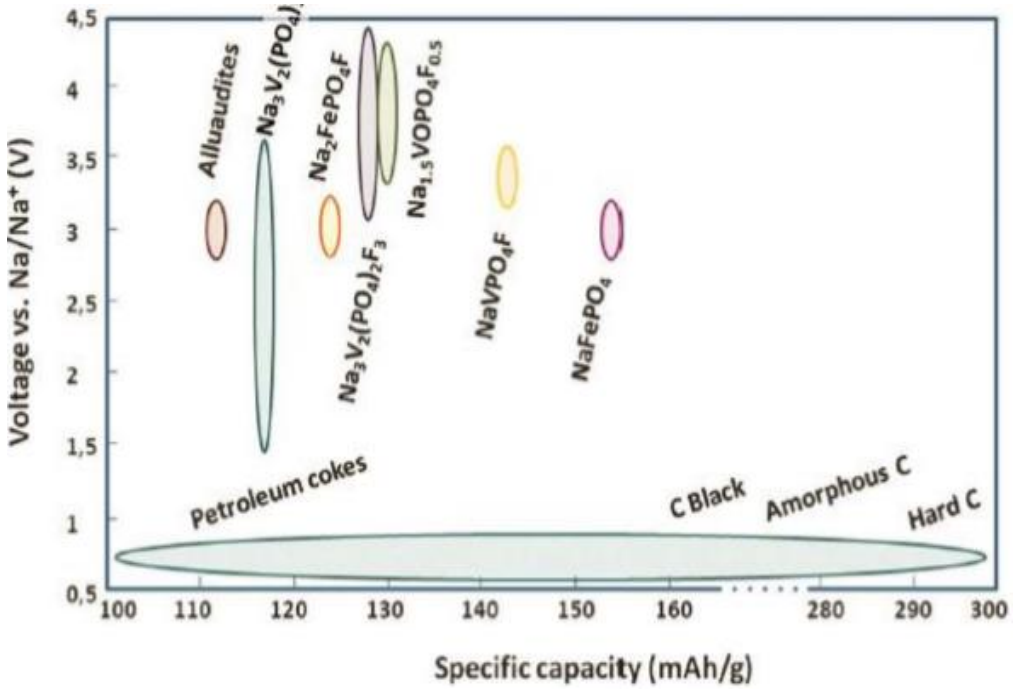

Figure 1.4 Different types of cathode and anode materials for NIBs [16]

1.5. Problem Statement of Thesis

Among different available anode materials, tin chalcogenide-based are considered as a promising anode material for sodium-ion batteries yet they suffer from poor initial coulombic efficiency, electronic conductivity, and capacity retention upon cycling. This is owed to large amount of volume expansion that occurs in the material during sodiation/desodiation and an effective strategy is required that not only buffers the volumetric expansion of the electrode to increases its capacity retention, but also improves the kinetics of a reaction.

1.6. Summary

Due to ever-decreasing reserve in fossil fuels, the focus for electricity generation is shifting towards renewable source of energy such as solar, wind and biomass. To store surplus electricity generated by these sources as a power backup, secondary batteries are required but LIBs are proving to be too costly for large-scale energy system storage. Owing to very high concentration of sodium reserves in earth crust, NIBs can be a cheap alternate source for that. Moreover, NIBs operate under the same mechanism as that of LIBs in terms of charge storage which could prove to be an ideal drop in technology. However, they face hinderance towards commercialization because of large ionic radius, high standard reduction potential, low gravimetric and volumetric energy density, large volume expansion of active materials upon cycling and high initial capacity loss because of SEI formation. Thus, strategies are required to minimize these problems that are being faced by NIBs at the moment in order facilitate them towards commercialization.

1.7. References

[1] Y. Fang, X.-Y. Yu, and X. W. (David) Lou, "Nanostructured Electrode Materials for Advanced Sodium-Ion Batteries," *Matter*, vol. 1, no. 1, pp. 90–114, 2019.

[2] B. C. Melot and J.-M. Tarascon, "Design and Preparation of Materials for Advanced Electrochemical Storage," *Acc. Chem. Res.*, vol. 46, no. 5, pp. 1226–1238, May 2013.

[3] A. Vlad, N. Singh, C. Galande, and P. M. Ajayan, "Design Considerations for Unconventional Electrochemical Energy Storage Architectures," *Adv. Energy Mater.*, vol. 5, no. 19, p. 1402115, Oct. 2015.

[4] K. Chayambuka, G. Mulder, D. L. Danilov, and P. H. L. Notten, "Sodium-Ion Battery Materials and Electrochemical Properties Reviewed," *Adv. Energy Mater.*, vol. 8, no. 16, pp. 1–49, 2018.

[5] C. Vaalma, D. Buchholz, M. Weil, and S. Passerini, "The demand for lithium-ion batteries (LIBs) has been increasing since their commer- cialization in 1991 and their widespread use in portable electronics," *Nat. Perspect.*, 2018.

[6] L. Chen, M. Fiore, J. E. Wang, R. Ruffo, D.-K. Kim, and G. Longoni, "Readiness Level of Sodium-Ion Battery Technology: A Materials Review," *Adv. Sustain. Syst.*, vol. 2, no. 3, p. 1700153, 2018.

[7] Z. Hu, Q. Liu, S. L. Chou, and S. X. Dou, "Advances and Challenges in Metal Sulfides/Selenides for Next-Generation Rechargeable Sodium-Ion Batteries," *Adv. Mater.*, vol. 29, no. 48, pp. 1–24, 2017.

[8] M. S. Whittingham, "Electrical energy storage and intercalation chemistry," *Science (80-.).*, vol. 192, no. 4244, pp. 1126–1127, Feb. 1976.

[9] J. B. Goodenough and K.-S. Park, "The Li-Ion Rechargeable Battery: A Perspective," *J. Am. Chem. Soc.*, vol. 135, no. 4, pp. 1167–1176, Jan. 2013.

[10] J. M. Tarascon, "Is lithium the new gold?," *Nature Chemistry*, vol. 2, no. 6. Nature Publishing Group, p. 510, Jun-2010.

[11] J. M. Tarascon, "Key challenges in future Li-battery research," *Philosophical Transactions of the Royal Society A: Mathematical, Physical and Engineering Sciences*, vol. 368, no. 1923. Royal Society, pp. 3227–3241, 28-Jul-2010.

[12] L. P. Wang, L. Yu, M. Srinivasan, Z. J. Xu, and X. Wang, "Recent developments in electrode materials for sodium-ion batteries," *Journal of Materials Chemistry A*, vol. 3, no. 18. Royal Society of Chemistry, pp. 9353–9378, 14-May-2015.

[13] N. Yabuuchi, K. Kubota, M. Dahbi, and S. Komaba, "Research development on sodium-ion batteries," *Chemical Reviews*, vol. 114, no. 23. American Chemical Society, pp. 11636–11682, 10-Dec-2014.

[14] M. D. Slater, D. Kim, E. Lee, and C. S. Johnson, "Sodium-Ion Batteries," *Adv. Funct. Mater.*, vol. 23, no. 8, pp. 947–958, Feb. 2013.

[15] S. Y. Hong, Y. Kim, Y. Park, A. Choi, N. S. Choi, and K. T. Lee, "Charge carriers in rechargeable batteries: Na ions vs. Li ions," *Energy and Environmental Science*, vol. 6, no. 7. The Royal Society of Chemistry, pp. 2067–2081, 21-Jul-2013.

[16] V. Palomares, P. Serras, I. Villaluenga, K. B. Hueso, J. Carretero-González, and T. Rojo, "Na-ion batteries, recent advances and present challenges to become low cost energy storage systems," *Energy and Environmental Science*, vol. 5, no. 3. The Royal Society of Chemistry, pp. 5884–5901, 01-Mar-2012.

[17] H. Pan, Y. S. Hu, and L. Chen, "Room-temperature stationary sodium-ion batteries for large-scale electric energy storage," *Energy and Environmental Science*, vol. 6, no. 8. The Royal Society of Chemistry, pp. 2338–2360, 17-Aug-2013.

[18] D. Kim, E. Lee, M. Slater, W. Lu, S. Rood, and C. S. Johnson, "Layered Na[Ni 1/3Fe 1/3Mn 1/3]O 2 cathodes for Na-ion battery application," *Electrochem. commun.*, vol. 18, no. 1, pp. 66–69, Jan. 2012.

[19] S.-W. Kim, D.-H. Seo, X. Ma, G. Ceder, and K. Kang, "Electrode Materials for Rechargeable Sodium-Ion Batteries: Potential Alternatives to Current Lithium-Ion Batteries," *Adv. Energy Mater.*, vol. 2, no. 7, pp. 710–721, Jul. 2012.

[20] M. Zarrabeitia, M. Á. Muñoz-Márquez, F. Nobili, T. Rojo, and M. Casas-Cabanas, "Influence of using metallic na on the interfacial and transport properties of Na-Ion batteries," *Batteries*, vol. 3, no. 2, pp. 1–13, 2017.

[21] K. Kubota and S. Komaba, "Review—Practical Issues and Future Perspective for Na-Ion Batteries," *J. Electrochem. Soc.*, vol. 162, no. 14, pp. A2538–A2550, 2015.

[22] J. Deng *et al.*, "Sodium-Ion Batteries: High Energy Density Sodium-Ion Battery with Industrially Feasible and Air-Stable O3-Type Layered Oxide Cathode (Adv. Energy Mater. 5/2018)," *Adv. Energy Mater.*, vol. 8, no. 5, p. 1870019, 2018.

[23] N. Koteeswara Reddy, M. Devika, and E. S. R. Gopal, "Review on Tin (II) Sulfide (SnS) Material: Synthesis, Properties, and Applications," *Crit. Rev. Solid State Mater. Sci.*, vol. 40, no. 6, pp. 359–398, 2015.

CHAPTER 2: Literature Review

2.1. Anode Materials for Sodium-ion Batteries

Sodium metal cannot be considered ideal choice for an anode material NIBs owing to its extremely high reactivity status which can pose a lot of safety concerns (such as sodium react vigorously with air and can explode when comes in contact with water). Furthermore. It's low melting point (97.7 º C), low specific capacity and short circuiting of cells due to unwanted dendrite growth in sodium during cyclic process also plays their role in not using sodium as an anode material [1]. Since sodium ion batteries follow majorly same reaction mechanism as LIBs, we can classify anode materials into three types as shown in figure 2.1, namely (1) insertion type (2) alloy- type (3) conversion type anode materials [2].

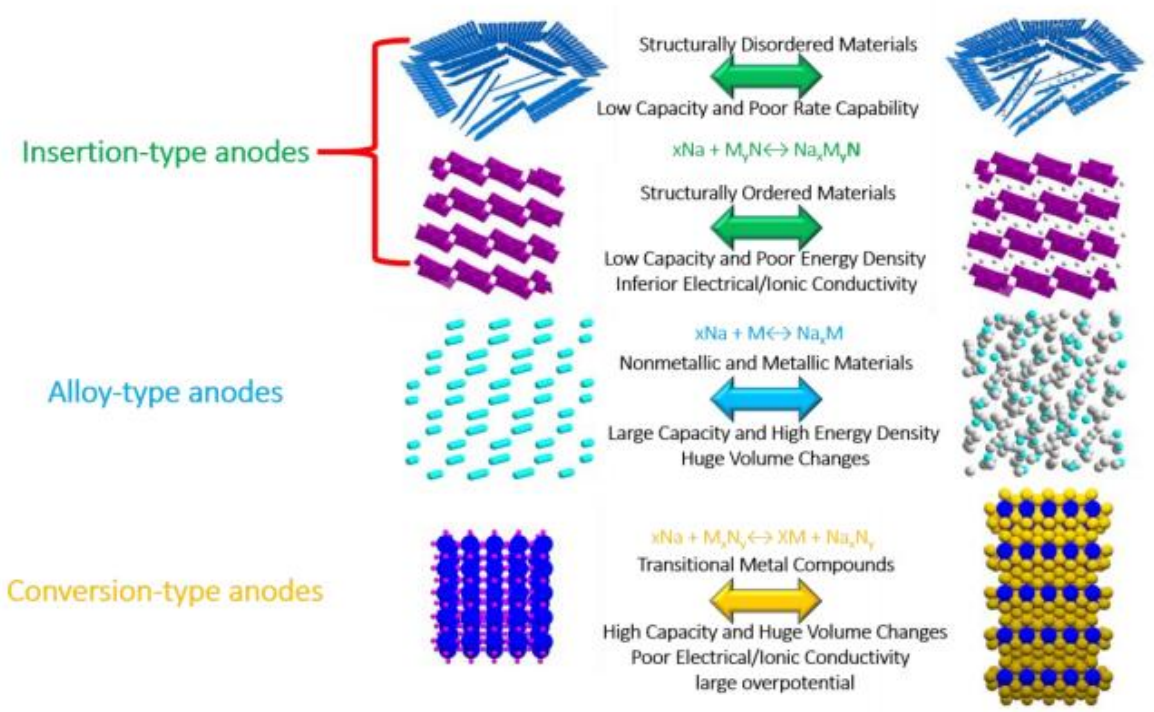

Figure 2.1 Different type of anode materials based on their insertion mechanism. [2]

Insertion type anode materials as their name suggests, has the ability to store and release sodium ions from their active sites which can be vacancies, defects, lattice spacing etc. [3]. This storage and release on sodium ion from active materials also depend a lot on whether the electrode material is behaving as crystalline or amorphous. When it comes to alloying type anode

materials for sodium ion batteries, they behave in a manner that during sodiation/desodiation process, sodium ions can create or break a bond with the metal and form an alloy which can also decompose during charging process [4]. Lastly, conversion type materials including different fluorides and sulfides undergoes a reversible reaction releasing transition metals and sodium compounds which can be identified during cyclic voltammetry [4].

Among these different types of anode materials, insertion materials usually give good cyclic ability with better rate capability since they undergo single electron transfer from anode to cathode and vice versa during charging/discharging. However, these electrodes deliver poor specific capacity which can be due to single electron transfer as a result, these materials intrinsically have poor theoretical capacity and this limits their commercialization in market as a reliable anode material. In contrast, conversion type anode materials and alloying type anode materials have high theoretical and reversible capacity owing to multi electron charge transfer process which occurs during cyclic process but large volume changes in electrode material as number of cycles are increased along with severe voltage hysteresis, their capacity decreases rapidly limiting their practical use [3]–[5].

2.2. Recent progress in Anode Materials

So far, the research on SIBs anode has gained substantial pace in the past decade to counteract these problems which are possessed by insertion, alloying and conversion type anode materials.

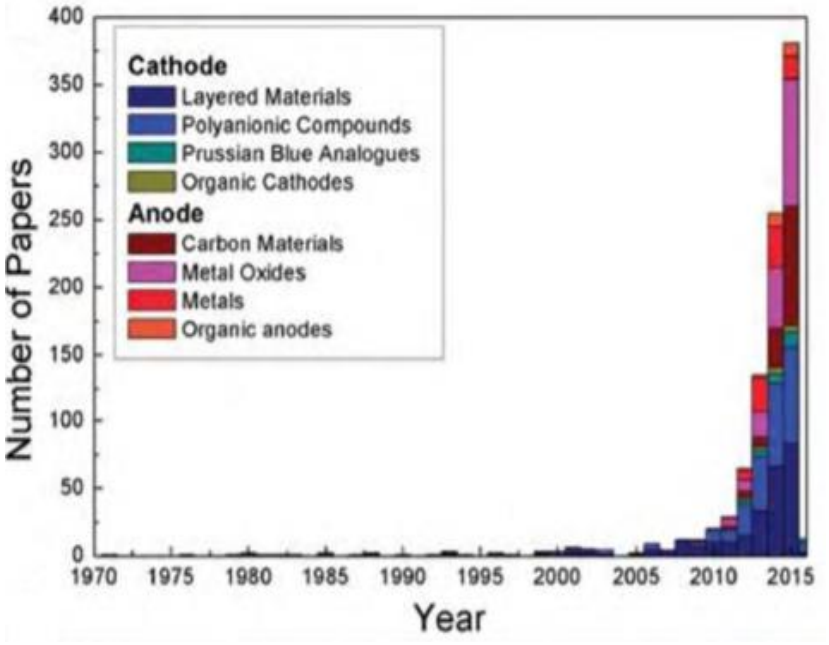

Figure 2.2 Research pattern on anode and cathode type materials over the years. [8]

2.2.1. Carbon Based Anode Materials

It is well knowns so far that when LIBs were commercialized, graphite played a big role in it by proving to be an effective anode material which can store and release Li ions during charging and discharging process. However, when graphite was used as an anode materials for NIBs, it failed to prove a good cyclic life and also delivered very less reversible capacity [6]. When analyzed, it was found that this peculiar behavior of graphite in NIBs is simply owed to its large ionic radii which require hosts materials with bigger interlamellar spacing than they were require for LIBs and this incapability of graphite was also reported by few other groups [7]. Figure 2.2 shows the electrochemical profile of graphite anodes, and it can be seen that the required anode material in LIBs can store 1 lithium ion corresponding to 6 carbon atoms while NIBs barely allow intercalation of sodium ions to happen. Mele and DiVincenzo via theoretical calculations came to conclusion Na-C bond is not thermodynamically favorable to form thus developing a weak interaction when sodium ions get inserted between carbon layers [8].

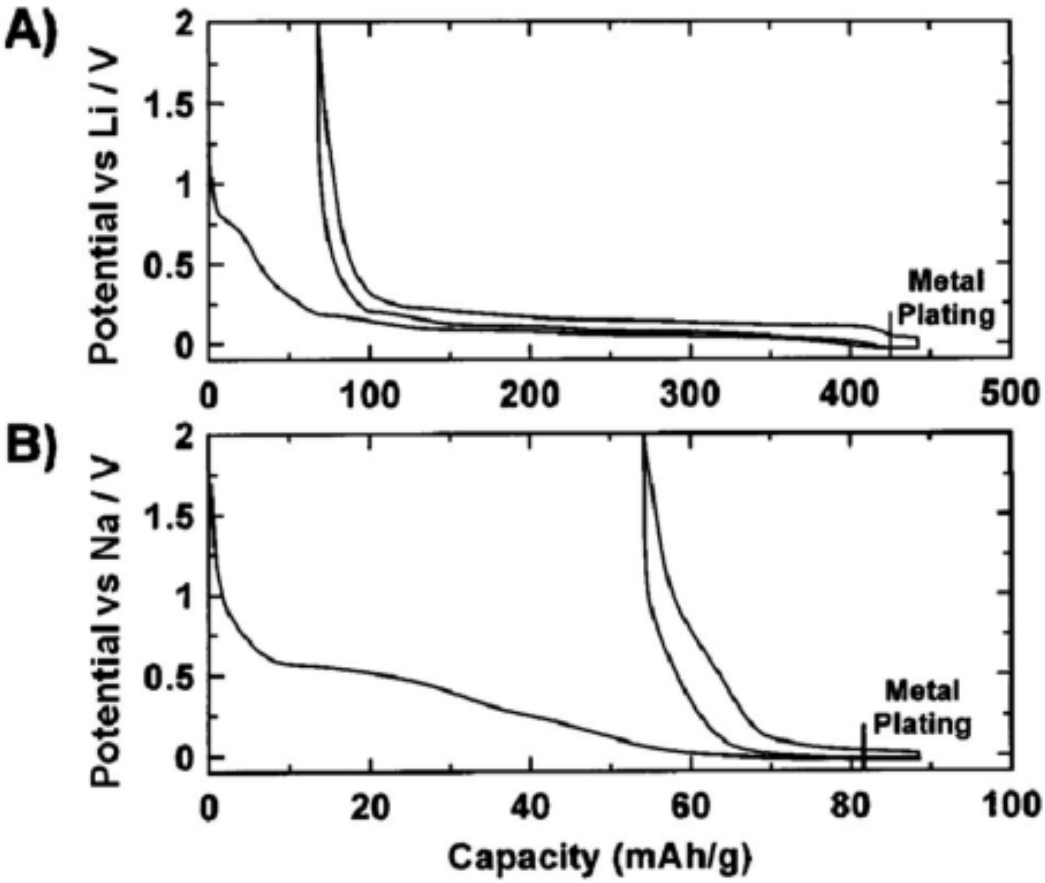

Figure 2.3 Electrochemical profile of graphite anode material for (A) LIBs (B) NIBs. [7]

Among different carbon based which have gained attention as an anode material for NIBs, hard carbon is one of them due to its high interlamellar d- spacing than graphite and rather high reversible capacity of 300 mAh/g. Unfortunately, due to low degree of graphitization, they exhibit poor cyclic life and rate capability [9].

2.2.2. Alloy Based Anodes

Based on their high theoretical, volumetric and gravimetric capacity, these electrode materials are considered as the most promising type of anode materials for SIBs. Alloy based anode materials include number of elements including Sb, Bi, P, Sn, Ge etc. which can form binary alloys with sodium [9]–[15]. So far, the major focus in alloy based anode material has been on tin, antimony and phosphorus because of their relatively high theoretical capacity which is why only these type of alloy based anodes will be discussed.

2.2.2.1 Tin and Antimony-based Alloy Anodes

Tin (Sn) have a theoretical capacity of 847 mAh/ g while antimony (Sb) show theoretical capacity of 660 mAh /g. This high theoretical capacity shown by these both electrode materials is due to the formation of $Na_{15}Sn_4$ [14], an alloying phenomena in tin while for antimony Na_3Sb forms. Electrochemical reaction of Na-Sn system occurs stepwise such as $Sn \rightarrow NaSn_5 \rightarrow NaSn \rightarrow Na_9Sn_4 \rightarrow Na_{15}Sn_4$ [14]. In antimony, first an amorphous phase Na_xSb forms from crystalline Sb which then reduces to crystalline Na_3Sb having hexagonal crystal lattice. When oxidation occurs, this crystalline Na_3Sb converts back into amorphous Sb. Scientists believe that this formation of amorphous intermediate phase before final crystalline Na_3Sb can act as a buffer to release volumetric strains induced during sodiation/ desodiation [14]. This property shown by bulk antimony particles is opposite to bulk tin particles which showed poor electrochemical performance when their particle size was increased. Furthermore, when the particle size of antimony was more decreased to nano size ~ 20 nm, they show improvement in electrochemical performance with enhanced cyclic stability. However, during alloying reactions of Sn and Sb, when $Na_{15}Sn_4$ and Na_3Sb forms, it is accompanied with huge volume expansion of 420% and 293% respectively [16][17].

So far, many strategies have been devised to deal with large volume expansion such as by increasing surface area of electrodes through the introduction of graphene, CNTs etc. which act as a matrix material and can counteract these large volume changes. One such example is shown in figure 2.4 in which a hierarchical tin@ carbon/ graphene composite was synthesized which prevented nanomaterial agglomeration due to high surface area of graphene matrix and

thus providing enough space to cater volume expansion in the structure hence, improving cyclic life [18].

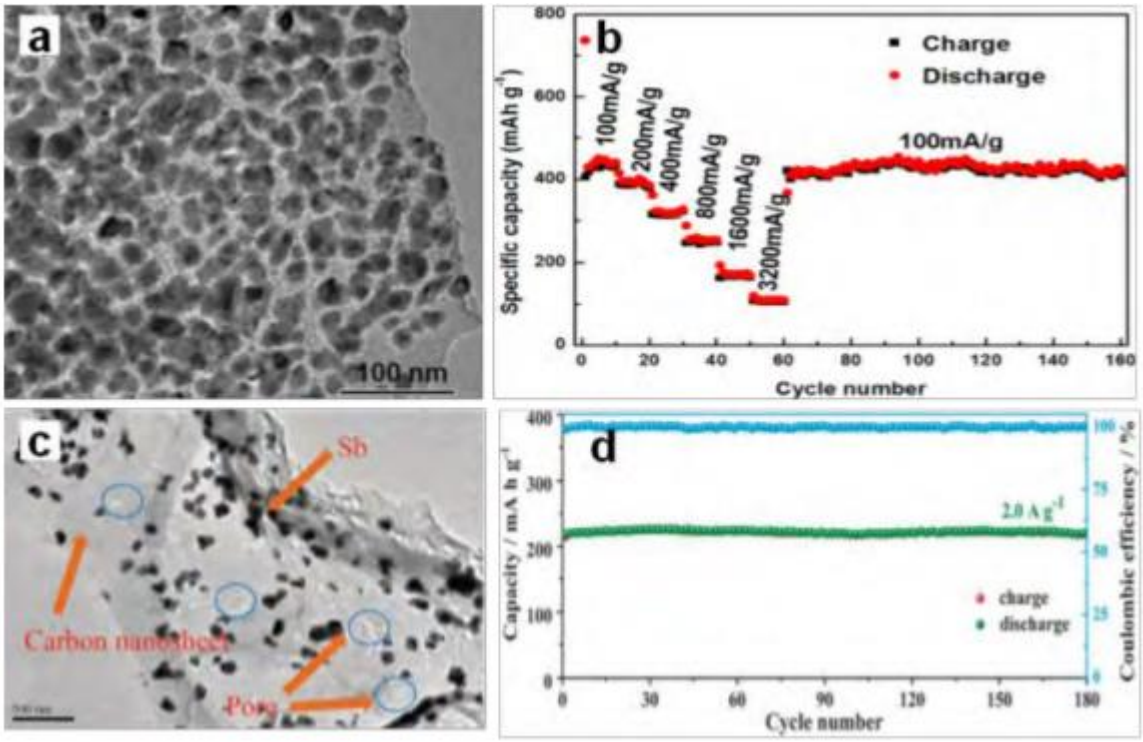

Figure 2.4 (a) TEM image of tin@ carbon / graphene composite (b) Rate capability test (c) TEM image of Sb-N/C composite (d) Cycling performance. [18]

2.2.2.2 Phosphorus Based Anodes

Among all the available anode materials, phosphorus has one of the highest theoretical capacity (2596 mAh/ g) owing to the formation of Na_3P [19], [20]. They show redox potential of 0.4 V in NIBs which is appropriate for them as we require an anode material with low reduction potential. However, they face the same problem as that is faced is tin and antimony-based alloys i-e their electrodes undergo large volume expansion during ion insertion and extraction phenomenon. White phosphorus, red phosphorus and black phosphorus are its 3 main allotropes but for secondary battery applications, only red and black are suitable [21]. Among them, only red phosphorus is available in the market and it exhibits an amorphous nature with extremely low electronic conductivity of 10^{-14} S/cm [22]. This develops the need of having a secondary matrix material to cater volume expansion that these electrodes experience and to improve the electronic conductivity [23]. This was perfectly exhibited by song et al. as shown in figure 2.5, who developed phosphorus/ graphene nanosheets through ball milling method.

The nanosheets of graphene in it chemically bonds with phosphorus particles and they deliver a reversible capacity of 2077 and good cyclic stability (1700 mAh/ g after 60 cycles) [24].

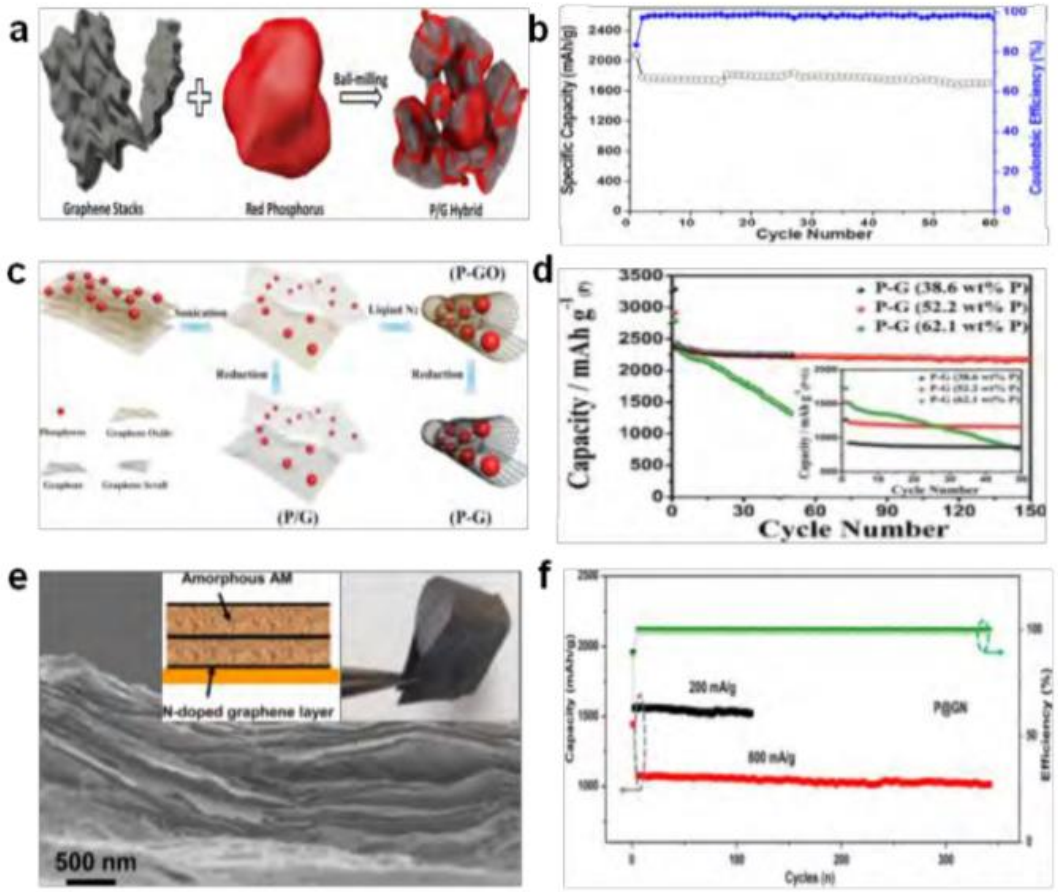

Figure 2.5 (a) schematic of P/ graphene nanosheet composite (b) cyclic stability (c) schematic of P/G composite (d) cycling performance of P/G composite at 250 mA/ g (e) SEM of P/ graphene nanosheet (f) cycling. [24]

2.2.3 Conversion Based Anodes

Like in LIBs, conversion type materials have also been studied as an anode material for NIBs owing to their high theoretical capacity. These types of materials usually include metal sulfides and oxides which has the ability to store sodium ions through either a conversion reaction or both conversion/ alloy reaction.

2.2.3.1 Metal Oxides

Metal oxides, which behave as a conversion-based anode undergo large volume changes during their cyclic life and so far various remedies have been designed to overcome this shortcoming.

One such was the synthesis of ultrathin NiO nanosheets through solvothermal route for sodium storage as shown in figure 2.6. This electrode delivered a reversible capacity of 299 mAh/ g at 1 A/ g and after 100^{th} cycle, it was still 266 mAh/ g [25]. Similar to alloy based anodes, we can design a matrix of graphene and combine it with different oxide materials such as Fe_3O_4, FeO, NiO, CuO, MoO_3, SnO_2, and Mn_3O_4 [26]. Among all of them, SnO_2 has gained special attention because of relatively high theoretical capacity of 782 mAh/ g. To counteract volume changes in tin oxide, chen et al. designed SnO_2/ 3DG composite, compared it with SnO_2/2DG composite and obtained a reversible capacity of 432 mAh /g after 200 cycles at 0.1 A/ g, which was grater than the later composite [27].

2.2.3.2 Metal Sulfides

In contrast to metal oxide anodes, metal sulfide anode show several advantages such as: (1) due to lower lower atomic mass of Sulfur atom, gravimetric density shown by metal sulfide is high; (2) They undergo less volume expansion as compared to metal oxides and other alloy based anode materials (3) Formation of Na_2S lead these electrodes to deliver better initial coulombic efficiency as compared to Na_2O which forms in metal oxides [28]. Some metal sulfides which have gained attention in the past decade include FeS, FeS_2, Ni_3S_2, NiS, CoS, MnS, ZnS, SnS_2, SnS and Bi_2S_3 [28]–[35]. Among these metal sulfides, layered metal sulfide, because of their unique layered structure have relatively large interlayer spacing and this makes them feasible for sodium ion intercalation along with compensating volume changes. However, in bulk, these material still suffers from this issue and to add to that, they also have sluggish kinetics in a reaction [33]. Like discussed before, several strategies have been designed to overcome these problems. Hu et al. showed that MoS_2 nanoflower if anchored on a graphene structure reduces barrier to Na^+ diffusion across electrodes and thus provide more active sites for sodium ion to store (figure 2.7) [36].

2.3 Tin sulfide-based Anode Materials

SnS_2 and SnS in the past decade because of their high theoretical capacity (1022 and 1136 mAh/ g) have found their application in NIBs. During charge and discharge, tin can dissociate itself from SnS through a conversion reaction and forms $Na_{3.75}Sn$ which leads them to deliver high specific capacity [37]–[40]. The mechanism of reaction that is being followed by these materials can be summarized below as:

$$SnS + 2xNa \rightarrow Sn + xNa_2S$$
$$Sn + 3.75Na \rightarrow Na_{3.75}S$$

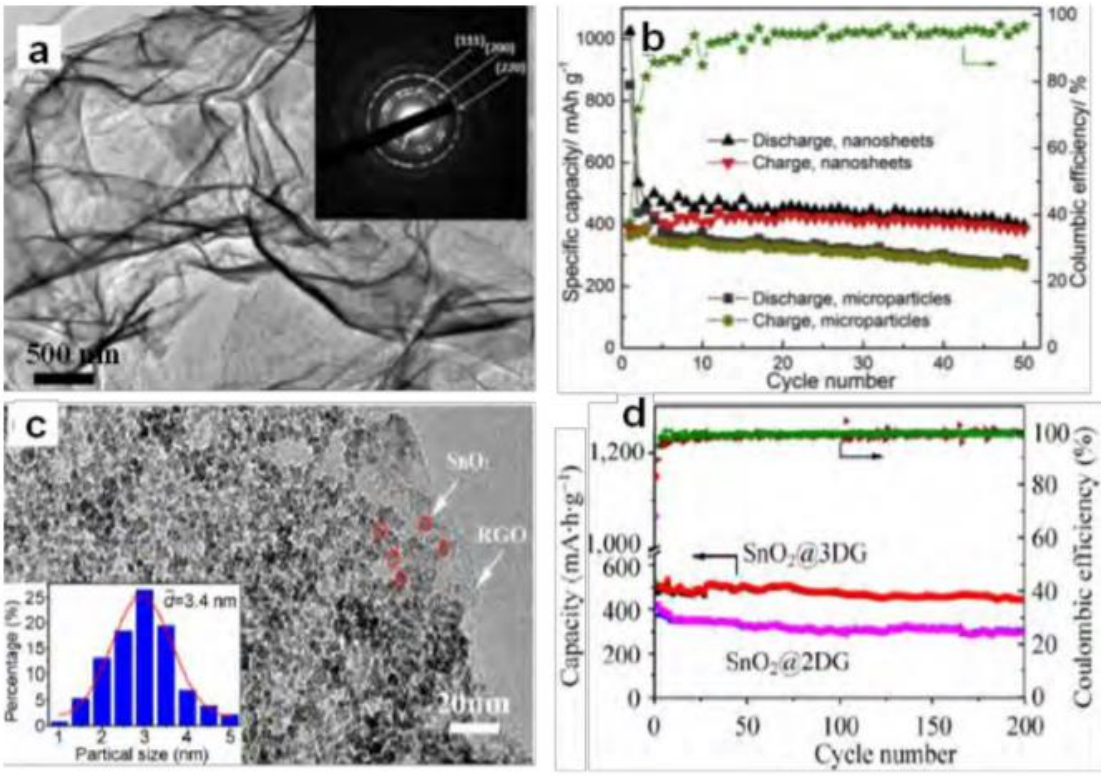

Figure 2.6 (a) HRTEM of NiO (b) cyclic stability of NiO at 0.1 A/ g (c) TEM of SnO_2/3DG (d) cycling performance comparison at 0.1 A/ g for SnO2/3DG and SnO2/2DG. [26, 27]

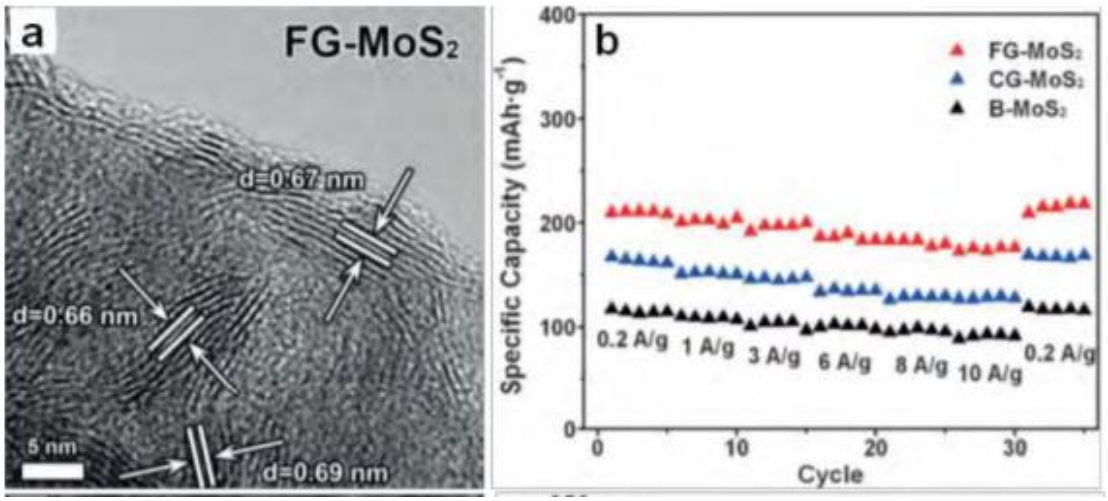

Figure 2.7 (a) HRTEM of FG-MoS_2 (b) cyclic stability of FG MoS_2 at 0.1 A/ g. [36]

Like other metal oxide and sulfides, composites of SnS with graphene has also received attention. Using this as a motivation, Zhou et al. was able to develop SnS/ graphene composite which exhibited reversible capacity of 492 and 308 mAh/ g at a current density of 810 and

7290 mAh/ g respectively (250 cycles) [41]. Tuning morphologies of nanomaterials is also another way to achieve good cyclic life and similarly, SnS with nano-wall, nano honeycomb and nano-flake morphology anchored on graphene-foam was reported [42]. This study revealed that among them, nano honeycomb SnS exhibited highest reversible capacity as shown in figure 2.8

Apart from graphene, modification through carbon in tin sulfide material has also gained attention. Choi et al. prepared SnS/C composite through spray pyrolysis method and after 50 cycles, he obtained discharge capacity of 433 mAh/ g at 0.5 A/ g with an average coulombic efficiency of 89% [43]. Similarly, carbon nanotubes (CNTs) because of their very less weight and high conductivity, they were used by Ren et al as he SnS_2/CNTs electrode which delivered a reversible capacity of 317 mAh/ g at 20 mA/ g [44].

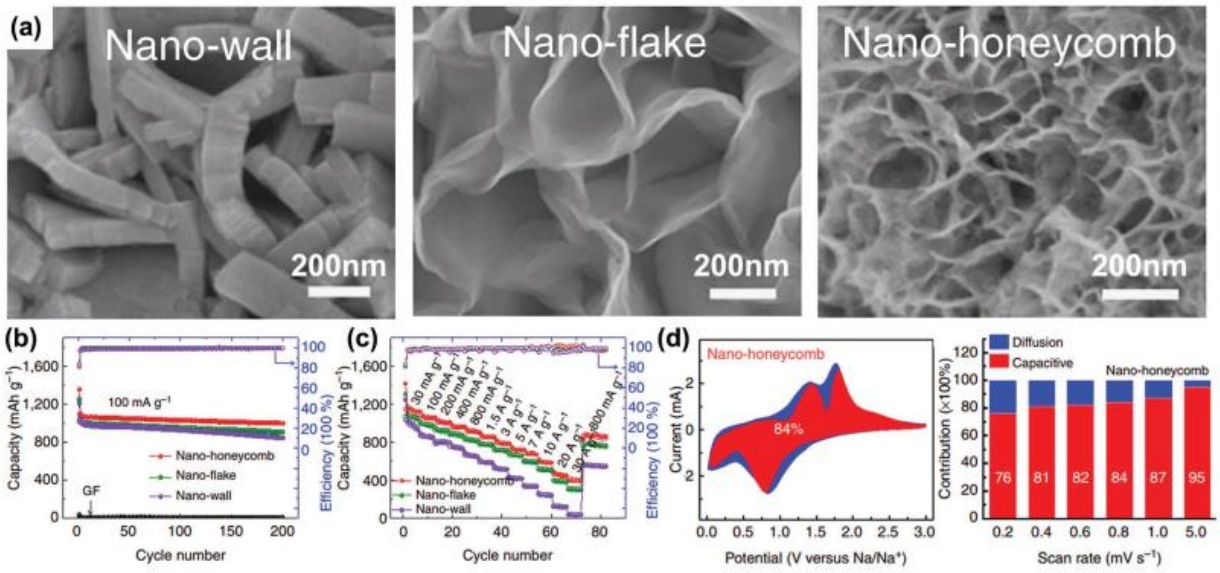

Figure 2.8 (a) SEM of SnS having different morphologies (b) cyclic life (c) rate capability tests (d) CV curve of nano-honeycomb morphology (e) pseudocapacitive behaviour of SnS honeycomb. [42]

2.4 Summary

This chapter starts with highlighting the different type of anode materials that are currently available for NIBs such as insertion, alloy based and conversion-based materials. Graphite, which is predominately used as an anode material for LIBs cannot be used in NIBs because of large ionic radii of sodium ion, which decreases its cyclic life. However, hard carbon can be suitable for commercialized NIBs because of high interlamellar spacing than that is provided

by graphite to store Na^+ but overall, the theoretical capacity shown by this material is less (300 mAh/ g). Thus alloy-based and conversion-based anode materials are looked at for their potential application in NIBs. Alloy based material such as tin and phosphorous show high theoretical capacity as they make an alloy with sodium ion but during sodiation/desodiation, this alloy material undergo large volume changes which decreases their rate capability as well as cyclic life. Finally, conversion-based materials such as metal oxides and metal suflides have shown promising results when they are used as an anode material for NIBs. They form Na_2O and Na_2S during charge/ discharge thus leading to ultrahigh theoretical capacity. However, metal oxides undergo large volume expansion as compared to metal sulfides and they also show less gravimetric capacity than metal sulfides. Tin sulfide over the past few years have gained importance because of its high theoretical capacity (1022 mAh/ g) and to counter volume expansion in to for improving cyclic life, different strategies have been proposed so far such as tuning morphology of active material, make it's composite with carbon based material such as graphene, carbon black and CNTs which can act as a buffer to volume expansion and provides short path for sodium ion to move between electrodes.

2.5 References

[1] J. Deng *et al.*, "Sodium-Ion Batteries: High Energy Density Sodium-Ion Battery with Industrially Feasible and Air-Stable O3-Type Layered Oxide Cathode (Adv. Energy Mater. 5/2018)," *Adv. Energy Mater.*, vol. 8, no. 5, p. 1870019, 2018.

[2] M. D. Slater, D. Kim, E. Lee, and C. S. Johnson, "Sodium-ion batteries," *Adv. Funct. Mater.*, vol. 23, no. 8, pp. 947–958, Feb. 2013.

[3] G. Yang *et al.*, "Carbon-Based Alloy-Type Composite Anode Materials toward Sodium-Ion Batteries," *Small*, vol. 15, no. 22. Wiley-VCH Verlag, p. 1900628, 29-May-2019.

[4] L. Wang *et al.*, "Promises and challenges of alloy-type and conversion-type anode materials for sodium–ion batteries," *Materials Today Energy*, vol. 11. Elsevier Ltd, pp. 46–60, 01-Mar-2019.

[5] N. Koteeswara Reddy, M. Devika, and E. S. R. Gopal, "Review on Tin (II) Sulfide (SnS) Material: Synthesis, Properties, and Applications," *Crit. Rev. Solid State Mater. Sci.*, vol. 40, no. 6, pp. 359–398, 2015.

[6] Z. L. Xu *et al.*, "Tailoring sodium intercalation in graphite for high energy and power sodium ion batteries," *Nat. Commun.*, vol. 10, no. 1, pp. 1–10, Dec. 2019.

[7] D. A. Stevens and J. R. Dahn, “The Mechanisms of Lithium and Sodium Insertion in Carbon Materials,” *J. Electrochem. Soc.*, vol. 148, no. 8, p. A803, Aug. 2001.

[8] D. P. DiVincenzo and E. J. Mele, “Self-consistent effective-mass theory for intralayer screening in graphite intercalation compounds,” *Phys. Rev. B*, vol. 29, no. 4, pp. 1685–1694, Feb. 1984.

[9] X. Dou *et al.*, “Hard carbons for sodium-ion batteries: Structure, analysis, sustainability, and electrochemistry,” *Materials Today*, vol. 23. Elsevier B.V., pp. 87–104, 01-Mar-2019.

[10] V. L. Chevrier and G. Ceder, “Challenges for Na-ion Negative Electrodes,” *J. Electrochem. Soc.*, vol. 158, no. 9, p. A1011, Sep. 2011.

[11] D. F. Qiu, X. Ma, J. D. Zhang, Z. X. Lin, and B. Zhao, “Mesoporous Silicon Microspheres Produced from In Situ Magnesiothermic Reduction of Silicon Oxide for High-Performance Anode Material in Sodium-Ion Batteries,” *Nanoscale Res. Lett.*, vol. 13, 2018.

[12] K. Song, C. Liu, L. Mi, S. Chou, W. Chen, and C. Shen, “Recent Progress on the Alloy-Based Anode for Sodium-Ion Batteries and Potassium-Ion Batteries,” *Small*. Wiley-VCH Verlag, p. 1903194, 23-Sep-2019.

[13] B. Q. Xiong *et al.*, “Boosting Superior Lithium Storage Performance of Alloy-Based Anode Materials via Ultraconformal Sb Coating–Derived Favorable Solid-Electrolyte Interphase,” *Adv. Energy Mater.*, vol. 10, no. 4, p. 1903186, Jan. 2020.

[14] W. T. Jing, C. C. Yang, and Q. Jiang, “Recent progress on metallic Sn- and Sb-based anodes for sodium-ion batteries,” *J. Mater. Chem. A*, vol. 8, no. 6, pp. 2913–2933, Feb. 2020.

[15] L. Guo, L. Cao, J. Huang, J. Li, and S. Chen, “ Carbon capsule confined Sb 2 Se 3 for fast Na + extraction in sodium-ion batteries ,” *Sustain. Energy Fuels*, vol. 4, no. 2, pp. 797–808, Feb. 2020.

[16] J. Huang *et al.*, “Nanostructures of solid electrolyte interphases and their consequences for microsized Sn anodes in sodium ion batteries,” *Energy Environ. Sci.*, vol. 12, no. 5, pp. 1550–1557, May 2019.

[17] W. Liu *et al.*, “Gassing in Sn-Anode Sodium-Ion Batteries and Its Remedy by

Metallurgically Prealloying Na," *ACS Appl. Mater. Interfaces*, vol. 11, no. 26, pp. 23207–23212, Jul. 2019.

[18] B. Luo, T. Qiu, D. Ye, L. Wang, and L. Zhi, "Tin nanoparticles encapsulated in graphene backboned carbonaceous foams as high-performance anodes for lithium-ion and sodium-ion storage," *Nano Energy*, vol. 22, pp. 232–240, Apr. 2016.

[19] J. Qian, X. Wu, Y. Cao, X. Ai, and H. Yang, "High capacity and rate capability of amorphous phosphorus for sodium ion batteries," *Angew. Chemie - Int. Ed.*, vol. 52, no. 17, pp. 4633–4636, Apr. 2013.

[20] Y. Kim *et al.*, "An amorphous red phosphorus/carbon composite as a promising anode material for sodium ion batteries," *Adv. Mater.*, vol. 25, no. 22, pp. 3045–3049, Jun. 2013.

[21] W. Liu, H. Zhi, and X. Yu, "Recent progress in phosphorus based anode materials for lithium/sodium ion batteries," *Energy Storage Materials*, vol. 16. Elsevier B.V., pp. 290–322, 01-Jan-2019.

[22] L. E. Marbella *et al.*, "Sodiation and Desodiation via Helical Phosphorus Intermediates in High-Capacity Anodes for Sodium-Ion Batteries," *J. Am. Chem. Soc.*, vol. 140, no. 25, pp. 7994–8004, Jun. 2018.

[23] X. Ma *et al.*, "High-performance red phosphorus/carbon nanofibers/graphene free-standing paper anode for sodium ion batteries," *J. Mater. Chem. A*, vol. 6, no. 4, pp. 1574–1581, Jan. 2018.

[24] J. Song *et al.*, "Chemically bonded phosphorus/graphene hybrid as a high performance anode for sodium-ion batteries," *Nano Lett.*, vol. 14, no. 11, pp. 6329–6335, Nov. 2014.

[25] Y. Pang, J. Zhang, D. Chen, and X. Jiao, "3D hierarchical porous NiO nanoflowers as an advanced anode material with remarkable lithium storage performance," *RSC Adv.*, vol. 6, no. 36, pp. 30395–30400, 2016.

[26] H. Kang *et al.*, "Update on anode materials for Na-ion batteries," *Journal of Materials Chemistry A*, vol. 3, no. 35. Royal Society of Chemistry, pp. 17899–17913, 08-Jul-2015.

[27] Y. X. Wang *et al.*, "Ultrafine SnO2 nanoparticle loading onto reduced graphene oxide as anodes for sodium-ion batteries with superior rate and cycling performances," *J. Mater. Chem. A*, vol. 2, no. 2, pp. 529–534, Jan. 2014.

[28] X. Guo, H. Gao, and G. Wang, “A Robust Transition-Metal Sulfide Anode Material Enabled by Truss Structures,” *Chem*, vol. 6, no. 2, pp. 334–336, Jan. 2020.

[29] Z. Hu *et al.*, “Pyrite FeS2 for high-rate and long-life rechargeable sodium batteries,” *Energy Environ. Sci.*, vol. 8, no. 4, pp. 1309–1316, Apr. 2015.

[30] J. Mao, T. Zhou, Y. Zheng, H. Gao, H. K. Liu, and Z. Guo, “Two-dimensional nanostructures for sodium-ion battery anodes,” *Journal of Materials Chemistry A*, vol. 6, no. 8. Royal Society of Chemistry, pp. 3284–3303, 2018.

[31] Y. X. Wang *et al.*, “Uniform yolk-shell iron sulfide-carbon nanospheres for superior sodium-iron sulfide batteries,” *Nat. Commun.*, vol. 6, no. 1, pp. 1–9, Oct. 2015.

[32] W. Ji, L. Hu, X. Hu, Y. Ding, and Z. Wen, “Nitrogen-doped carbon coating mesoporous ZnS nanospheres as high-performance anode material of sodium-ion batteries,” *Mater. Today Commun.*, vol. 19, pp. 396–401, Jun. 2019.

[33] M. Hu *et al.*, “Revealing the Critical Factor in Metal Sulfide Anode Performance in Sodium-Ion Batteries: An Investigation of Polysulfide Shuttling Issues,” *Small Methods*, vol. 4, no. 1, p. 1900673, Jan. 2020.

[34] L. Shen *et al.*, “Hierarchical Metal Sulfide/Carbon Spheres: A Generalized Synthesis and High Sodium-Storage Performance,” *Angew. Chemie - Int. Ed.*, vol. 58, no. 22, pp. 7238–7243, May 2019.

[35] J. K. Kim, S. K. Park, J. S. Park, and Y. C. Kang, “Uniquely structured composite microspheres of metal sulfides and carbon with cubic nanorooms for highly efficient anode materials for sodium-ion batteries,” *J. Mater. Chem. A*, vol. 7, no. 6, pp. 2636–2645, Feb. 2019.

[36] Z. Hu *et al.*, “MoS2 Nanoflowers with Expanded Interlayers as High-Performance Anodes for Sodium-Ion Batteries,” *Angew. Chemie - Int. Ed.*, vol. 53, no. 47, pp. 12794–12798, Nov. 2014.

[37] Z. Li, J. Ding, and D. Mitlin, “Tin and Tin Compounds for Sodium Ion Battery Anodes: Phase Transformations and Performance,” *Acc. Chem. Res.*, vol. 48, no. 6, pp. 1657–1665, Jun. 2015.

[38] P. K. Dutta, U. K. Sen, and S. Mitra, “Excellent electrochemical performance of tin monosulphide (SnS) as a sodium-ion battery anode,” *RSC Adv.*, vol. 4, no. 81, pp.

43155–43159, Sep. 2014.

[39] E. Cho, K. Song, M. H. Park, K. W. Nam, and Y. M. Kang, “SnS 3D Flowers with Superb Kinetic Properties for Anodic Use in Next-Generation Sodium Rechargeable Batteries,” *Small*, vol. 12, no. 18, pp. 2510–2517, May 2016.

[40] Y. Zheng, T. Zhou, C. Zhang, J. Mao, H. Liu, and Z. Guo, “Boosted Charge Transfer in SnS/SnO2 Heterostructures: Toward High Rate Capability for Sodium-Ion Batteries,” *Angew. Chemie - Int. Ed.*, vol. 55, no. 10, pp. 3408–3413, Mar. 2016.

[41] T. Zhou *et al.*, “Enhanced sodium-ion battery performance by structural phase transition from two-dimensional hexagonal-SnS2 to orthorhombic-SnS,” *ACS Nano*, vol. 8, no. 8, pp. 8323–8333, 2014.

[42] D. Chao *et al.*, “Array of nanosheets render ultrafast and high-capacity Na-ion storage by tunable pseudocapacitance,” *Nat. Commun.*, vol. 7, p. 12122, Jun. 2016.

[43] S. H. Choi and Y. C. Kang, “Aerosol-assisted rapid synthesis of SnS-C composite microspheres as anode material for Na-ion batteries,” *Nano Res.*, vol. 8, no. 5, pp. 1595–1603, May 2015.

[44] Y. Ren, J. Wang, X. Huang, and J. Ding, “Three-dimensional SnS2 flowers/carbon nanotubes network: Extraordinary rate capacity for sodium-ion battery,” *Mater. Lett.*, vol. 186, pp. 57–61, Jan. 2017.

CHAPTER 3: Material Processing & Characterization Techniques

3.1. Overview of Some Material Preparation Techniques Used for Anode Synthesis

There are variety of material preparation techniques which can be utilized to synthesize materials that can be used an anode material for NIBs. Some of them are solid state reaction method, electrospinning method, chemical vapor deposition (CVD) and hydrothermal method.

3.1.1. Solid State Reaction

Briefly, in stolid state reaction the solid precursor materials are mixed with each other to get the product. However, in order to overcome thermodynamic barrier that is faced by these precursor materials to react, materials are sintered between temperature range of 500 to 1500°C. For products to nucleate (1) the difference between initial structure of precursor and final structure of products should be less (2) structural reorganization should be less. Thus, the key ingredient is to homogenously mix precursors with a precise amount to maximize surface area of reactants.

3.1.2. CVD

CVD, is one of the most sophisticated technique to produce good quality high performance anode material and its schematic is shown in figure 3.1 [1]. In CVD, substrate which provide nucleation sites for growth of product is fed with single or more than single volatile precursor gas. These precursors at a very high temperature decompose and react with each other to form a uniform layer of product on substrate. This uniformity in obtained layer can be ascribed high degree of control and high deposition rate which is controlled by controlling gas flow rate.

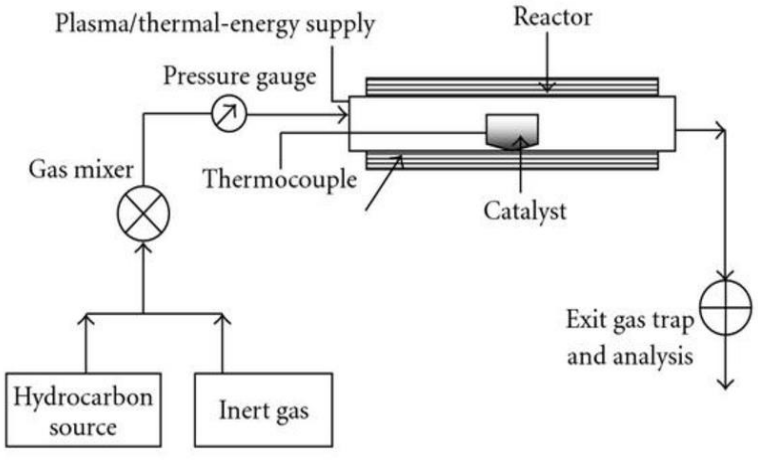

Figure 3.1 Schematic of CVD. [1]

3.1.3. Electrospinning Method

Electrospinning method is another way, which is a much simpler technique than CVD and it is used to deposit uniform fibers on the substrate (figure 3.2). It comprises of three main components (1) collector (2) injection spring (3) voltage supply [2]. A voltage difference is developed between collector and syringe, fiber comes out from the top of syringe and gets deposited on a collector due to this voltage difference. One can optimize this deposition technique by varying voltage, flow velocity and distance between collector and syringe needle

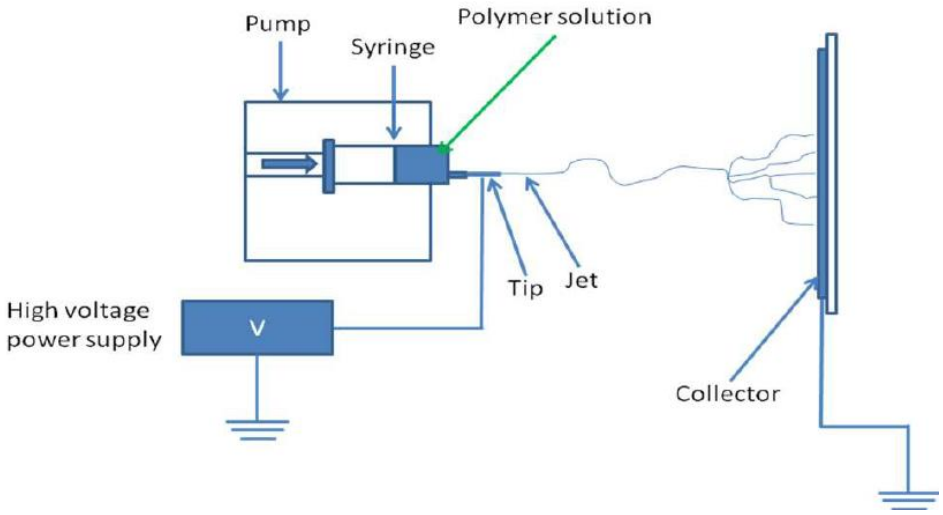

Figure 3.2 Schematic of Electrospinning. [2]

3.1.4. Hydrothermal/ Solvothermal Method

Hydrothermal/ solvothermal is another synthesis technique which is sued to synthesize electrode materials with tuned degree of crystallinity in a powder form in a relatively large quantity than CVD and electrospinning. In this technique, precursors are first homogenously mixed in a solvent which can be water in case of hydrothermal reaction or another liquid in case of solvothermal. After mixing homogenously, this solution is transferred into a Teflon cup which gets put into an autoclave to get sealed completely (figure 3.3) [3]. This autoclave is then heated to a high temperature for a specific amount of time to obtain the desired product. The vapor pressure generated inside an autoclave dictates the morphology. size and crystallinity of the product that we get which in turn depends on the precursor amount ratio, temperature that we set and time allowed for the reaction.

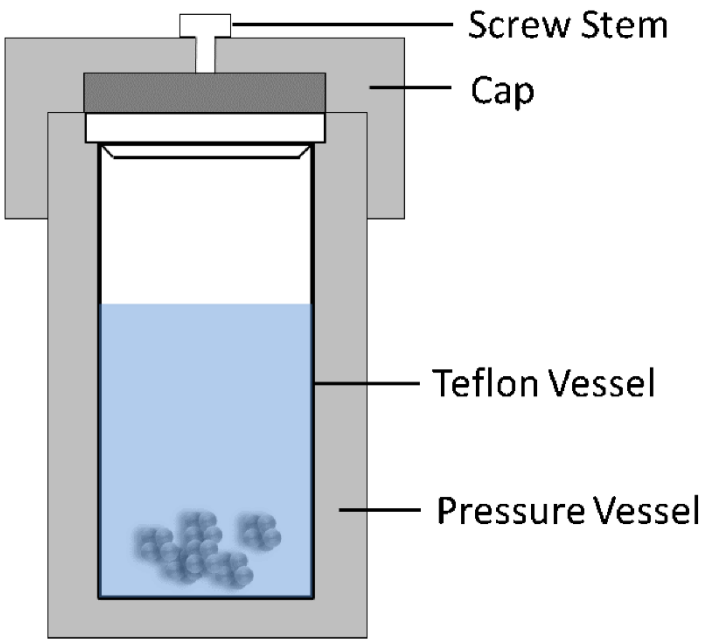

Figure 3.3 Teflon lined autoclave for hydrothermal/ solvothermal method. [3]

3.2. Materials Characterization

3.2.1. X-ray Diffraction (XRD)

Crystal structure and phase of as prepared materials are identified using XRD. In this technique, X-rays, produced through a Cu kα source is incident on prepared sample material. These X-rays diffract from crystal lattices of the material, comes back and produces constructive interference when these rays satisfy Bragg's law [4]:

$$n\lambda = 2d \sin\theta \quad \rightarrow \quad \text{equation (1)}$$

In equation (1), d is the interplanar spacing, θ is the Bragg's angle, n tells us about the order of reflection and λ is the wave length of incident X-rays. The XRD pattern of each material is different and they also different according to phases that they form. So, by comparing XRD pattern (JCPDS no) obtained sample electrode material with its reference sample pattern, we can identify our material accurately with its phase. The XRD equipment used for this thesis had a model D8 Advanced by Bruker and the schematic of its working principle is show in figure 3.4. It is to be noted that in a crystal lattice, each atom acts as a scattering point and all these points are coherent in nature thus, when an X-ray strikes these atoms they get diffracted

and when more than one X-ray get scattered from a coherent source and also satisfy Bragg's law condition, constructive interference in rays occur which detected by the detector. The intensity of the signal detected depends on the crystallinity of the sample i-e. for how long, a specific order of atoms in a sample is being maintained. Higher the range of order, higher will be the obtained intensity of the signal and vice versa.

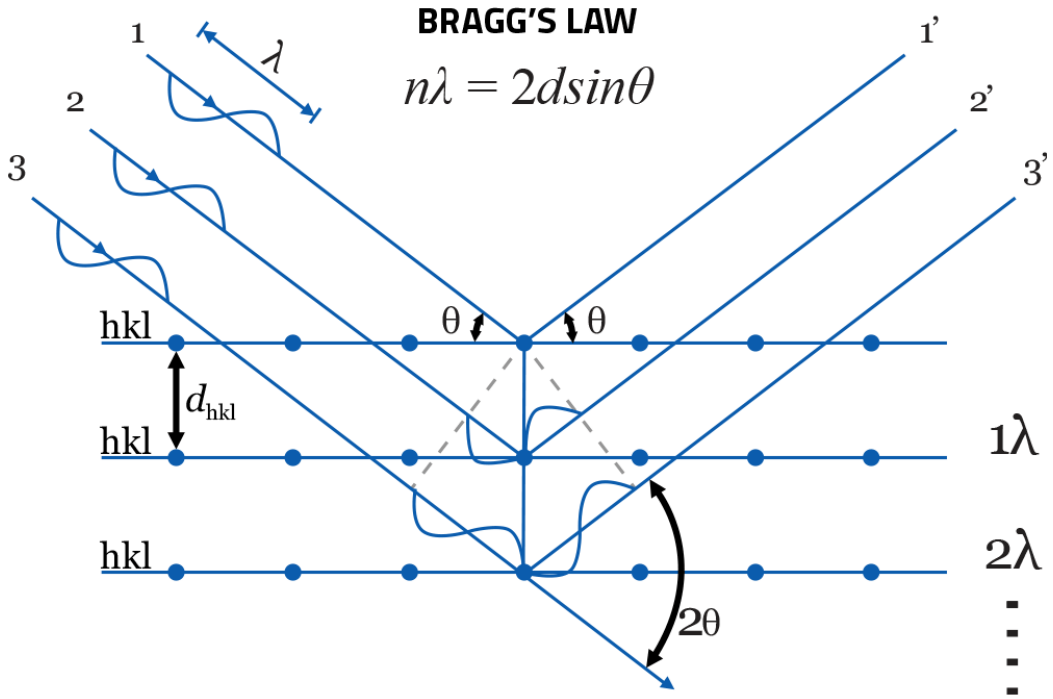

Figure 3.4 Schematic of XRD working principle. [4]

3.2.2. Scanning Electron Microscopy (SEM)

In order to identify the morphology and size of nano materials, SEM is utilized for it. SEM is a type of electron microscopy that utilizes high energy beam of electrons to analyse the sample in an ultrahigh vacuum [5]. These electrons with a high energy when gets bombarded on to the sample surface, it interacts with the atoms of the material and this interaction can either yield back scattered effect of secondary electron effect. In secondary electron effect, the primary electron beam strikes the electron of specimen atom and yields an electron from its valance band through inelastic collusion. This emitted electron is detected through a secondary electron detector and detector converts electrical signal into the form of an image which is viewed on the screen. In back scattered effect, primary beam of electron gets scattered back through an

elastic collusion from the specimen atoms. Back scattered effect is mostly used to study heavy elements as we get a white and black contrast difference (white representing heavy atom, dark representing light atom). Thus, SEM is mainly used to identify surface morphology of electrode materials as the atoms which interact with primary beam of electrons are present at a few nanometer distance from the base of sample and the equipment that was used for this thesis had a model VEGA 3 LMU by TESCAN. The schematic of its working principle is shown in figure 3.5.

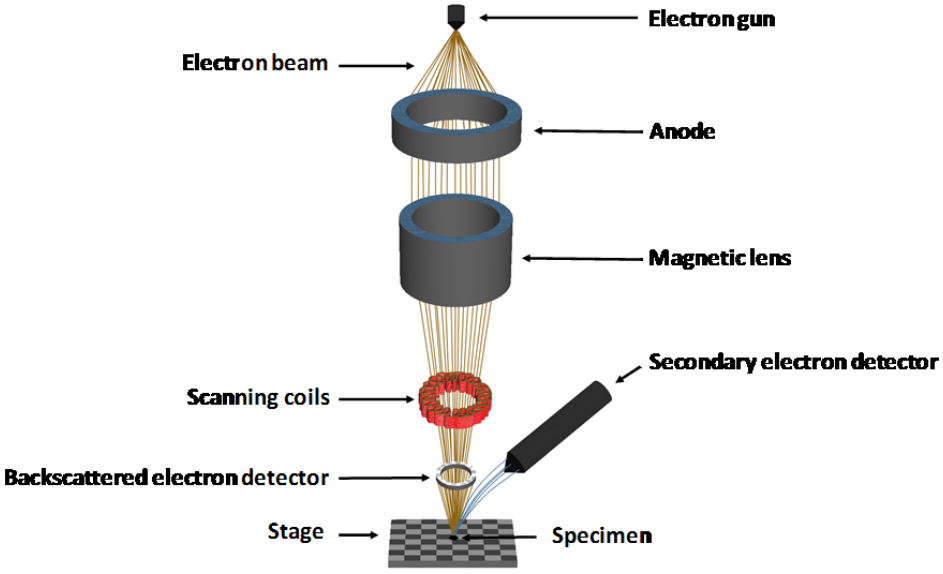

Figure 3.5 SEM working principle. [5]

3.2.3. Thermogravimetric Analysis (TGA)

TGA is a technique which is used to measure changes that occur in a sample physically or chemically when they are heated at a constant rate. These changes are measure according to reference sample which is also heated to a high temperature at a constant rate thus, all the changes that take place in the sample electrode material is measured relative to the sample present in the reference pan [6]. In batteries, we require TGA result to measure the accurate amount of active material that is present our nanocomposite or hybrid material or to estimate the amount of impurities that are present in the sample. The equipment that is used for this purpose had a model DTG-60/60H and its schematic is shown in figure 3.6.

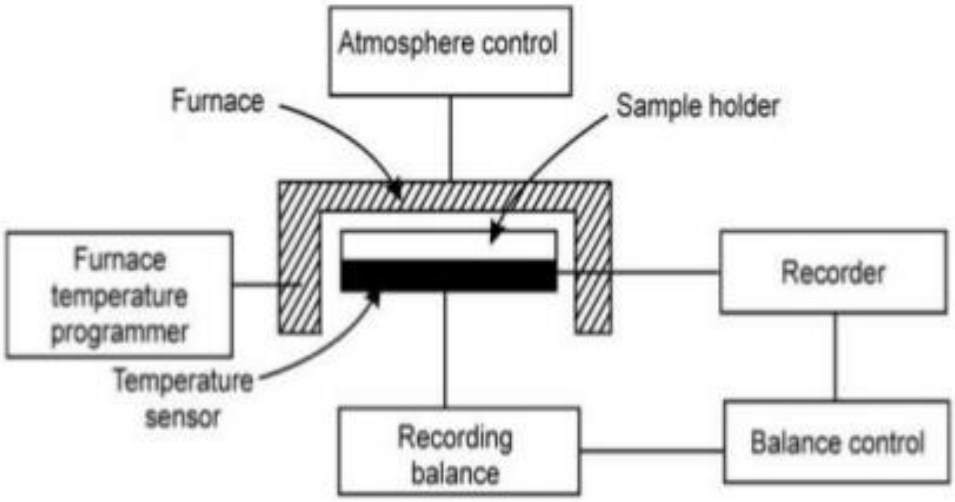

Figure 3.6 TGA working principle. [6]

3.2.4. Fourier Transform Infrared Spectroscopy (FTIR)

To obtain emission and absorption spectrum of a sample, FTIR is utilized for it which can be done for solid, liquid or gas samples. It collects a spectral absorption or transmission spectrum over a wide range of wavelength. To achieve that, a monochromatic light is radiated on the sample and we observe how much of that light gets absorbed or emitted, and then this process is continued for a large number of wavelengths. Each material has the capability to absorb or emit light of a specific wavelength which is governed by the types of covalent bonds that are present in it. Each covalent bond is associated with definite bond bending and bending stretching. The later one comprises of asymmetric or symmetric vibrations meanwhile, the bending vibrations in it is usually classified as high energy vibrations. However, when it comes to limitations, the FTIR characterization technique only detects those polar bonds which are infrared active i-e. which can absorb infrared radiations. Thus, in turn this technique is usually utilized to analyze the type of covalent bonds that are present in out electrode material.

While analyzing data obtained from FTIR, at vertical axis we can take either absorption or transmittance intensity vs IR frequency, indicated in term of wavenumber (cm^{-1}) which can vary from 650 to 4000 cm^{-1} for a model Agilent Cary 360. The transmission or absorption intensity in infrared spectra depends on how strong is the dipole moment of the polar bond which is detected. Thus, for bonds which are highly polar in nature show strong

absorption/transmittance intensity band. Similarly, for medium intensity band is observed for medium polar bond and low intensity band is observed for weakly polar bond. The schematic of FTIR is shown in figure 3.7.

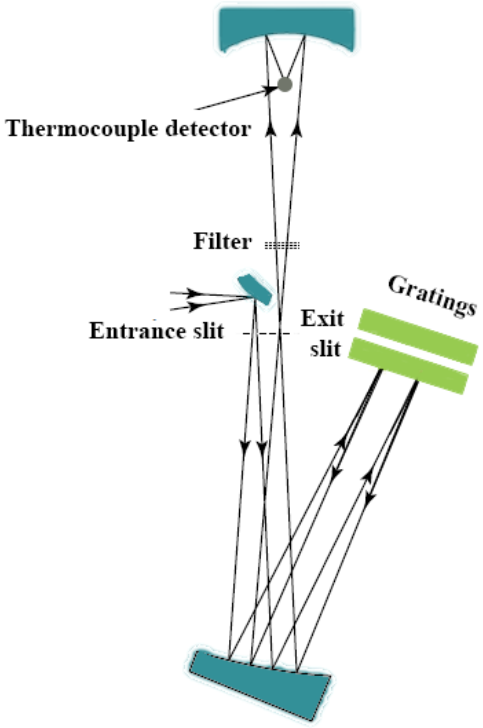

Figure 3.7 FTIR schematic

3.3. Electrode Fabrication and Assembly

3.3.1. Electrode Preparation

To fabricate a coin cell, we need to prepare an electrode. To synthesize that, firstly, the active material is mixed homogeneously with conductive agent and a binder in a specific ratio. The slurry of these three materials is prepared afterward in a solvent in such a way that it has enough viscosity to stick to the surface and not flow freely which is usually analyzed through naked eye. Then this slurry is coated on to a current collector foil by using a doctor blade process and throughout this process it is made sure that thickness of coating should be kept around a constant range. Following this, the coated foil is dried afterwards in a vacuum overnight to evaporate the solvent present in it. During drying process, the coating shrinks and some wrinkles can create on the surface due to which the foil is passed through a roller which presses it to remove non-uniformities present on the surface. To convert it into a electrode shape, the

coated collector foil is punched through a 16 mm diameter to get an electrode disc which is then stored in a glove box for coin cell preparation.

3.3.3. Coin Cell Assembly

CR 2032-coin cell assembly is usually carried out in an Ar filled glove box because of high reactivity of sodium and lithium. To synthesize a coin cell, firstly an active electrode i-e anode pasted on a current collector foil is place on a larger cap end (with a + sign) which is covered with a porous separator. Then few drops of electrolyte are dropped on a porous separator which also wets the electrode disc. On the separator, the cut sodium disc is placed which also comes in contact with the electrolyte. On top of sodium disc, a stainless-steel spacer is attached followed by an O-ring which keeps the component of cell in a required shape [7]. This whole is assembly is then placed on a crimper which seals the electrode to carry out further electrochemical analysis. The schematic of coin cell assembly is shown in figure 3.8.

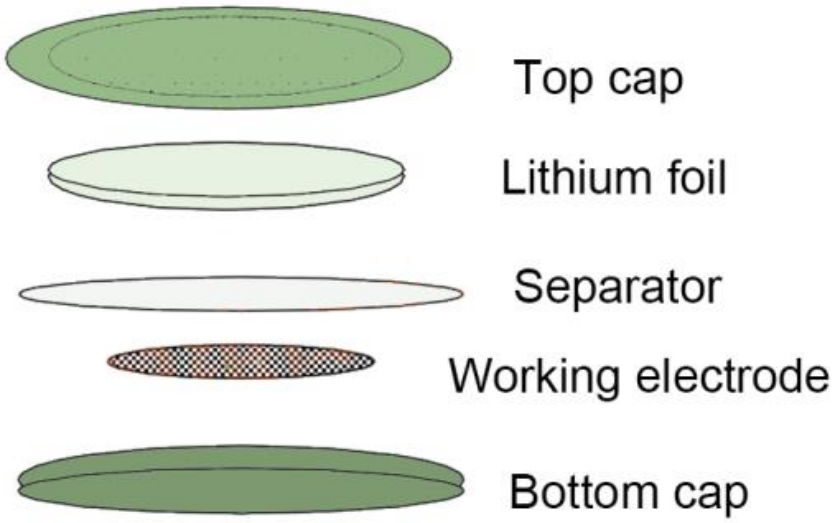

Figure 3.8 Coin cell assembly. [7]

3.4. Electrochemical Characterization

3.4.1. Galvanostatic Charge/Discharge Analysis

To analyse the cyclic life of a coin cell in this thesis, charge discharge analysis is carried out on 8-channel battery analyser test station at a constant current mode. To do that, coin cell connected to the positive and negative terminal of test station accordingly and through a software, constant current mode is selected. In this mode, current in amperes is given according

to the weight of active material and starting as well as cut-off voltage is given. This process is repeated for as many numbers of cycles as desired and this is how cyclic life of an is analysed. The capacity of a cell given during charge/discharge can be calculated as

$$Q = I \times t \quad \rightarrow \quad \text{equation (2)}$$

Where 't' in equation (2) is the time take by a cell to fully charge/discharge while 'I' is the current density given to the cell (according to its active material weight), at which it is charged or discharged. When determining rate capability of a cell, we change current density that is given to a cell after specific number of cycles and a capacity/cycle graph is obtained as a result.

3.4.2. Cyclic Voltammetry (CV)

Cyclic voltammetry (CV) is another technique which is utilized in this thesis to find out the electrochemical reactions that are taking in our anode material during charge/discharge process. A graph is obtained between current and voltage at a specific scan rate, which is usually kept low (in mV/ S). In a graph we will obtain several peaks which corresponds to oxidation and reduction phenomenon that are occurring within the cell during charge/discharge. Thus, cyclic voltammeter gives information about electrochemical reactions that are occurring in a coin cell having novel electrode materials. To connect a coin cell with an electrochemical workstation (CHI 660E), the counter and reference electrode of workstation is connected to that end of cell which has sodium foil present as sodium can act as both counter and reference electrode. The working electrode of workstation (schematic 3.9 (a)) is connected to the active anode material end of the cell and thus we get redox peaks of reactions that are occurring in a cell during cycling phenomena [8]. When a potential is given between working electrode and reference electrode, a current is obtained as a result which is monitored.

3.4.3. Electrochemical Impedance Spectroscopy (EIS)

Another technique which aids in studying the electrochemical performance of a cell is EIS which gives a deeper insight about phenomenon that are occurring in a cell. In this technique, which is also carried out on same electrochemical workstation (figure 3.9), we measure the internal resistance of a cell [8]. A Nyquist plot is obtained at a constant voltage within a frequency range which is usually given between 100kHz to 10 mHz. In Nyquist plot, we obtain two semi circles at a high and mid frequency range corresponding to electrode interface resistance that sodium ions face during discharging or charging and a linear tail corresponding to Warburg impedance which tells about sodium ion diffusion constant. At a very high

frequency of the plot, the spectrum obtained gives information about resistance shown by metallic wire or connections because of its inductive behaviour, while part of the spectrum where first semi-circle forms at a high frequency range tells us about ohmic resistance present in a cell (active material, electrolyte and separator). Second semi-circle at mid-frequency range corresponds to charge transfer resistance and a linear tail afterwards corresponds to diffusion processes.

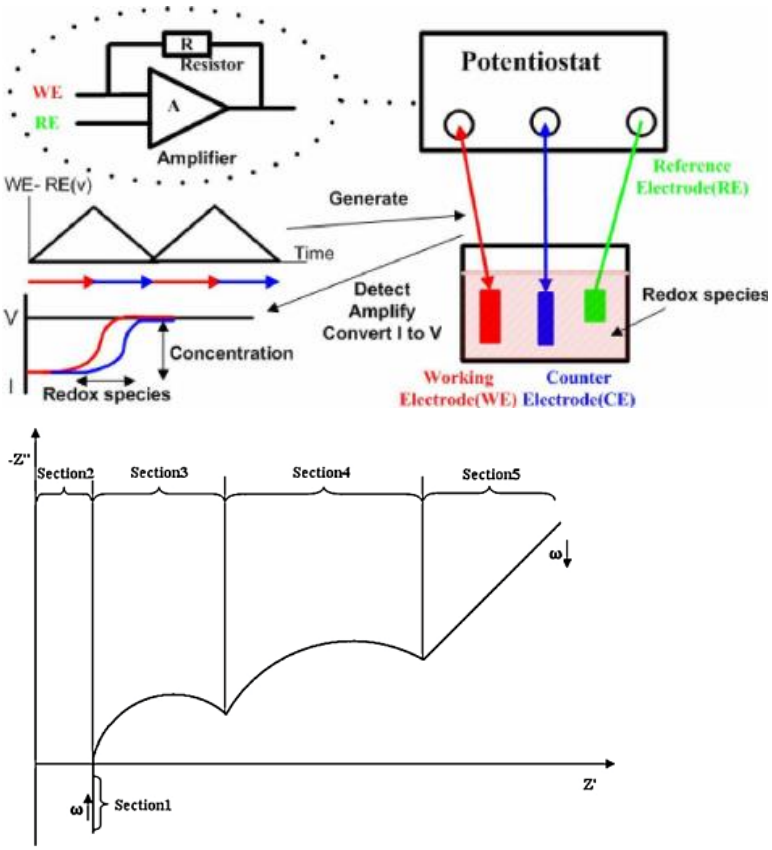

Figure 3.9 (a) Schematic diagram of CV (b) EIS Nyquist plot schematic. [8]

3.5. Summary

In this chapter, various electrode synthesis techniques have been discussed along with their advantages among them, solvothermal technique will be used to synthesize electrode material for this thesis as we can tune crystallinity of a material in it as well as being able to synthesize in large quantity. The as prepared material has to be characterized structurally, morphologically and electrochemically. For this technique such as XRD, SEM, TGA and FTIR are discussed. In XRD, we can analyse the material structure and phase which is synthesized, while SEM gives information about its morphology and size of particles etc. TGA analyses the amount of impurities or the amount of active material which is present in our sample while FTIR can give

us covalent bonding analysis. Electrochemically, galvanostatic charge/discharge analysis tells us about electrode cyclic life, CV give information the redox reactions that are occurring in our cell and EIS provide analysis about the internal resistance that sodium ion faces while from anode to cathode or vice versa.

3.6. References

[1] "(PDF) Role of Reaction and Factors of Carbon Nanotubes Growth in Chemical Vapour Decomposition Process Using Methane—A Highlight." [Online]. Available: https://www.researchgate.net/publication/44849850_Role_of_Reaction_and_Factors_of_Carbon_Nanotubes_Growth_in_Chemical_Vapour_Decomposition_Process_Using_Methane-A_Highlight. [Accessed: 21-Feb-2020].

[2] "Effect of Poly(vinyl alcohol)/Chitosan Ratio on Electrospun-Nanofiber Morphologies | Scientific.Net." [Online]. Available: https://www.scientific.net/AMR.463-464.734. [Accessed: 21-Feb-2020].

[3] G. Yang and S. J. Park, "Conventional and microwave hydrothermal synthesis and application of functional materials: A review," *Materials*, vol. 12, no. 7. MDPI AG, p. 1177, 11-Apr-2019.

[4] Q. Shen, Z. Liu, Y. Hua, J. Zhao, W. Lv, and A. Mohsan, "Effects of Cutting Edge Microgeometry on Residual Stress in Orthogonal Cutting of Inconel 718 by FEM," *Materials (Basel).*, vol. 11, no. 6, p. 1015, Jun. 2018.

[5] C. Suryanarayana, "Microstructure: An Introduction," Springer, Singapore, 2017, pp. 105–123.

[6] R. J. Longbottom *et al.*, "2) Bragg Institute, Australian Nuclear Science and Technology Organisation," *ISIJ Int.*, vol. 56, no. 9, pp. 1–6, 2016.

[7] C. Liu and L. Liu, "Optimal Design of Li-Ion Batteries through Multi-Physics Modeling and Multi-Objective Optimization," *J. Electrochem. Soc.*, vol. 164, no. 11, pp. E3254–E3264, Jan. 2017.

[8] D. Li, K. Xu, J. Wang, Z. Ye, Y. Ying, and Y. Li, "Quartz Crystal Au Electrode-Based Electrochemical Immunosensor for Rapid Detection of Escherichia coli O157:H7," *Trans. ASABE*, vol. 51, no. 5, pp. 1847–1852, 2008.

CHAPTER 4: Experimentation

4.1. Material Synthesis:

Thiourea, $Sncl_2.2H_20$ and ethylene glycol of analytical grade was purchased from Sigma-Aldrich (USA). Nitric acid (67% conc.) was obtained from Merck (USA) and CNTs with a diameter of 30-60 nm were attained from NESCOM (Pakistan). Conductive agent such as carbon black, and poly(vinylidene fluoride) binder was purchased from MTI Corporation (USA). n methyl-2-pyrrolidone, was bought from RCI Labscan (Thailand) and the electrolyte used to prepare cell was procured from Xiamen TOB New Energy Technology (China).

4.2. Functionalization of CNTs

It is important for CNTs to be functionalized and to achieve that, CNTs were added in a beaker containing 40% nitric acid solution and was stirred at 110°C for 2 hours [1]. Afterwards CNTs were removed from this solution and to extract left over acid from nanotubes, functionalized CNTs were washed with deionized water and acetone till its pH reaches to near 7. The product obtained was dried in a vacuum oven at 80°C for 12 hours to remove any solvent present in it

4.3. Synthesis of Co-doped of CNTs (NS- CNTs)

Functionalized carbon nanotubes were then doped with both nitrogen and sulfur atoms. To achieve that firstly, 60 ml of ethylene glycol was taken in a 100 ml beaker and in it, 0.152 g of thiourea was added, which acts as a source of both sulfur and nitrogen atoms [2, 4]. Then 0.05 g of as obtained functionalized CNTs were taken and added to the above solution of thiourea in an ethylene glycol. The solution was stirred for 30 minutes followed by ultrasonication procedure. This was done to get a uniformly dispersed, homogenous solution of CNTs, thiourea and ethylene glycol, which was transferred to an autoclave having maximum capacity of 100 ml. The autoclave was kept at 180°C for 12 hours which gives enough time for thiourea to dissociate, release nitrogen and sulfur atoms that gets doped in CNTs. The Nitrogen, sulfur co-doped CNTs (NS-CNTs) product was washed with both deionized water and acetone to remove the ethylene glycol solvent from it. It was then dried in a vacuum oven at 60°C for 12 hours.

4.4. Synthesis of co-doped SnS/CNTs Nanocomposite (NS-SnS/CNTs)

To synthesize NS-SnS/CNTs nanocomposite, 0.75 g of thiourea and 0.145 g of $SnCl_2.2H_2O$ was added into two different beakers having 30 ml ethylene glycol each [5]. Solutions in both beakers were stirred for 30 minutes each and then both solutions were mixed with each other. To this solution, having 60 ml ethylene glycol now, 0.05 g of NS-CNTs was added and after stirring it for 30 minutes, it was ultrasonicated for 1 hour. When the homogenous mixture was obtained, the solution was then transferred to an autoclave of 100 ml capacity and was kept at 180°C for 24 hours. After heating of 24 hours, the autoclave was allowed to cool naturally to a room temperature and the product obtained was washed repeatedly with deionized water and acetone to remove ethylene glycol solvent from it and to completely remove any solvent present, it was dried at 60°C for 12 hours. The product that obtained from the reaction was NS-SnS_2/CNTs and to synthesize NS-SnS/CNTs, it was annealed at 400°C for 1 hour with a ramp rate of 2°C/ min so that it doesn't affect the microstructure and morphology of the samples. During annealing, phase transformation occurs and NS-SnS_2/CNTs convert into NS-SnS/CNTs and this whole procedure for better understanding is explained schematically in figure 4.1. To synthesize pure SnS and SnS/CNTs, it follows the same mechanism as described above except for the fact that CNTs were not added when pure SnS was being synthesized and CNTs were

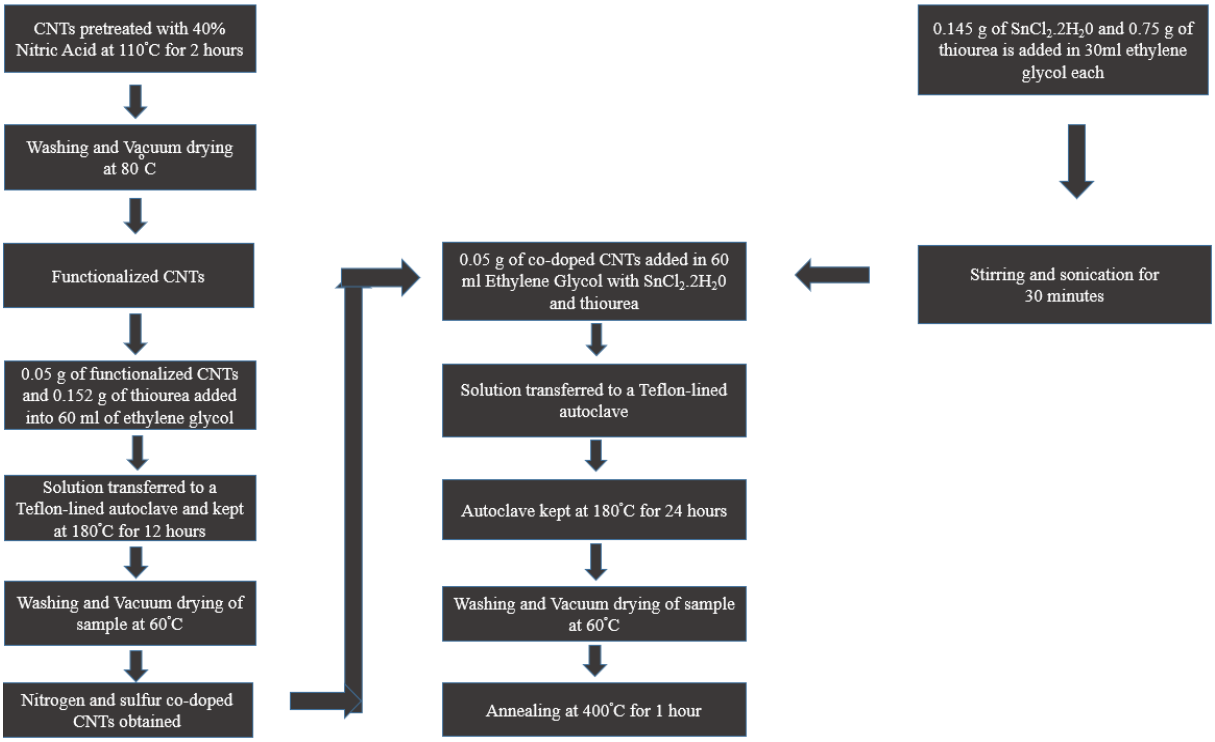

Figure 4.1 Schematic of NS-SnS/CNTs synthesis

not co-doped with nitrogen and sulfur atoms when SnS/CNTs sample was being prepared, which is also explained schematically in figure 4.2 and 4.3.

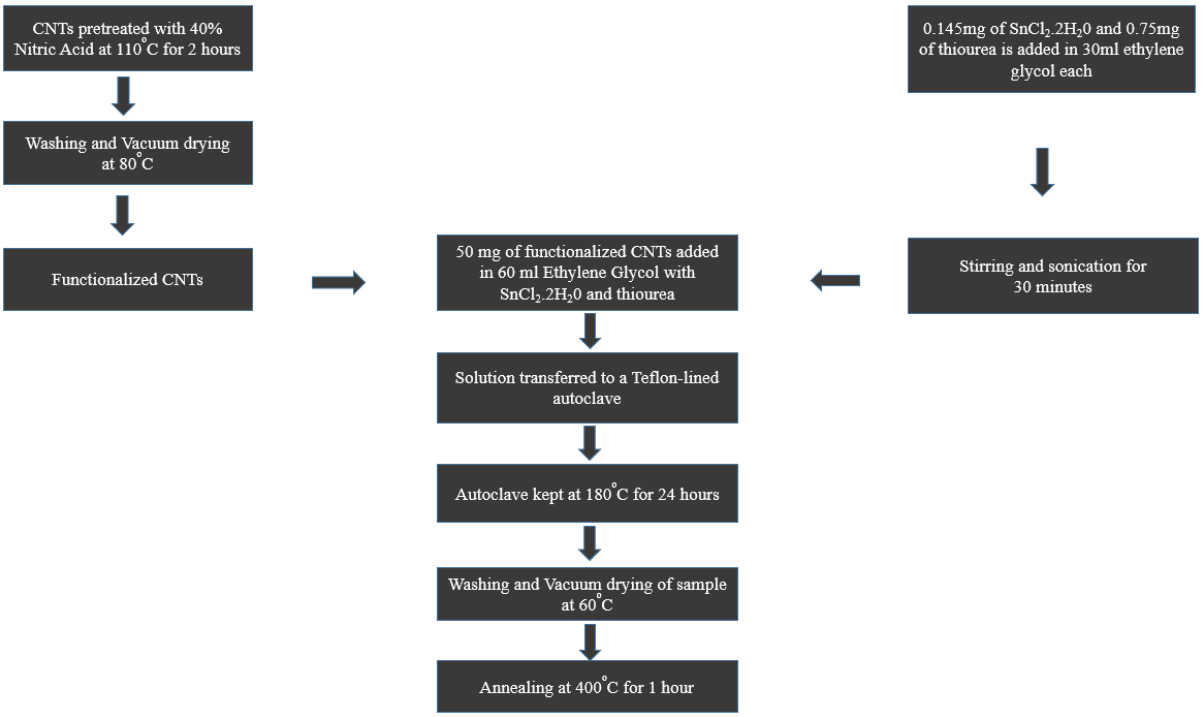

Figure 4.2 Schematic of SnS/CNTs synthesis

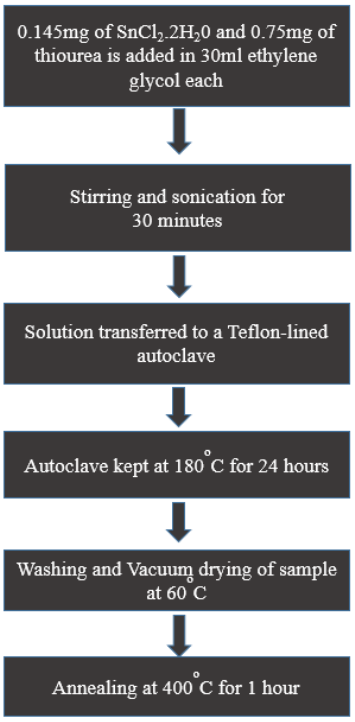

Figure 4.3 Schematic of SnS synthesis

4.5. Coin Cell Fabrication

To fabricate coin cell for electrochemical performance analysis, CR-2032 cells was prepared in a glove box under standard operating conditions. To synthesize this cell, firstly we require a working electrode which was synthesized by making a slurry of active materials which were prepared. For slurry preparation, a homogenous mixture of (poly(vinylidene fluoride) binder, carbon black conductive agent and active material in N-methyl pyrrolidinone (NMP) is required at a weight % of 80:15:5. This homogenous slurry was applied to a copper foil (for anode) by using doctor blade technique and it was made sure that coating prepared was also homogenous in nature. The foil was dried instantly after this at 80°C to remove wet NMP and it was vacuum dried at 80°C for 12 hours to completely remove NMP. During drying process, the coating could shrink due to removal of solvent and to overcome this shrinkage, the foil was passed to a roller several times which also removes any wrinkles that might have formed at the surface of coating. Then 16 mm electrode discs were prepared by using a puncher of same diameter and these discs were transferred to a glove box where coin cell is assembled. To

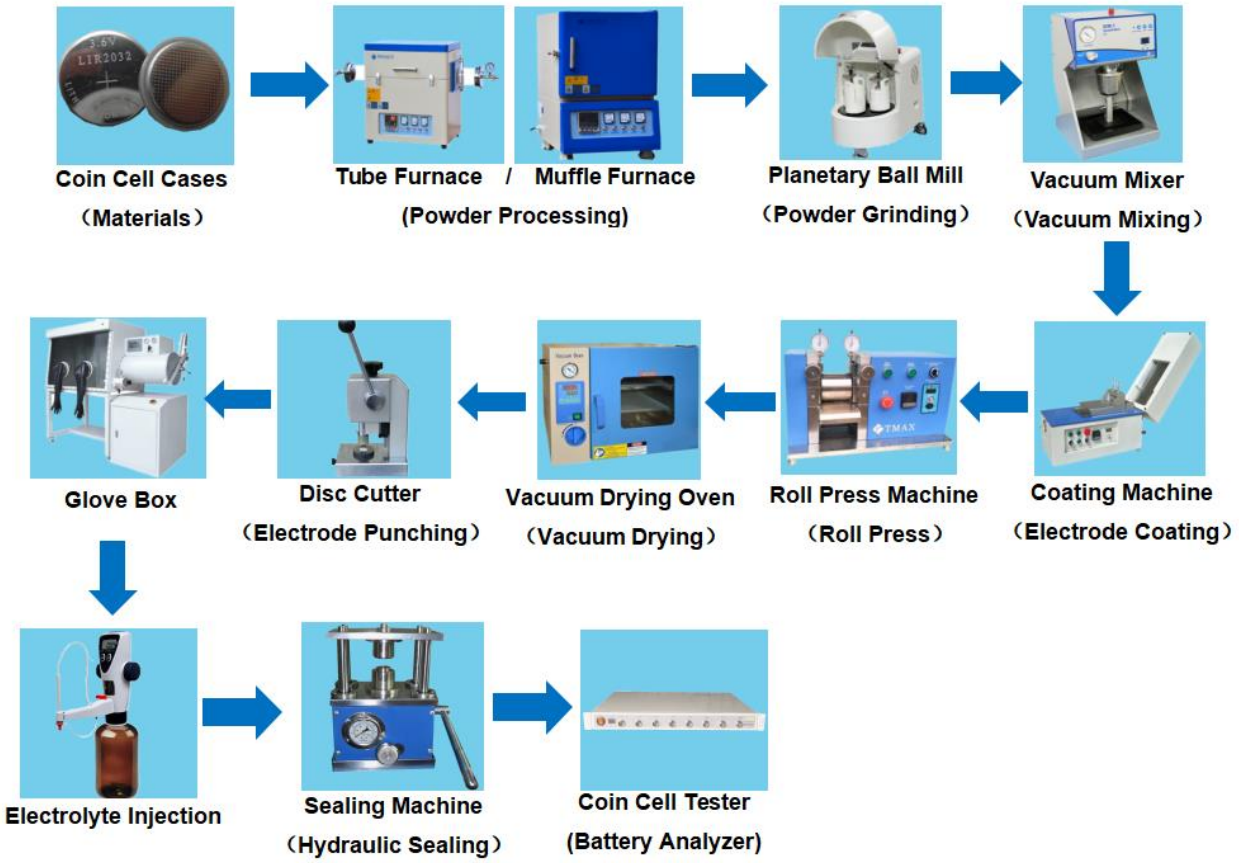

Figure 4.4 Schematic of coin cell fabrication line

assemble a coin cell, working electrode was place at one end of the disc which is covered by a polypropylene sheet separator so that cell might not get short circuited when sodium is placed on top of it, which acts as both counter and reference electrode. On that separator, few drops of electrolyte (1 M $NaClO_4$ in a (1:1) volume mixture of ethylene carbonate/dimethyl carbonate having 5 wt.% fluoroethylene carbonate in it) were added thus allowing sodium ions to migrate from one electrode to another. Then the cell was crimped by using a high-pressure crimper and this completely seals the components of cell, which is shown in the schematic of coin cell fabrication line (figure 4.4). To analyse electrochemical performance, 8-channel battery analyser was used for sodiation/ desodiation cycle analysis and CV was used for studying the redox behaviour of anode at a scan rate of 0.1 mV/ s. To analyze the kinetic of reaction, EIS was performed within a frequency range of 100 kHz and 0.1 Hz.

4.6. Summary

To improve the electrochemical performance of sodium ion battery anode materials, different active materials including SnS, SnS/CNTs and NS-SnS/CNTs were prepared by using a solvothermal reaction technique. For co-doping procedure, the only difference is that CNTs had to go through a solvothermal reaction with thiourea in it, to get sulfur and nitrogen atoms doped in CNTs. After structural and morphological characterization, as prepared anode materials were analysed electrochemically by synthesizing a coin cell after creating electrode disc. Battery analyser was required for cyclic life analysis, while CV and EIS were important in studying the electrochemical reactions that might occur in a cell and resistance shown by cell during charge transfer.

4.7. References

[1] S. Zhang, L. Yue, H. Zhao, Z. Wang, and J. Mi, "Mwcnts wrapped flower-like SnS composite as anode material for sodium-ion battery," *Mater. Lett.*, vol. 209, pp. 212–215, 2017.

[2] M. Wang *et al.*, "SnS Nanosheets Confined Growth by S and N Codoped Graphene with Enhanced Pseudocapacitance for Sodium-Ion Capacitors," *ACS Appl. Mater. Interfaces*, vol. 11, no. 44, pp. 41363–41373, 2019.

[3] J. Xiong *et al.*, "N/S Co-doped carbon derived from cotton as high performance anode materials for Lithium ion batteries," *Front. Chem.*, vol. 6, no. APR, pp. 1–9, 2018.

[4] L. Fan *et al.*, “Promising Dual-Doped Graphene Aerogel/SnS2 Nanocrystal Building High Performance Sodium Ion Batteries,” *ACS Appl. Mater. Interfaces*, vol. 10, no. 3, pp. 2637–2648, 2018.

[5] S. Mohebbi, S. Mikaeily, and A. R. J. Azar, “Cauliflower-like tin sulphide nanoparticles: An amazing material for adsorption of methylene blue dye,” *Micro Nano Lett.*, vol. 10, no. 4, pp. 220–223, 2015.

CHAPTER 5: Results and Discussion

Schematically, the synthesis of NS-SnS/CNTs by using solvothermal route is shown in figure 5.1. As illustrated, nitrogen and sulfur doping in CNTs was carried out by using thiourea as a dopant source, which was added in a stochiometric amount. During solvothermal reaction, high temperature and high-pressure breaks thiourea, which releases nitrogen and suflur atoms. These atoms because of enough reaction time diffuses into carbon nanotube walls and makes a covalent bond there. NS-CNTs formed along with thiourea was used a precursor for next solvothermal reaction and to that, $SnCl_2.2H_2O$ was also added. $SnCl_2.2H_2O$ at high pressure and temperature releases Sn^{+4} ions which makes a bond with S^{-2} ions that were released by thiourea and forms SnS_2. However, the growth of SnS_2 here takes place on CNTs whose wettability was improved by heteroatoms doping. CNTs with improved wettability can allow more nucleation sites for SnS_2 to grow and this results in development of amorphous structure in NS- SnS_2/CNTs but with a morphology of cauliflower like, which also remain same in other samples because of stochiometric concentration of precursors that were used. NS- SnS_2/CNTs was annealed for one hour at 400°C, which is above its phase transformation temperature and we get NS- SnS/CNTs [1].

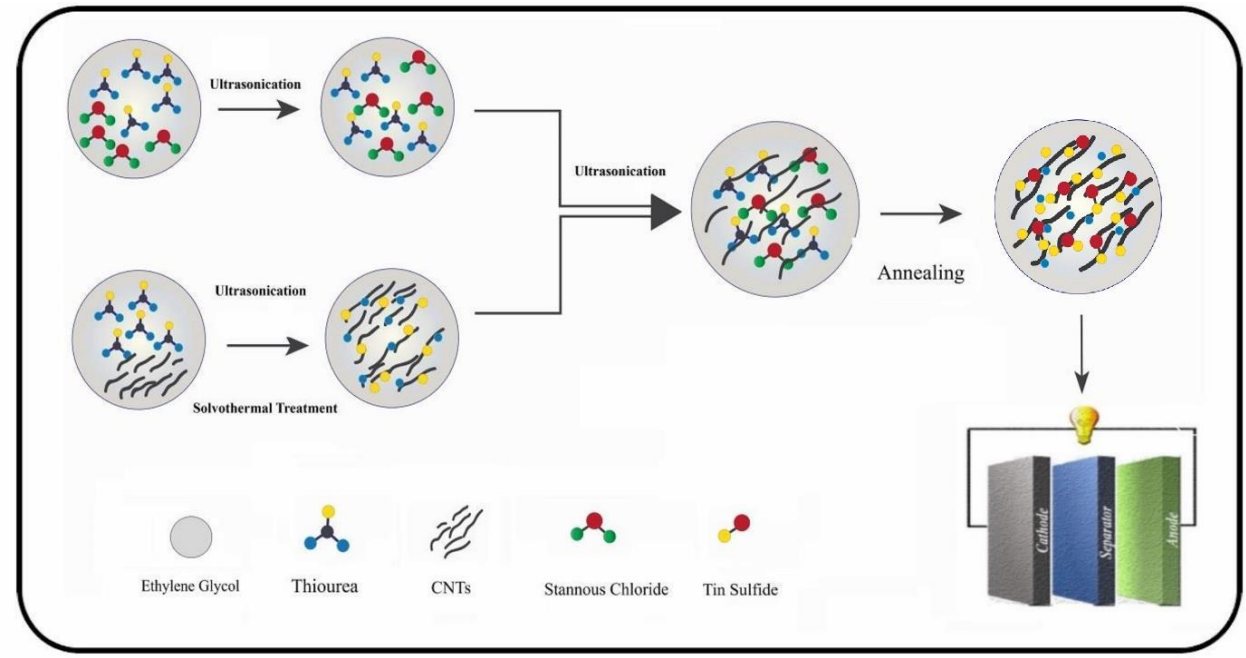

Figure 5.1 Proposed growth mechanism of NS-SnS/CNTs

5.1. Structural Characterization

5.1.1. X-Ray Diffraction Analysis

Figure 5.2 shows XRD pattern for NS-SnS/CNTs, SnS/CNTs and SnS. The XRD pattern for all 3 samples can be indexed to JCPDS 39-0354 which shows that lattice constants of SnS i-e. a, b and c are 4.32, 11. 19, and 3.98 nm respectively. As can be observed from the graph, CNTs exhibits a wide pattern of diffraction at $2\theta = 26^{\circ}$ and 42° having lattice index of (002) and (001) respectively and for those samples in which nanocomposite was made with SnS, the peak of CNT at 26° overlaps with a peak of SnS at plane (120). However, as compared to SnS/CNTs, NS-SnS/CNTs shift in 2θ values of both CNTs peak to a lower angle. At 26°, this peak shift can be due to the presence of carbon-nitrogen bond which is shorter that carbon-carbon bond that CNTs previously had before doping while at 42°, it can be because to increase in lattice spacing of CNTs due to addition of nitrogen and sulfur atoms as a dopant [2]. Moreover, the presence of doping atoms increases available nucleation sites for SnS to grow which reduces crystallite size of NS-SnS/CNTs to 20 nm from 22 nm (for SnS/CNTs) and this reduction in size, which can be identified by broad pattern in XRD, forces NS-SnS/CNTs to develop more of an amorphous type nature as compared to its counterpart samples.

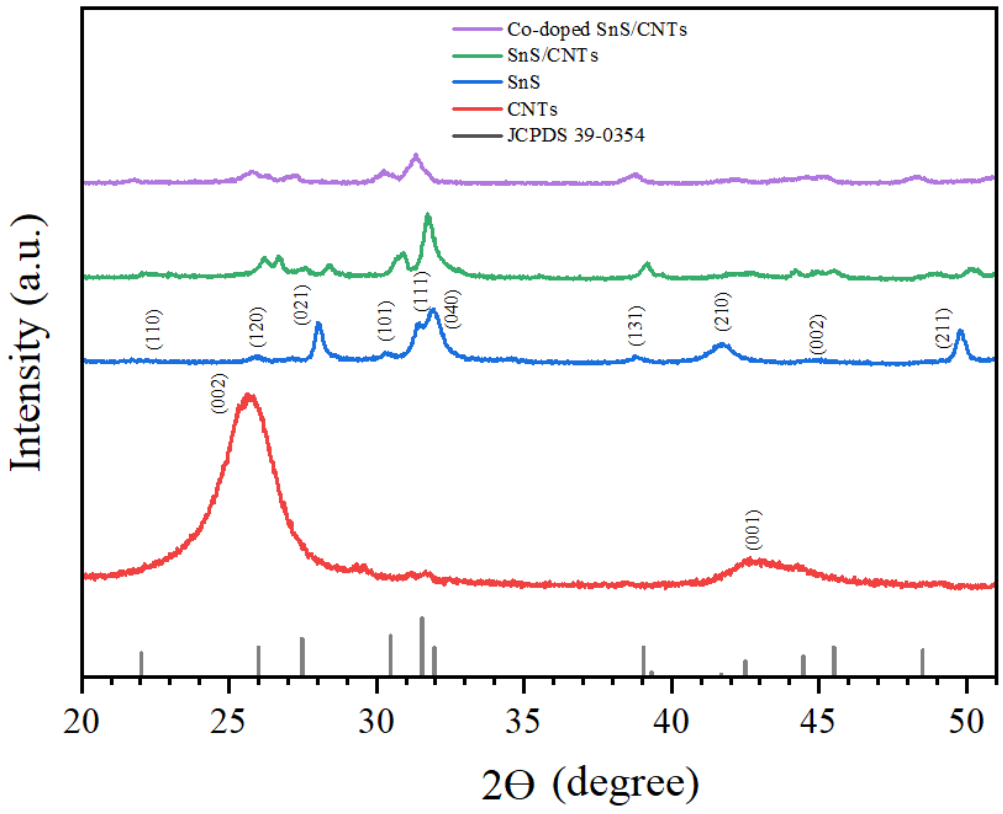

Figure 5.2 XRD peaks of active materials for NIBs

5.1.2. SEM Analysis

SEM image of as prepared samples show cauliflower like morphology (figure 5.3) which was achieved by controlling Sn to S ratio as well as temperature and time. Figure 5.3a show SEM of CNTs which show a diameter in the range of 30-60 nm, and when were introduced into cauliflower like SnS, it connects them together and form a framework (5c and 5d). This is because length of CNTs is larger than the diameter of SnS. The framework of CNTs and SnS improves their conductivity by providing a shorter pathway for sodium ion to diffuse from anode to cathode [3]. This improvement in conductivity can also be confirmed from impedance spectra results of nanocomposites. By analyzing SEM images of all samples, it was found that introduction of CNTs reduces thickness of nanosheet of SnS from 65 nm to 45 nm for SnS/CNTs. This reduction in thickness of nanosheet increases further to 39 nm for NS-SnS/CNTs because of heteroatoms introduction, which backs the result of reduction in crystallite size of SnS for doped sample in XRD.

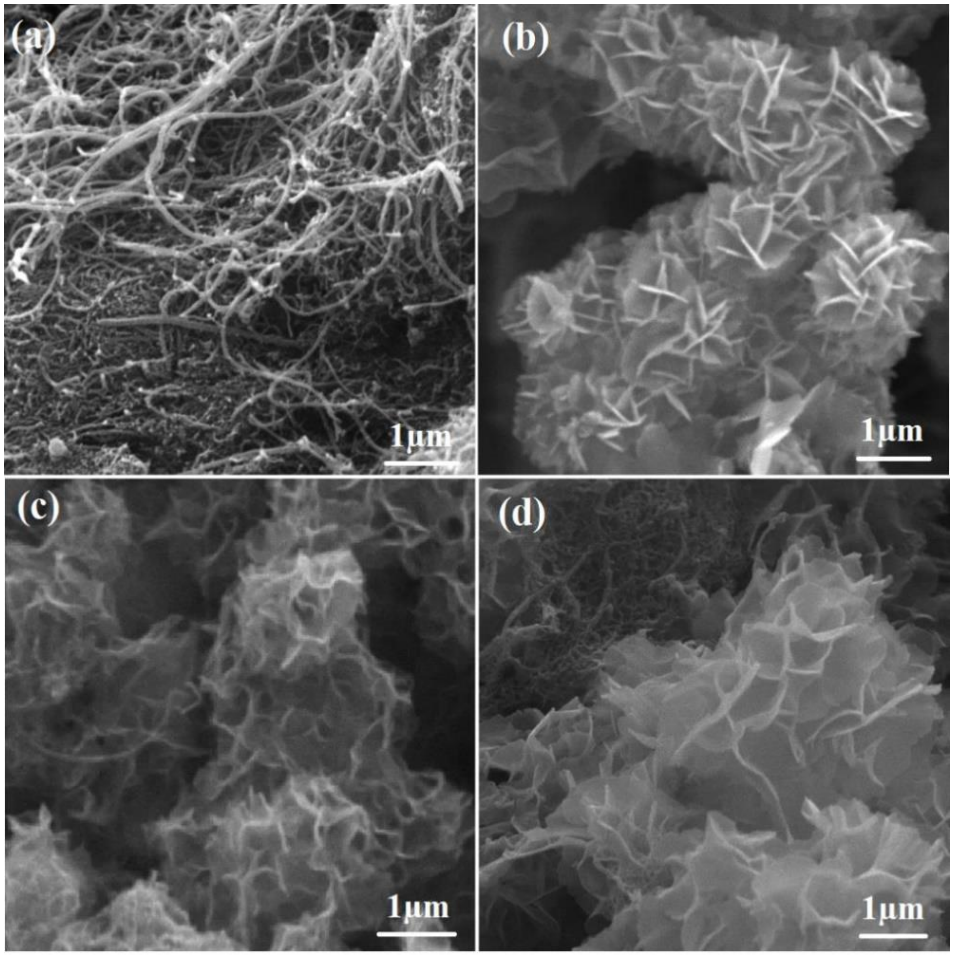

Figure 5.3 SEM images of (a) CNTs (b) SnS (c) SnS/CNTs (d) NS-SnS/CNTs

5.1.3. TGA

Thermogravimetric analysis was carried out to determine the weight% of each component in the sample and it can be seen in figure 5.4. While analysing the curves obtained for SnS/CNTs and NS-CNTs, two major region of weight losses were observed. First was from the temperature it starts to 400°C which is because of removal of adsorbed water molecules and organic residues. The curve from 450°C to 800°C show weight loss because of removal of carbon nanotubes from both composites as the carbon in them forms CO or CO_2 and gets removed as a gas leaving only SnS behind. After calculating, the content of CNTs in NS-SnS/CNTs amounts to 42% while the other nanocomposite showed 38 wt% of CNTs. Overall, it was observed that nanotube content was higher than previously reported which plays an important role in reducing charge transfer resistance of sodium ions during cycling process [4].

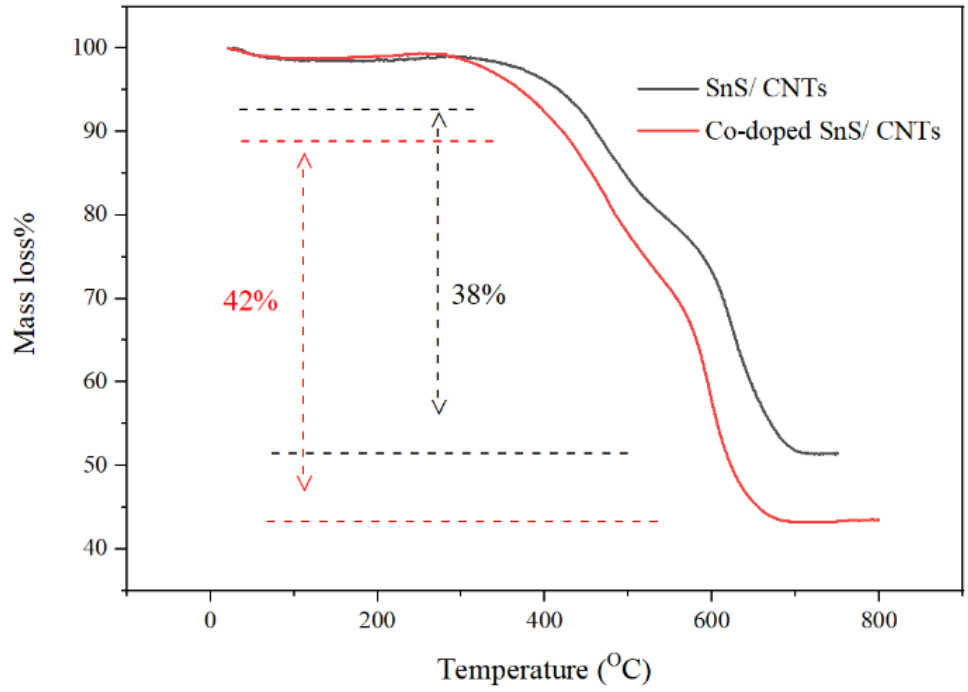

Figure 5.4 TGA of (a) SnS/CNTs (b) NS-SnS/CNTs

5.1.4. FTIR Analysis

FTIR spectrum obtained within the range of wavenumber 650-4000 cm^{-1} for synthesized samples are shown in figure 5.5. SnS show a typical band at 1040 cm^{-1} and 2350 cm^{-1} while the spectrum of CNTs can be seen from 1100 to 1200 cm^{-1} [4][5]. The reason for wide range of CNTs spectrum is down to the fact that nanotubes have a diameter within 30-60 nm and the band in this region suggests due to the presence of defects in it resembling SP3 carbon state.

Since, for synthesizing NS-SnS/CNTs, the procedure followed had similarities with previous reports and that's why at 1320 cm^{-1}, C-N band can be seen which indicates the presence of nitrogen doping in it [6]. Furthermore, it can also be observed that metal- thiourea complex, O-H bond and other absorption bands intensity decreases because of introduction CNTs in it to make a nanocomposite.

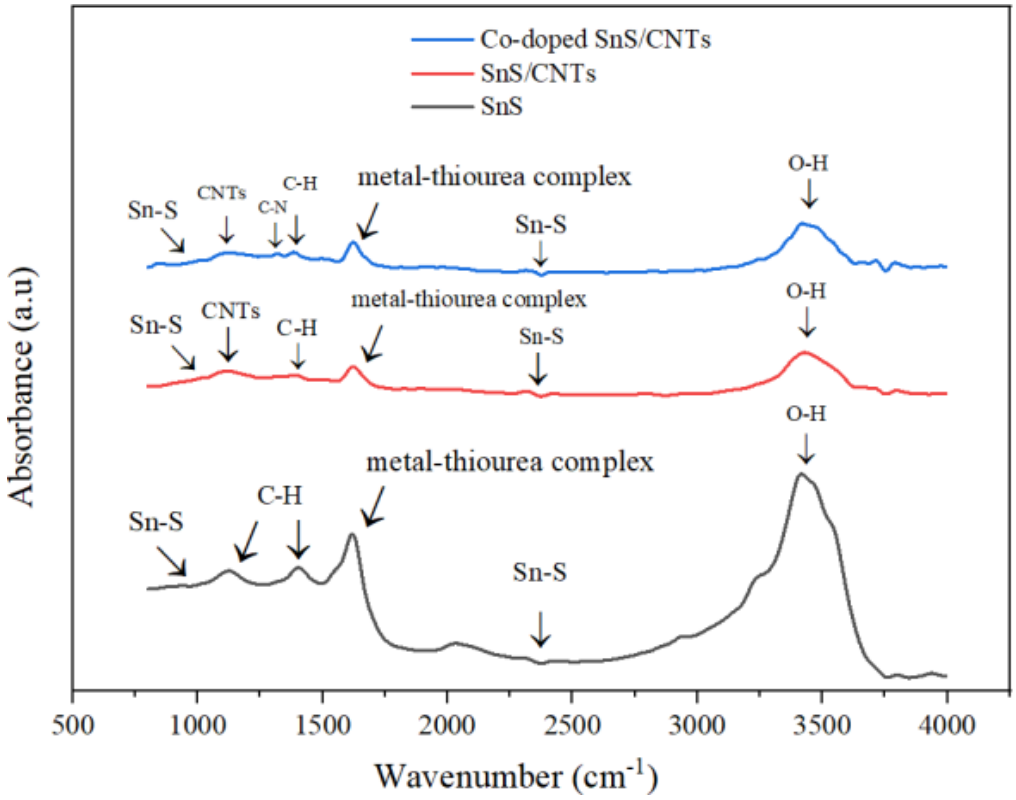

Figure 5.5 FTIR of SnS, SnS/CNTs and NS-SnS/CNTs

5.2. Electrochemical Characterization

5.2.1. Galvanostatic Charge/Discharge Performance

To study charge/(dis)charge performance of electrodes synthesized from these samples, a current density of 100 mA/ g was given, and cut off voltage for discharging was kept at 10 mV and 2.5 V for charging. From figure 5.6a it can be seen that nanocomposites deliver better initial discharge capacity, especially SnS/CNTs which showed highest capacity of 1406.9 mAh/ g, as compared to pure SnS which only delivered 597.4 mAh/ g. This discharge capacity shown by SnS/CNTs nanocomposite was even higher than the theoretical capacity of SnS i-e. 1022 mAh/ g. NS-SnS/CNTs also showed a good initial discharge of 947.96 mAh/ g while it

delivered a its counterpart charge capacity of 466.6 mAh/ g. This corresponding charge capacity shown by SnS/CNTs was higher than pure SnS initial charge capacity but less than SnS/CNTs anode. However, this increased initial charge/(dis)charge capacity of nanocomposite with respect to pure SnS can be simply down to the framework created by CNTs connecting cauliflower like SnS together and thus increasing conductivity and providing flexibility to the structure. Furthermore, these nanotubes reduce SnS nanosheets thickness which increases surface area for both nanocomposites. This increase in surface area allows more liquid based electrolyte to come in contact with the anode and hence, increases capacity.

Nevertheless, the relative decrease in discharge capacity shown by NS-SnS/CNTs can be ascribed to the fact that nitrogen doping in it results in development of an electron rich structure and this structure would prevent electrons originating from sodium atoms to pass from anode to cathode. Due to this, sodium will also face hinderance to get adsorbed in the structure easily and hence less sodium ions will leave its structure during charging/(dis)charging [7]. Figure 5.6b shows capacity/voltage profile SnS/CNTs nanocomposite during its 1^{st}, 2^{nd}, 10^{th}, 20^{th} and 50^{th} cycle and this profile result is completely in sync with the CV results of SnS/CNTs, and this same pattern was also observed for other 2 samples. It is also reported that solid electrolyte interphase formation results in high initial discharge capacity and that's why 1^{st} charge capacity is always very less than 1^{st} discharge capacity. Keeping that in mind, the initial coulombic efficiency shown by SnS, SnS/CNTs, NS-SnS/CNTs was 36.6%, 39.4% and 44% respectively. The increase in first coulombic efficiency for co-doped electrode can be ascribed to the less crystalline nature and more amorphous behavior shown by it. After 50 cycles, the SnS/CNTs electrode because of its more crystalline nature showed better reversible capacity of 183.3 mAh/ g which was more than twice than SnS. NS-SnS/CNTs after 50 cycles showed less reversible capacity (154.5 mAh/ g) than SnS/CNTs but overall, average coulomb efficiency, after 1^{st} cycle was increased to 34.1% from 29.9% (for SnS/CNTs). Improvement in capacity retention can be given to the isotropic nature of NS-SnS/CNTs electrode, due to which it can maintain its structural integrity when sodium ions leave or insert itself in the structure. Hence, this electrode has the capability to provide more space to release strains which can develop because of volume changes in the structure. The capacity retention in SnS/CNTs electrode is poor because of the fact that SnS crystals formed in it are large in size, which tend to collapse during cycling and the electrode loses its structural integrity [8]–[10].

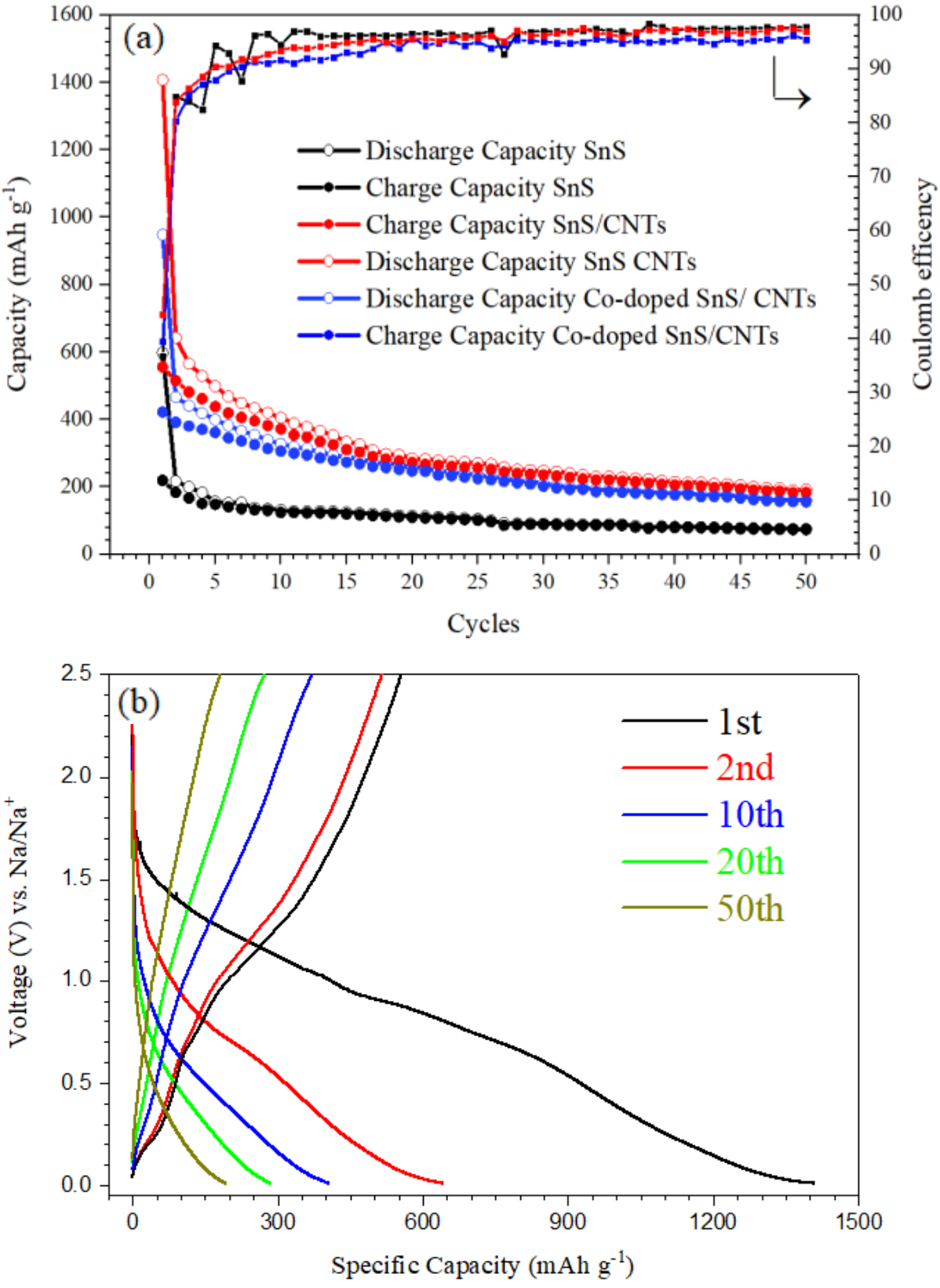

Figure 5.6 (a) Cyclic stability of electrodes at 100 mA/ g (b) capacity/voltage profile of SnS/CNTs

5.2.2. Cyclic Voltammetry Analysis

To analyze redox reactions occurring in electrodes, CV was carried out its result is shown in figure 5.7. First three CV scans of SnS/CNTs reveal various reduction and oxidation peaks. For first scan of discharge, a peak at ~ 0.65 V was observed which can be due to various reasons (1) formation of Na_2S because of SnS conversion reaction (2) Sn partial alloying reaction (3) Irreversible loss in capacity because of SEI formation [11], [12]. While analyzing CV curve, it has to be kept in mind that flat regions correspond capacitive contribution of electrode while peaks represent those phenomena which are limited due to the diffusion process. In next two cycles, reduction/oxidation peaks can be identified to partial alloying/dealloying process, at 0.01/0.24 V, 0.60/0.73 V and 1.12/1.17 V. At 1.12 V, the reduction peak can be linked to the conversion reaction, while 0.60 and 0.01 V reduction peaks are because of step wise alloying process [13]. The reaction that SnS undergoes is as follows:

$$SnS + 2Na^+ + 2e^- \rightarrow Sn + Na_2S$$

$$4Sn + 15Na^+ + 15e^- \rightarrow Na_{15}Sn_4$$

While charging, the dealloying anode peaks can be observed at 0.24 and 0.73 V. These peaks show that Na_xSn converts to Sn and at 1.17 V, conversion reaction takes place during which SnS again forms [14][15]. Same CV pattern was also observed for other electrodes thus indicating that same reduction/oxidation reactions take place in them. All of them, like SnS/CNTs, showed high initial capacity loss in their first relating to SEI.

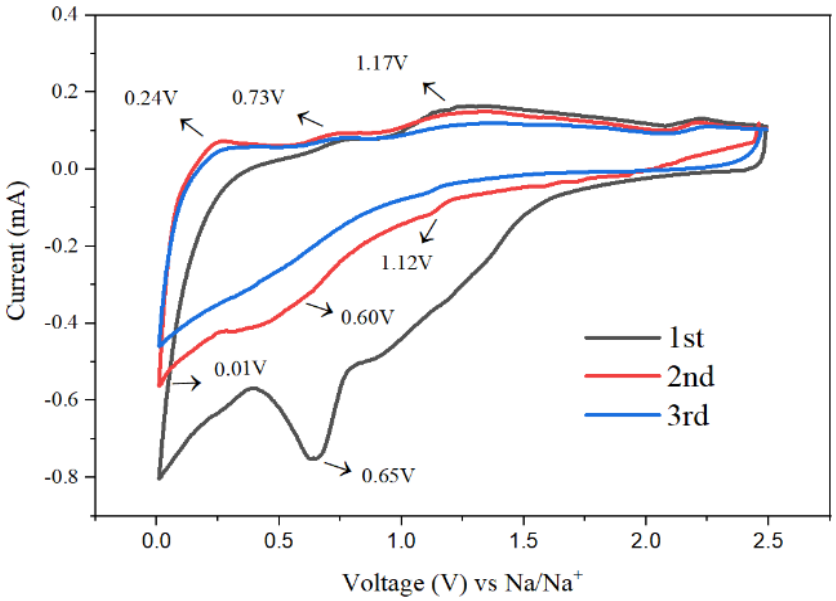

Figure 5.7 CV of SnS/CNTs electrode

5.2.3. EIS Analysis

To analyze kinetics of reaction, EIS was used to obtain Nyquist plots for SnS/CNTs and NS-SnS/CNTs is shown in figure 5.8. After drawing an equivalent circuit for EIS spectra of nanocomposites, we can obtain information about sodium ion diffusion coefficient within the bulk material at low frequency of spectra, resistance to charge transfer (R_{ct}) at medium frequency of and solid electrolyte interface formation resistance at high frequency of spectra [16][17]. From the graph, it can be seen that diameter of formed semicircle for SnS/CNTs is smaller than that formed for NS-SnS/CNTs at medium to high frequency region. This means that R_{ct} of SnS/CNTs is smaller than the later one and this comes out to be 44 Ω vs 76 Ω. This charge transfer resistance is remarkably lower than what have been mostly reported so far for tin sulfide-based systems which can be owed to unique cauliflower like morphology of tin sulfide and nanotube network bridging those sulfides together hence, shortening path to sodium ion diffusion [10][18][19][20]. Furthermore, this is also due to addition of CNTs in high concentration in nanocomposites, and very low binder concentration that was kept while making electrodes. Spectra at low frequency show linear line but the slope of this line is much steeper for NS-SnS/CNTs electrode indicating that sodium ion diffusivity is higher in SnS/CNTs electrode. When compared with each other, the R_{ct} value for SnS/CNTs electrode is much smaller than what is shown by NS-SnS/CNTs electrode because of the fact that later one shows more resistance to Na^+ diffusion. This is because more defects are present in the later one due to nitrogen and sulfur atom dopants which forces it to develop amorphous structure. This isotropic behavior shown by NS-SnS/CNTs electrode decreases its charge transfer resistance.

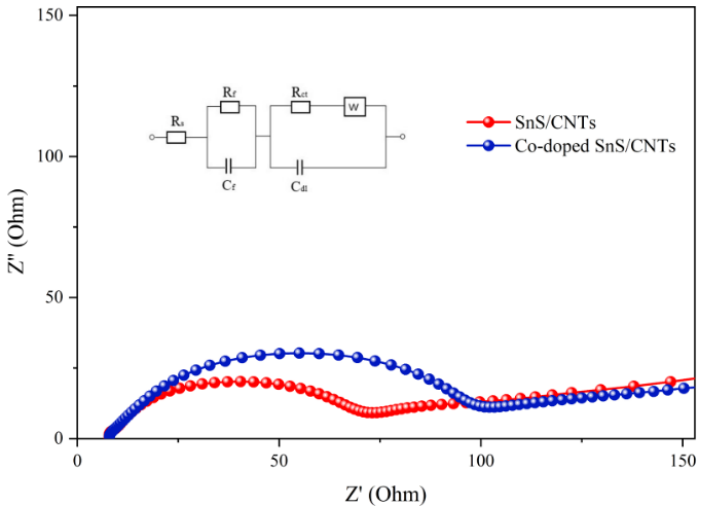

Figure 5.8 Nyquist plots of nanocomposites

5.3. Discussion:

To analyze the results, the reversible capacity obtained for nanocomposite anodes was compared with commercially available anode materials of LIBs after few hundred cycles. The data has been taken from different companies including Sony, Panasonic, LG, Samsung and Toshiba etc. Table 2. below compares the capacity of different anode materials as.

Table 5.1 Reversible capacity comparison between commercialized LIBs anode and as synthesized nanocomposite [21]

Reversible Capacity in Commercial cells after few hundred cycles (mAh/g)		**Reversible Capacity obtained in this project after 50 cycles (mAh/g)**
$LiCoO_2$	**148**	**154.5**
$LiNi_{0.33}Mn_{0.33}Co_{0.33}O_2$	**280**	
$LiMn_2O_4$	**120**	
$LiFePO_4$	**165**	
$Li_4Ti_5O_{12}$	**175**	

From the table it can be seen that the reversible capacity shown by nanocomposite electrodes not is quite as good as commercialized anode materials. This can be down to number of factors (i) large Na^+ as compared to Li^+ which makes it difficult for host material to maintain the structure upon charging/discharging, (ii) the commercialized chemistries are of intercalation type rather than of alloying-conversion type as it is here, in which the electrode undergoes a chemical reaction followed by an alloy formation with a metal ion upon charging and thus, resulting capacity improves significantly but at an expense of poor cyclability, because of large amount of volume expansion that occurs in the material.

However, the obtained results show that the strategy employed for this project is a step in a right direction. This is due to the improvement in capacity retention obtained for codoped nanocomposite as compared to undoped sample, because dopants had created defects in the

structure leading to the formation of an amorphous phase in it. Secondly, the charge transfer kinetics of both nanocomposite electrodes has improved a lot as compared to what was reported in the literature previously so far. That happened due to addition of CNTs in a large amount as what have been reported previously, and this decreased the charge transfer resistance of electrodes suggesting, that this strategy can be employed to enhance the rate performance of NIBs electrode in future. To further clear this, charge transfer resistance data is compared with recently reported literature of NIBs below in table 3.

Table 5.2 Comparison of charge transfer resistance data with literature

Sr. No	**Research Title**	**Authors**	**Year of Publication and Journal**	**Charge Transfer Resistance (Ω)**
1	Pomegranate-inspired SnS/ZnS@C heterostructural nanocubes towards high-performance sodium ion battery [13]	Ai et al.	Applied Surface Science (2019)	127.8
2	Hierarchical assembly and superior lithium/sodium storage properties of a flowerlike C/SnS@C nanocomposite [18]	Zhang et al.	Electrochimica Acta (2019)	100
3	Enhanced electrochemical performance of SnS nanoparticles /CNTs composite as anode material for sodium-ion battery [19]	Chen et al.	Chinese Chemical Letters (2018)	273.6
4	Low crystallinity SnS encapsulated in CNTs decorated and S-doped carbon fibers as excellent anode for NIBs [10]	Zhang et al.	Electrochimica Acta (2018)	90
5	This work			44

5.4. Summary

This chapter begins with predicting growth mechanism of NS-SnS/CNTs and how heteroatom dopants forces the nanocomposite to develop more of an amorphous nature. Then the samples that were prepared as an active material for NIBs anode were characterized structurally and electrochemically. XRD revealed decrease in the crystallite size of NS-SnS/CNTs as compared to SnS/CNTs which indicates that this decrease in crystallite size can be attributed to defects that were introduced in it via doping process. The more amorphous nature of NS-SnS/CNTs was also observed in its XRD pattern which was rather broad than other samples. Moreover, these results were further backed by SEM analysis which also showed reduction in SnS nanosheet thickness as the defects were increased. SEM revealed that unique cauliflower like SnS was formed by controlling Sn/S ratio, temperature and time in a solvothermal reaction and this cauliflower like SnS formed a network with CNTs which is responsible for enhanced electrochemical performance in nanocomposites. FTIR revealed C-N band which was developed due to nitrogen doping while TGA gave information about weight % of CNTs that were present in nanocomposites.

Electrochemically, nanocomposites gave batter charge/(dis)charge performance as compared to pristine SnS due to the fact that a network is created between SnS and CNTs, which enhances its surface area of electrode, shortens path for ion diffusion during sodiation and desodiation. However, NS-SnS/CNTs deliver better initial and average coulombic efficiency than SnS/CNTs because of it's more amorphous nature. Due to its isotropic behavior, it can provide enough voids for SnS to undergo volume expansion and release strains hence, this amorphous behavior of electrode act as a buffer to volume fluctuations. CV results confirmed that partial alloying-conversion redox reaction takes place during discharging and charging process. EIS results reveal that nanocomposite exhibit small charge transfer resistance than most of the electrodes which were reported previously. However, due to more crystalline nature and presence of less defects in SnS/CNTs, it showed more reduction to charge transfer resistance than NS-SnS/CNTs.

5.5. References

[1] B. Yang *et al.*, "Structural Phase Transition from Tin (IV) Sulfide to Tin (II) Sulfide and the enhanced Performance by Introducing Graphene in Dye-sensitized Solar Cells," *Electrochim. Acta*, vol. 176, pp. 797–803, 2015.

[2] Y. Li *et al.*, "Sulfur-nitrogen doped multi walled carbon nanotubes composite as a

cathode material for lithium sulfur batteries," *Int. J. Hydrogen Energy*, vol. 39, no. 28, pp. 16073–16080, 2014.

[3] S. Zhang, H. Zhao, M. Wu, L. Yue, and J. Mi, "One-pot solvothermal synthesis 2D SnS2/CNTs hybrid as a superior anode material for sodium-ion batteries," *J. Alloys Compd.*, vol. 737, pp. 92–98, 2018.

[4] S. Li *et al.*, "Stannous sulfide/multi-walled carbon nanotube hybrids as high-performance anode materials of lithium-ion batteries," *Electrochim. Acta*, vol. 136, pp. 355–362, 2014.

[5] M. Gurubhaskar, N. Thota, M. Raghavender, Y. P. V. Subbaiah, G. H. Chandra, and K. T. R. Reddy, "A Facile and TGA Free Hydrothermal Synthesis of SnS Nanoparticles," *Nano*, vol. 12, no. 10, pp. 1–10, 2017.

[6] A. Misra, P. K. Tyagi, M. K. Singh, and D. S. Misra, "FTIR studies of nitrogen doped carbon nanotubes," *Diam. Relat. Mater.*, vol. 15, no. 2–3, pp. 385–388, 2006.

[7] P. Sehrawat, C. Julien, and S. S. Islam, "Carbon nanotubes in Li-ion batteries: A review," *Mater. Sci. Eng. B Solid-State Mater. Adv. Technol.*, vol. 213, pp. 12–40, 2016.

[8] J. R. Rodriguez, Z. Qi, H. Wang, M. Y. Shalaginov, M. Kang, and K. A. Richardson, "Ge2Sb2Se5 Glass as High-Capacity Promising Lithium-ion Battery Anode," *Nano Energy*, p. 104326, 2019.

[9] F. Han, W. C. Li, C. Lei, B. He, K. Oshida, and A. H. Lu, "Selective formation of carbon-coated, metastable amorphous ZnSnO 3 nanocubes containing mesopores for use as high-capacity lithium-ion battery," *Small*, vol. 10, no. 13, pp. 2637–2644, 2014.

[10] S. Zhang, H. Zhao, M. Wang, Z. Li, and J. Mi, "Low crystallinity SnS encapsulated in CNTs decorated and S-doped carbon fibers as excellent anode material for sodium-ion batteries," pp. 1–9, 2019.

[11] Y. Wang *et al.*, "Tin sulfide nanoparticles embedded in sulfur and nitrogen dual-doped mesoporous carbon fibers as high-performance anodes with battery-capacitive sodium storage," *Energy Storage Mater.*, vol. 18, no. August 2018, pp. 366–374, 2019.

[12] B. Qin *et al.*, "Exploring SnS nanoparticles interpenetrated with high concentration nitrogen-doped-carbon as anodes for sodium ion batteries," *Electrochim. Acta*, vol. 296, pp. 806–813, 2019.

[13] J. Ai *et al.*, “Pomegranate-inspired SnS/ZnS@C heterostructural nanocubes towards high-performance sodium ion battery,” *Appl. Surf. Sci.*, vol. 496, no. August, p. 143631, 2019.

[14] S. H. Choi, Y. Jang, Y. J. Choi, and Y. N. Ko, “Facile synthesis of macroporus SnS microspheres as a potential anode material for enhanced sodium ion batteries,” *J. Ind. Eng. Chem.*, vol. 80, pp. 130–135, 2019.

[15] Y. Zhang *et al.*, “Heterostructured SnS/TiO2@C hollow nanospheres for superior lithium and sodium storage,” *Nanoscale*, vol. 11, no. 27, pp. 12846–12852, 2019.

[16] S. S. Zhang, K. Xu, and T. R. Jow, “Electrochemical impedance study on the low temperature of Li-ion batteries,” *Electrochim. Acta*, vol. 49, no. 7, pp. 1057–1061, 2004.

[17] N. R. Srinivasan, S. Mitra, and R. Bandyopadhyaya, “Improved electrochemical performance of SnO2-mesoporous carbon hybrid as a negative electrode for lithium ion battery applications,” *Phys. Chem. Chem. Phys.*, vol. 16, no. 14, pp. 6630–6640, 2014.

[18] Y. Zhang *et al.*, “Hierarchical assembly and superior lithium/sodium storage properties of a flowerlike C/SnS@C nanocomposite,” *Electrochim. Acta*, vol. 296, pp. 891–900, 2019.

[19] Y. Chen *et al.*, “Enhanced electrochemical performance of SnS nanoparticles / CNTs composite as anode material for sodium-ion battery,” *Chinese Chem. Lett.*, vol. 29, no. 1, pp. 187–190, 2018.

[20] Y. Zhang *et al.*, “Carbon coated amorphous bimetallic sulfide hollow nanocubes towards advanced sodium ion battery anode,” *Carbon N. Y.*, vol. 150, pp. 378–387, 2019.

[21] Nitta, Naoki, et al. "Li-ion battery materials: present and future." *Materials today* vol. 18, no. 5 , pp. 252-264, 2015

CONCLUSION

Tin sulfide-based systems were synthesized as an anode material for NIBs because of its high theoretical capacity. However, they face the problem of high-volume expansion during cycling process which fades its capacity with time. To mitigate this issue, in this dissertation, SnS nanocomposite was synthesized with carbon nanotubes which was doped with nitrogen and sulfur atoms. Due to these dopants, defects were introduced in the structure and those defects reduced the crystallite size and nanosheet thickness of SnS in NS-SnS/CNTs nanocomposite, which resulted in the development of an amorphous structure in it. Due to the formation of unique cauliflower like morphology of SnS and CNTs bridging those cauliflowers together, surface area of nanocomposite increased and at 100 mA/ g, it delivered reversible capacity of more than 2.5 times higher than pristine SnS after 50 cycles. It also showed high first and average coulombic efficiency than other electrodes thus indicating better capacity retention than them. This increase in capacity retention can be attributed to isotropic behavior of electrode, which can provide sufficient space to act as a buffer to volume expansions that may occur in electrode when sodium ion inserts or extracts itself from the structure. Furthermore, due to this robust ion transport network created in a nanocomposite, it showed reduction to charge transfer resistance than most of those electrodes which were reported previously.

RECOMMENDATIONS

Several studies but not limited to them, can be carried out to build on the results that are obtained in this dissertation however. These studies may require different material preparation techniques with different precursors, additives, binders and conductive agents etc. It is suggested by exploring these novel ideas, NIBs electrochemical performance can be improved further. These suggestions are as follows:

1. Using 3D graphene as a matrix material to create a framework with cauliflower like morphology of SnS.
2. Nickel foam can further enhance surface area and thus electrochemical performance of nanocomposites if it is incorporated as a matrix material in the structure.
3. By exploring a novel morphology of SnS with this nanocomposite and analyzing the impact of that morphology electrochemically.
4. By creating a heterostructure of SnS with another metal sulfide or metal oxide to enhance the capacity of anodes.
5. By carefully tuning the crystallinity of SnS i-e. partial crystalline/amorphous structure, we can achieve high reversible capacity with good coulomb efficiency
6. Creating an electrostatic charge on matrix materials such as graphene, CNTs, nickel foam which can help with anchoring SnS particles on the matrix thus obtaining high reversible capacity with good cyclic stability

ACKNOWLEDGEMENTS

I would like to express my sincere gratitude to my research supervisor, Dr. Zuhair S. Khan of USPCAS-E, NUST, Islamabad for letting me be part of the research group at Advanced Energy Materials and Fuel Cells lab, USPCAS-E, NUST, Islamabad. I feel privileged to have worked under his kind auspices. It's the blend of his patience, persistence, guidance and motivation that made me accomplish my research aims in due time.

I would also like to thank Dr. Naseem Iqbal who allowed me to use the facilities of Energy Storage Lab, USPCAS-E, NUST for preparing electrodes, coin cell and characterizing though battery analyzer.

Finally, I would like to express gratitude towards PGP NUST for providing a financial assistance to carry out this project.

APPENDIX A: Publication

Amorphous codoped SnS/CNTs nanocomposite with improved capacity retention as an advanced sodium-ion battery anode

Ahmed A. Qayyum[1*], Zuhair S. Khan[1,], Sheeraz Ashraf[1], Nisar Ahmed[1]

1) Advanced Energy Materials & Systems Lab., Department of U.S.-Pakistan Center for Advanced Studies in Energy, National University of Sciences and Technology, Islamabad, 44000, Pakistan

*****Corresponding Author: Ahmed A. Qayyum

Email: ahmedqayyum@hotmail.com

Abstract:

Tin-based chalcogenides are considered as a promising anode material for sodium-ion batteries yet they suffer from poor electronic conductivity, initial coulombic efficiency and capacity retention. Herein, using facile solvothermal route, cauliflower like SnS/CNTs and codoped SnS/CNTs nanocomposites were synthesized. Heteroatom dopants in codoped SnS/CNTs create an amorphous structure which provides sufficient space to release volumetric strains induced during sodiation/desodiation, resulting in superior capacity retention and initial coulombic efficiency of 44% as compared to 39.4% for SnS/CNTs and 36% for SnS. Carbon nanotubes create a framework by connecting cauliflower like SnS together and at 0.1 A g^{-1}, it delivers a reversible capacity of 183.3 mAh g^{-1} after 50 cycles in SnS/CNTs, which is more than twice as high as is delivered by pure SnS, and also with a very small resistance to charge transfer. Therefore, these novel nanocomposites provide a robust platform for application in sodium-ion batteries.

1. Introduction:

Since 1991, lithium ion batteries (LIBs) have dominated the market in terms of electricity energy storage system however, with an ever-increasing market of electromobility and stationary energy storage, industries dealing with these products are in a pursuit of developing a more energy efficient storage technology [1]. So far, majority of these needs are being met by LIBs because of their good energy density, cyclic life and compact design, which in turn also increases the cost of raw materials like lithium and cobalt, that comprise the core component of LIB technology, making large-scale storage systems too expensive to aid in shifting from dependence on fossil fuels to renewable energy sources [1]. Fortunately, sodium ion batteries (NIBs) have gained much more attention as an alternative source to LIBs because of relatively high abundance of sodium in earth crust (2.75% vs 0.0065% for Li) and seawater as well, which would decrease the manufacturing cost of batteries [2,3]. Moreover, NIBs follow the same electrochemical energy storage mechanism as shown by LIBs. However, these batteries, so far, have failed to deliver same volumetric and gravimetric energy density, limiting their practical applications to only where size of battery is not the biggest constraint. This can be owed to the fact that sodium has higher standard reduction potential of -2.71 in electrochemical series than that to lithium (-3.04) hence, less cyclic capacity per unit mass and volume is obtained [1, 4].

One of the major reasons for success in commercialization of LIBs is the adoption of graphite as an anode material but in NIBs, it exhibits poor storage capacity because of the fact that Na^+ is larger (ionic radius of 1.02 A^o vs 0.76 A^o) and 3 times as heavier as Li^+ , which makes it difficult for graphite to maintain its lattice structure during charging/discharging mechanism hence, the capacity retention of anode reduces significantly after few cycles [5, 6]. Therefore, the major hinderance that NIBs are facing towards commercialization includes finding a suitable anode material, which can deliver a good capacity retention upon cycling [7]. Among different materials, transition metal chalcogenides (TMCs) and transition metal dichalcogenides (TMDs) such as MoS, WS, FeS, CuS, PbS, TiS, TiS_2 SbS_2 MOS_2, WS_2, FeS_2 Sb_2S_3 etc. have gained importance for their use in various energy applications including batteries, owing to their high theoretical specific capacity[8-10]. Stannous sulfide (SnS) is one of those material (theoretical specific capacity ~ 1028 mAh g^{-1}) which can deliver high energy density when it is used as an anode material for NIBs and this is basically because of partial alloying-conversion reaction mechanism that it follows [10]. However, the problem with SnS is that they provide poor cyclic life because of large volume changes that occur in its structure during sodiataion/desodiation [11]. One way to cater these problems is to introduce conductive agents like graphene, carbon powder, amorphous carbon, carbon nanorods etc. in active materials that can not only counter the effect volume change but also improves the conductivity of active material and so far many approaches have been designed to incorporate these agents with active materials [11,12].

Among different available carbon-based matrix materials that can act as a conductive agent, carbon nanotubes (CNTs) have been investigated intensively in the past decade because of its high aspect ratio and superior mechanical strength (tensile strength ~ 63 GPA) [13]. Moreover, along with all these remarkable properties, they are also extremely light in weight and possess a very high electrical conductivity of ~ 10,000 cm^2 V^{-1} S^{-1}, which provides flexibility to structure and improves their performance in electrochemical energy storage devices [13]. To make a composite anode system with them, CNTs can either act as a self-supporting electrode for ion storage or it can be used as a scaffold on which active electrode materials (such as transition metal oxides and chalcogenides) possessing higher specific capacity can anchor [14]. Using later phenomena, Ren et al. showed that SnS_2/CNTs electrode at 20 mA g^{-1} delivered initial and final specific discharge capacity (after 20 cycles) of 649 mAh g^{-1} and 317 mAh g^{-1} respectively meanwhile, corresponding pure SnS_2 electrode delivered only 255 mAh g^{-1} for NIBs [15]. Using solvothermal method, Zhang et al. proposed 2D SnS_2/CNTs for NIBs and at

50 mA g^{-1}, got initial discharge capacity of 1063 mAh g^{-1} and after 100 cycles obtained final discharge of 476.3 mAh g^{-1} [16]. Moreover, it was demonstrated by Zhu et al. that for LIBs, SnS/CNTs exhibit an initial discharge of 1427 mAh g^{-1} at 100 mA g^{-1} and it remains up to 453 mAh g^{-1} after 100 cycles [17]. Importance of controlling the morphology of electrode active material have received a significant amount of attention in past few decades and among those morphologies, cauliflower is gaining attraction because of its high specific surface area that originated from its hierarchical porous structure containing micropores and mesopores in it [18-20]. These micro and mesopores enhances electrode/electrolyte contact area, making electrodes to exhibit superior electrochemical performance, which is also shown by He et al., who had synthesized cauliflower like FeS_2/graphene foam anode for LIBs and obtained a specific discharge capacity of 615 mAh g^{-1} at an high current density of 5000 mA g^{-1} [21]. Previously, through experimental and theoretical calculations, it was shown that doping of SP^2 based carbon structures with agents like N, S, P and Br have shown to increase their electrical conductivity, which was also analyzed by Linlin et al. when he synthesized doped N-S graphene/ SnS_2 aerogel, and after 50 cycles, attained a reversible capacity of 527 mAh g^{-1} at 20 mA g^{-1} for NIBs [22]. Recently, Zhang et al. revealed that compared to crystalline anode, bimetallic sulfide@C nanocubes, having amorphous nature, is more effective in releasing volume strain and restraining the pulverization of electrode [23]. Furthermore, it was realized that by introducing dopants, a more disordered structure is obtained due to increase in number of defects and in comparison, to unitary-heteroatom doping, binary-heteroatom dopants would produce more defects in the structure because of two elements creating a synergistic effect [25, 26]. So far, to the best of our knowledge, there is no study available analyzing the impact of nitrogen and sulfur doped CNTs, and its nanocomposite with SnS for NIBs.

Herein, self-assembled cauliflower like SnS, SnS/CNTS and codoped SnS/CNTs (with nitrogen and sulfur dopants) were applied as an anode material for NIBs after their synthesis was carried out via solvothermal method. The dopants create a disordered structure in codoped SnS/CNTs and it shows better initial coulombic efficiency with increased capacity retention because of its ability to provide sufficient space to rectify the impact of volume expansion during desodiation/sodiation. The SnS/CNTs nanocomposite electrode upon cycling delivered an enhanced reversible capacity with boosted charge transfer because of unique cauliflower like morphology of SnS and homogenous distribution of carbon nanotubes in it, connecting SnS together and creating a framework. This framework shortens the Na^+ diffusion distance, enhances surface area, increasing electrode/electrolyte contact area and thus, improving

electrochemical performance. Consider easy synthesis approach along with improved electrochemical performance, these nanocomposites can be very promising candidate for NIB anode.

2. Experimental Methods:

2.1. Synthesis of Nitrogen and Sulfur doped CNTs (codoped CNTs):

All reagents and chemicals involved in this work had an analytical grade and were used without any further processing. The doping procedure of CNTs with nitrogen and sulfur was extracted from the literature [14,27]. Briefly, CNTs were functionalized with 40% nitric acid at $110^{O}C$ for 2 hours and were vacuum dried afterwards for 12 hours. 0.152 g of thiourea was added in 60 ml of ethylene glycol and stirred for 30 minutes. Then 0.05 g of CNTs were added in the above solution and was homogenously dispersed for 1 hour via ultrasonication. The obtained dispersion was poured in 100 ml autoclave and was kept at $180^{O}C$ for 12 hours. Nitrogen-sulfur codoped CNTs were collected after washing the as obtained product with purified water, acetone and drying at $60\ ^{O}C$ for 10 hours in vacuum.

2.2. Fabrication of Codoped SnS/CNTs Nanocomposite:

To fabricate nanocomposite of codoped CNTs with SnS, the procedure was followed as it was carried out in the literature [5,28]. To summarize, 0.145 g of $SnCl_2.2H_20$ and 0.75g of thiourea was introduced to 30 ml of ethylene glycol each and stirring was carried out for 30 minutes. Afterwards, both solutions are mixed with each other and stirred. Then the as obtained codoped CNT product was added and dispersed homogeneously in this solution via ultrasonication for 1 hour followed 30 minutes stirring. This homogenously dispersed solution was poured in 100 ml autoclave and was heated at $180^{O}C$ for 24 hours. Nitrogen sulfur codoped SnS_2/CNTs nanocomposite was obtained after washing the product repeatedly with purified water, acetone and drying at $60^{O}C$ for 12 hours in vacuum. This is followed by annealing at $400^{O}C$ for 1 hour which resulted in a phase transformation and codoped SnS/CNTs nanocomposite was obtained [29]. For comparison, SnS/CNTs were prepared without doping and pure SnS was prepared without adding CNTs.

2.3. Characterization

X-ray diffraction (D8 Advance by Bruker) having Cu-kα as a source of radiation was used to identify materials and their morphologies were revealed by scanning electron microscopy (VEGA 3 LMU, TESCAN). Thermogravimetric analysis (DTG-60/60H) was employed to

determine the wt.% of CNTs in nanocomposites and FTIR (Agilent cary 630) was carried out to analyze covalent bonds in it. The electrical resistivity of samples was obtained from Hall Effect equipment (HMS 3000, Ecopia).

2.4. Electrochemical Measurements:

For electrochemical characterization, CR 2032 coin cell was fabricated (in a glove box). Working electrode paste was made by making a homogenous mixture of as synthesized active material, Super P and poly(vinylidene fluoride) with N-methyl pyrrolidinone in a ratio of 80:15:5. The slurry afterwards was pasted on a copper foil which was dried for an overnight in vacuum at $80^{O}C$. working electrodes were cut into 16 mm discs and sodium foil was taken as a reference and counter electrode while polypropylene layer was used as a separator. Electrolyte used was 1 M $NaClO_4$ in a (1:1) volume mixture of ethylene carbonate/dimethyl carbonate having 5 wt.% fluoroethylene carbonate in it. Charge/ discharge performance of cells were obtained by the help of 8 channel battery analyzer (BST8-3) where voltage range was kept between 0.01 V to 2.50 V. Cyclic Voltammetry (CV) was carried out between 0.01 V to 2.50 V at a scan rate of 0.2 mV s^{-1} while electrochemical impedance spectroscopy (EIS) was done between frequency of 100 mHz to 100 kHz. Both EIS and CV measurements were performed on electrochemical workstation (CHI 660E) at a room temperature.

3. Results and Discussion:

Formation of sulfur and nitrogen codoped SnS/CNTs composite via solvothermal method is illustrated in figure 1(a). Firstly, CNTs were mixed with thiourea which acts as a dopant source for both nitrogen and sulfur, in an ethylene glycol solution and solvothermal reaction was carried out. High temperature ($180^{O}C$) and pressure dissociates thiourea into its atomic form having both nitrogen and sulfur atoms. Both of these atoms get sufficient time (12 h) to make a covalent bond with CNTs and later these heteroatom dopants would play a crucial role in SnS growth mechanism [27,30]. The as prepared codoped CNTs were used as a precursor with $SnCl_2.2H_2O$, which acts as a source for tin by releasing Sn^{+4} ions, absorbs S^{-2} from thiourea during stirring. During solvothermal reaction, codoped CNTs with improved wettability, provides more nucleation sites to the growth of SnS, takes upon an amorphous cauliflower like morphology (dictated by high temperature and pressure inside an autoclave for 24h) while CNTs without heteroatom dopants develop SnS with more of a crystalline nature. After annealing this nanocomposite at $400^{O}C$ for 1 hour, Sn^{+4} reduces to Sn^{+2} or SnS_2 /CNTs undergoes a phase transformation and nanocomposite converts into codoped SnS/CNTs [29].

XRD patterns of CNTs, SnS, SnS/CNTs and codoped SnS/CNTs samples can be seen in Figure 1(b). The pattern of SnS was indexed to orthorhombic SnS (JCPDS No. 39-0354) having a lattice constant of a = 4.3291 Å, b = 11. 1923 Å, 3.9838 Å. CNTs exhibit a broad diffraction peak (002) at 2θ around 26^{O} and another peak at ~ 43^{O} which corresponds to (001). In SnS/CNTs and codoped SnS/CNTs, it was observed that CNTs peak overlap with a peak of

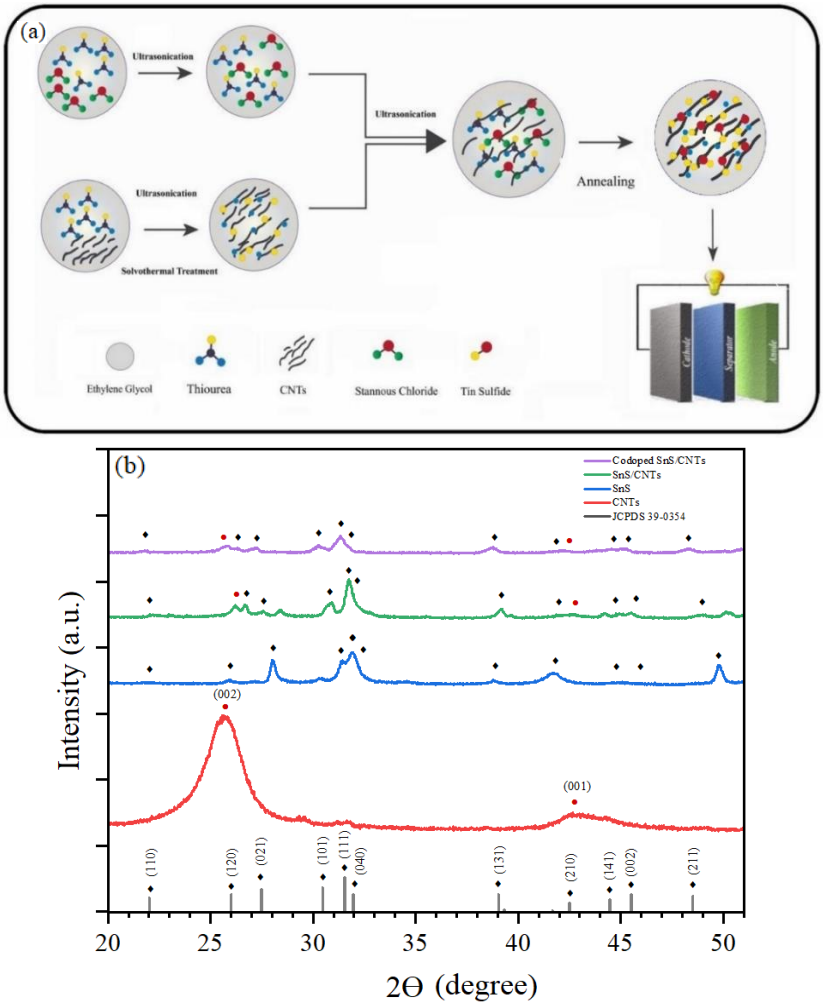

Figure 1(a) Schematic illustration of codoped SnS/ CNTs nanocomposite formation (b) XRD analysis

SnS at (120) plane. However, for codoped SnS/CNTs, a relative peak shift to lower 2θ values was also observed when compared with SnS/CNTs nanocomposite and pristine CNTs. At (100), the peak shift can be associated to the C-N bond whose introduction causes distortions within the carbon layer because of its relatively shorter bond length than C-C bond and the line shift at (002) can be ascribed to the expansion of interlayer distance between two graphitic layers to relax the distortions produced by sulfur and nitrogen dopants [25]. It is obvious that the presence heteroatom dopants introduce defects in the structure which produces lattice

strains and to accommodate those strains, crystallite size of SnS decreases from ~22nm (in SnS/CNTs) to ~ 20nm in codoped SnS/CNTs. This synergistic effect of reduced crystallite size and the presence of defects forces codoped SnS/CNTs to develop an isotropic nature leading to rather broad diffraction pattern with reduced intensity in XRD. It is noteworthy that few peaks SnS_2 are also present in the diffraction pattern indicating the existence of residuary hexagonal SnS_2 during the phase transformation.

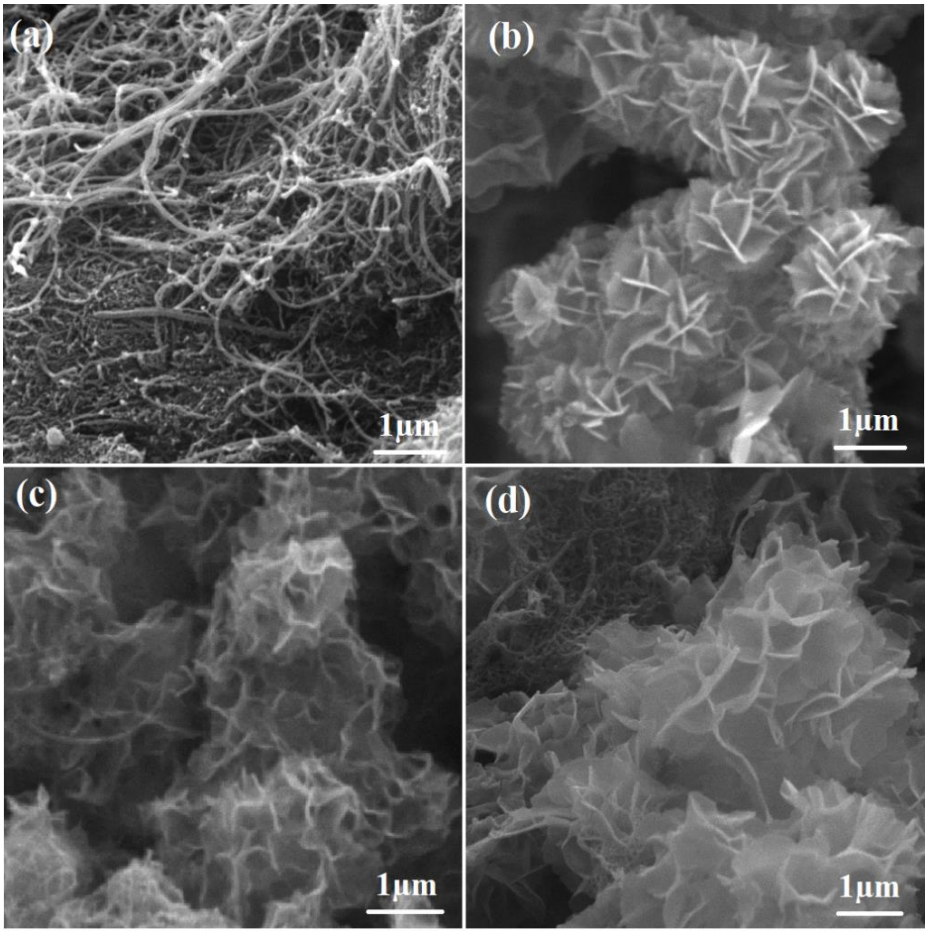

Figure 1: SEM images of (a) CNTs (b) SnS (c) SnS/CNTs
(d) codoped SnS/CNTs

Figure 2 shows SEM images of all the samples revealing their structure and morphology. Well defined cauliflower like morphology of SnS was obtained for all samples by carefully controlling time, temperature and Sn/S ratio. It can be seen in figure 2a that pristine CNTs have a diameter ranging from 30- 60 nm and when these CNTs are introduced to SnS, because their length is much longer than the diameter of cauliflower, they can be seen bridging adjacent cauliflowers together in nanocomposites (figure 2c and 2d) [16]. This effectively improves the

conductivity of nanocomposite electrodes and these results are in well agreement with their impedance spectra (will be discussed later). This cauliflower like SnS is actually an agglomeration of SnS nanosheets having a thickness of 65nm for bare SnS and 45 nm for SnS/CNTs. Interestingly, the thickness of nanosheets in nanocomposite further decreased to 39 nm after CNTs were doped (figure 2d) and this is in contrast with the result of XRD which also showed reduction to crystallite size of SnS, facilitating the formation of amorphous structure in codoped SnS/CNTs. Moreover, it has already been reported by Mohebbi et al. that cauliflower like morphology exhibit a high specific surface area of 28.005 $m^2 g^{-1,}$ and had an average pore diameter of 37.195 nm [28].

To determine the wt.% carbon nanotubes in SnS/CNTs and codoped SnS/CNTs nanocomposite, thermogravimetric analysis was employed and results are shown in figure 3a. It can be seen that both curves exhibit two major regions of weight loss. Weight loss from room temperature to $400^{O}C$ is can be ascribed to removal of organic residues and evaporation of adsorbed water molecules. The region from 450-$800^{O}C$ corresponds to the removal of CNTs as the carbon in it oxidizes to form CO or CO_2 [31]. Thus, the content of CNTs in SnS/CNTs and codoped SnS/CNTs comes out to be around 38% and 42% respectively. For codoped sample synthesis, since it was a two-step solvothermal process, the initial amount of CNTs taken was relatively high as there were chances of it being wasted. It is to be noted that overall, in our nanocomposites, the CNTs content was kept higher than what was reported previously which significantly reduces charge transfer resistance during cycling process [31]. Furthermore, on the basis of stoichiometry, the amounts of nitrogen and sulfur in codoped SnS/CNTs are calculated to be 5.2 atomic% and 2.5 atomic% respectively, which is close to what was reported previously [27].

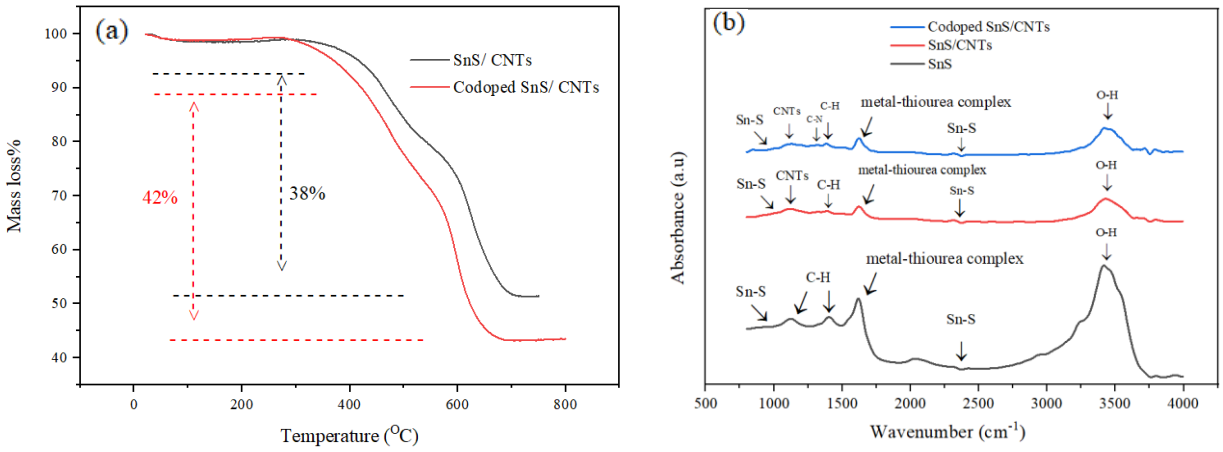

Figure 2(a): TGA analysis (b) FTIR spectrum

Figure 3b shows the FTIR spectra of SnS, SnS/CNTs and codoped SnS/CNTs over a wavenumber ranging of 800-4000 cm^{-1}. FTIR spectra shows the characteristic bands of SnS at 2350 and 1040 cm^{1}. The IR spectrum of carbon nanotubes can be found in the region of 1100-1200 cm^{-1} which represents the more disorder sp3 carbon state [32,33]. The broad absorption band of CNTs in IR spectrum is influenced by CNTs having a diameter from of 30-60 nm. As the doping procedure was followed exactly according to previous reports [27,30], only in codoped SnS/CNTs material , we observe the presence C-N band at 1320 cm^{-1}[32,34]. It was also observed that the absorbance of SnS, metal-thiourea complex, O-H and C-H alkyl deforming decreases when CNTs are introduced. This is because of its amorphous nature which doesn't allow IR light to transmit through it easily.

At current density of 0.1 A g^{-1}, charge/discharge profile of different electrodes were obtained within 0.01-2.50 V and results are shown in figure 4a. It can be seen that SnS/CNTs nanocomposite exhibited high initial discharge capacity as compared to codoped SnS/CNTs and pristine SnS sample. SnS/CNTs exhibited initial discharge capacity of as high as 1406.9 mAh g^{-1}, which is even greater than the theoretical capacity of SnS (1022 mAh g^{-1}), and a corresponding charge capacity of 555.5 mAh g^{-1}. The codoped sample delivered initial discharge and charge capacity of 947.96 mAh g^{-1} and 466.6 mAh g^{-1} respectively, while SnS only showed 597.4 mAh g^{-1} and 216.2 mAh g^{-1}. The low initial reversible capacity of pristine SnS as compared to nanocomposites can be ascribed to the large volumetric change that occurs in the structure during charging/discharging process, and also due to intrinsically high resistivity of the sample (3.75×10^{6} Ω cm). This resistivity of a sample decreases significantly to

1.83×10^{3} Ω cm when highly conductive CNTs are introduced to SnS however, it increases again to 9.33×10^{3} Ω cm when codoped CNTs are added into SnS [15,35]. The increase in electrical resistivity here can be due to the formation of smaller sized SnS crystals as dopants introduce disorders in the lattice site, thus leading to the development of amorphous structure in it and the results are in good consistent with XRD [36]. Overall, the increase of specific discharge capacity in both nanocomposites with respect of SnS can be ascribed to the homogenous distribution of CNTs in a cauliflower like SnS structure connecting them together to form a framework. CNTs provide flexibility, increases the conductivity of nanocomposite, decreases the thickness of SnS nanosheet (as shown previously in figure 2c and 2d) and increases the surface area of the electrodes. The framework formed in them enhances contact between electrolyte and anode material, shortens the Na^{+} diffusion length and ultimately, they

give better charge discharge performance as compared to bare SnS. The relatively less discharge capacity shown by codoped SnS/CNTs as compared to SnS/CNTs can be attributed to the fact that an electron rich structure forms due to nitrogen doping and this provide hinderance to the electrons coming from the absorbed Na atoms. As a result it increases the energy required by sodium to get absorbed in codoped SnS/CNTs electrode which would depress its discharge capacity [14]. figure 4b, show capacity/ voltage profile of SnS/CNTs electrode for 1^{st}, 2^{nd}, 10^{th}, 20^{th} and 50^{th} cycle, and the results are in well agreement with the CV curve. The initial capacity loss after first few cycles is because of solid electrolyte interphase (SEI) formation, which is an inevitable phenomenon, occurs majorly due to electrolyte decomposition [37]. The formed SEI films at the interface of electrode and electrolyte would hinder sodium ion diffusion across it and since diffusion is a concentration gradient phenomenon, the imbalance of sodium ion created across the interface contributes heavily to observed capacity loss [37]. It is understood that SEI formed can be fragile and gets damaged easily, which decomposes more electrolyte and new dendritic deposits are created on electrodes upon further cycling but the decrease in specific capacity after first few cycles is less which points to the formation of stable SEI afterwards [37,38]. Even though SEI forms, relatively, we obtain high initial coulombic efficiency of 44% codoped SnS/CNTs as compared to SnS/CNTs (39.4%) and bare SnS (36.6%). This demonstrates the advantages of having an electrode with an amorphous structure and the results of initial coulombic efficiency in nanocomposite electrodes are in well accordance with prior reports on NIBs[16, 39,40]. When it came to cyclic stability, after 50 cycles, highly crystalline SnS/CNTs exhibit a reversible capacity of 183.3 $mAhg^{-1}$ (with a capacity retention of 29.9% after 2^{nd} cycle), which is approximately 2.5 times higher than what is shown by pristine SnS, while amorphous codoped SnS/CNTs delivered a final charge capacity of 154.5 $mAhg^{-1}$ but that with an improved capacity retention of 34.1%. The reversible capacity shown by these electrodes are significant to previous report on NIBs by Ren et al., who had obtained 317 mAh g^{-1} at 20 mA g^{-1} for SnS_2/CNTs electrode (after 20 cycles), and comparable to Xu et al., who showed that MTP@rGO electrode exhibit a discharge capacity of 199.7 mAh g^{-1} after 100 cycles at 50 mA g^{-1} [15,41]. This enhancement in capacity retention in codoped SnS/CNTs electrode can be ascribed to the amorphous feature of an electrode, which owing to its intrinsically isotropic nature, upon cycling can retain better structure integrity as it can effectively release strains induced due to volume fluctuations during ion insertion/extraction. It has already been shown in figure 1(b) that crystals formed for SnS/CNTs nanocomposites are larger in size than amorphous codoped SnS/CNTs crystals. Because of this small crystallite size, upon cycling, codoped SnS/CNTs electrode exhibit less

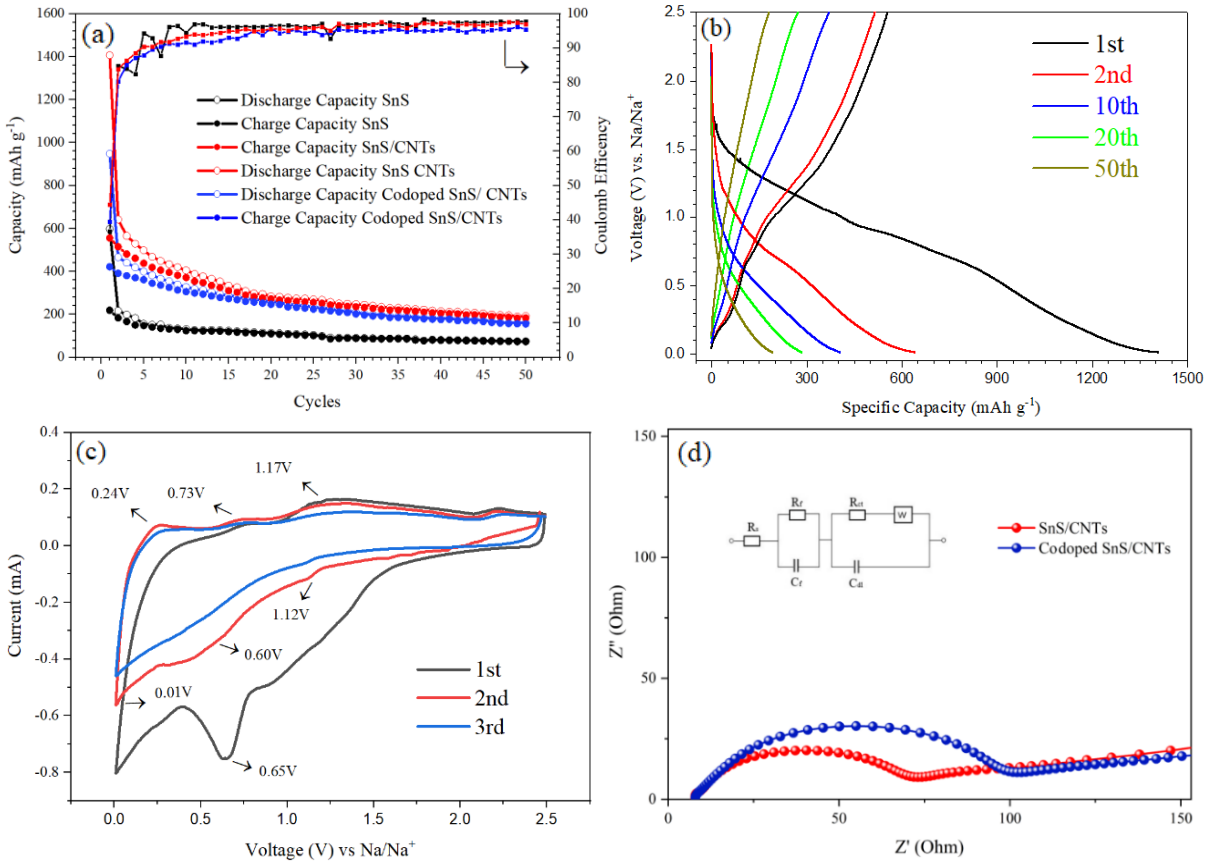

Figure 3(a) cycling performance of electrodes at 0.1 A g^{-1} (b) charge /discharge profile of SnS/CNTs at 0.1 A g^{-1} (c) CV of SnS/CNTs (d) nyquist plots of impedance spectra

tendency to collapse and pulverization [42,43,44]. Hence, incorporating codoped CNTs with tin sulfide-based systems can prove to be beneficial for enhancing capacity retention in NIBs.

Cyclic voltammetry was carried out to observe the storage behavior of Na^+ in SnS/CNTs nanocomposite and its result can be seen in figure 4(c). In an initial scan, reduction peak at ~ 0.65 V was obtained corresponding to conversion reaction of SnS to Sn and Na_2S, partial alloying reaction of tin, along with the formation of SEI i-e initial irreversible capacity loss, which is mainly a diffusion limited process [26,45]. It was already reported that in a CV curve, pseudocapacitive contribution is indicated by plateaus while diffusion limited processes are indicated by peaks in it [26]. In the corresponding two cycles, redox peak pairs are observed at 0.01/0.24, 0.60/0.73 V and 1.12/1.17 V, which can be ascribed to a reversible alloying/dealloying process. The reduction peaks at 1.12 V and 0.60V relates to conversion reaction and multi-step alloying process respectively, while the cathodic peak obtained at 0.01 V indicates that Na^+ intercalation is happening in CNTs matrix [42]. The alloying and conversion reaction that SnS undergoes during Na^+ insertion/extraction is as follows [46] :

$$SnS + 2Na^+ + 2e^- \rightarrow Sn + Na_2S$$

$$4Sn + 15Na^+ + 15e^- \rightarrow Na_{15}Sn_4$$

During charge cycle, the anodic peak at 0.24 V points to sodium ion extraction from CNTs. The remaining two anodic peaks at 0.73 V and 1.17 V indicates to multi-step dealloying process as Na_xSn changes to Sn and conversion reaction of Sn to SnS respectively. [26,47]. For other electrodes, no obvious difference in peak pleateus was seen which indicates that they undergo same charge/discharge reaction and also exhibit large initial capacity loss attributing to the formation of SEI [48].

EIS was utilized to know more about the kinetic properties of SnS/CNTs and codoped SnS/CNTs electrode and results are shown in figure 4(d) along with their equivalent circuit. The impedance spectra is comprised of low, medium and high frequency region which gives information about diffusion of Na^+ in bulk material (W_b), charge transfer resistance (R_{ct}) and SEI resistance (R_f) respectively [49,50]. It is apparent that SnS/CNTs electrode semicircle in medium-high frequency region has a smaller diameter as compared to codoped SnS/CNTs electrode and with the help of an equivalent circuit, SnS/CNTs electrode was seen to exhibit R_{ct} of only 44 Ω while the codoped electrode displayed 76 Ω. This boosted charge transfer in both electrodes reveal that SnS and CNTs have a strong interaction between them, bridging cauliflower like SnS together, enabling simple yet effective electronic configuration. It is also owed to (1) high concentration of CNTs which was used to make nanocomposite, (2) and relatively low concentration of binder that was used to synthesize electrodes. At low frequency of this Nyquist plot, the observed slope is much higher for codoped electrode than SnS/CNTs electrode and this indicates about high Na^+ diffusivity for the later one [47]. As compared to SnS/CNTs electrode, this relative increase in charge transfer resistance and decrease in sodium ion diffusivity for codoped electrode could be due to more amorphous nature of it, which doesn't allow sodium ion to diffuse as easily as they do in highly crystalline electrodes. Nevertheless, the boosted charge transfer in nanocomposite indicates a faster kinetic process in those electrodes, which is better than many of its tin chalcogenide counterparts [24,48,51,52,53].

4. Conclusion:

In summary, cauliflower like SnS was synthesized for sodium ion battery anode and its nanocomposite was also made with CNTs and nitrogen sulfur codoped CNTs. It was observed that heteroatoms doping in CNTs was mainly responsible for codoped SnS/CNTs electrode to develop an amorphous nature and upon cycling, this electrode showed enhancement in both capacity retention and initial coulombic efficiency as compared to highly crystalline SnS/CNTs electrode. It is worth emphasizing that this loosely dense structure formed in codoped electrode has voids in it which can not only act as a buffer to volume fluctuations during conversion-alloying reaction but also partly mitigates mechanical degradation of electrodes. SnS/CNTs electrode at 0.1 A g^{-1} delivers a reversible capacity of 183.3 mAh g^{-1}, which is more than twice as high as it was being delivered by bare SnS. Moreover, small charge transfer resistance of 44 Ω for SnS/CNTs and 76 Ω for codoped SnS/CNTs electrode was observed when CNTs were added in high concentration to form nanocomposites. These results suggest that an effective electronic configuration must have been established in nanocomposites because of the framework, that developed when CNTs interacted with cauliflower like SnS. Hence, by rationally tuning the amorphous nature and creating delicate designs, we can improve the capacity retention and charge transfer kinetics of electrode materials, which would provide a pathway for enhancing electrochemical performance in NIBs.

Acknowledgements

Authors would like to express gratitude towards US Pakistan Center for Advanced Studies in Energy and PGP NUST for providing a financial assistance to carry out this research.

References:

[1]J. Y. Hwang, S. T. Myung, and Y. K. Sun, “Sodium-ion batteries: Present and future,” Chemical Society Reviews, vol. 46, no. 12. Royal Society of Chemistry, pp. 3529–3614, 21-Jun-2017.

[2]C. Chen et al., “In-situ formation of tin-antimony sulfide in nitrogen-sulfur Co-doped carbon nanofibers as high performance anode materials for sodium-ion batteries,” Carbon N. Y., vol. 120, pp. 380–391, 2017.

[3]H. Lai et al., “Fabrication of graphene supported SnO_2 nanoparticles and their sodium storage properties,” Mater. Lett., vol. 166, pp. 292–295, 2016.

[4]M. H. Han, E. Gonzalo, G. Singh, and T. Rojo, “A comprehensive review of sodium layered oxides: powerful cathodes for Na-ion batteries,” Energy Environ. Sci., vol. 8, no. 1, pp. 81–102, 2015.

[5]S. Zhang, L. Yue, H. Zhao, Z. Wang, and J. Mi, “Mwcnts wrapped flower-like SnS composite as anode material for sodium-ion battery,” Mater. Lett., vol. 209, pp. 212–215, 2017.

[6]K. Chayambuka, G. Mulder, D. L. Danilov, and P. H. L. Notten, “Sodium-Ion Battery Materials and Electrochemical Properties Reviewed,” Adv. Energy Mater., vol. 8, no. 16, pp. 1–49, 2018.

[7]A. Ponrouch, D. Monti, A. Boschin, B. Steen, P. Johansson, and M. R. Palacín, “Non-aqueous electrolytes for sodium-ion batteries,” Journal of Materials Chemistry A, vol. 3, no. 1. Royal Society of Chemistry, pp. 22–42, Jan. 2015.

[8]F. U. Hassan, U. Ahmed, M. Muhyuddin, M. Yasir, M. N. Ashiq, and M. A. Basit, “Tactical modification of pseudo-SILAR process for enhanced quantum-dot deposition on TiO_2 and ZnO nanoparticles for solar energy applications,” Mater. Res. Bull., vol. 120, no. May, p. 110588, 2019.

[9]M. Muhyuddin, M. T. Ahsan, I. Ali, T. F. Khan, M. A. Akram, and M. A. Basit, “A new insight into solar paint concept: regeneration of CuS nanoparticles for paintable counter electrodes in QDSSCs,” Appl. Phys. A Mater. Sci. Process., vol. 125, no. 10, 2019.

[10]Z. Hu, Q. Liu, S. L. Chou, and S. X. Dou, “Advances and Challenges in Metal Sulfides/Selenides for Next-Generation Rechargeable Sodium-Ion Batteries,” Adv. Mater., vol. 29, no. 48, pp. 1–24, 2017.

[11]D. D. Vaughn, O. D. Hentz, S. Chen, D. Wang, and R. E. Schaak, “Formation of SnS nanoflowers for lithium ion batteries,” Chem. Commun., vol. 48, no. 45, pp. 5608–5610, 2012.

[12]L. Zhou et al., “Structural and chemical synergistic effect of CoS nanoparticles and porous carbon nanorods for high-performance sodium storage,” Nano Energy, vol. 35, pp. 281–289, May 2017.

[13]M. S. Balogun, Y. Luo, W. Qiu, P. Liu, and Y. Tong, A review of carbon materials and their composites with alloy metals for sodium ion battery anodes, vol. 98. Elsevier Ltd, 2016.

[14]P. Sehrawat, C. Julien, and S. S. Islam, “Carbon nanotubes in Li-ion batteries: A review,” Mater. Sci. Eng. B Solid-State Mater. Adv. Technol., vol. 213, pp. 12–40, 2016.

[15]Y. Ren, J. Wang, X. Huang, and J. Ding, “Three-dimensional SnS_2 flowers/carbon nanotubes network: Extraordinary rate capacity for sodium-ion battery,” Mater. Lett., vol. 186, pp. 57–61, Jan. 2017.

[16]S. Zhang, H. Zhao, M. Wu, L. Yue, and J. Mi, “One-pot solvothermal synthesis 2D SnS_2/CNTs hybrid as a superior anode material for sodium-ion batteries,” J. Alloys Compd., vol. 737, pp. 92–98, 2018.

[17]J. Zhu, Y. Li, and G. Hu, “Large-scale synthesis of SnS/carbon nanotube composites with enhanced reversible lithium-ion storage,” Ionics., vol. 24, no. 4, pp. 1265–1269, 2018.

[18]T. Anitha, A. E. Reddy, I. K. Durga, S. S. Rao, H. W. Nam, and H. J. Kim, “Facile synthesis of $ZnWO_4$@WS_2 cauliflower-like structures for supercapacitors with enhanced electrochemical performance,” J. Electroanal. Chem., vol. 841, pp. 86–93, May 2019.

[19]D. Amaranatha Reddy et al., “Facile synthesis of cauliflower-like cobalt-doped Ni_3Se_2 nanostructures as high-performance cathode materials for aqueous zinc-ion batteries,” Int. J. Hydrogen Energy, vol. 45, no. 13, pp. 7741–7750, Mar. 2020.

[20]V.G.R. Kummara, V. Rajangam, V.V. M.G. Chandu, M. Rao Kummara, and H. J. Kim, “Facile synthesis of hierarchical agglomerated cauliflower-like $ZnWO_4$@NiO nanostructures as an efficient electrode material for high-performance supercapacitor applications,” Mater. Lett., vol. 268, p. 127594, Jun. 2020.

[21]J. He et al., “Self-assembled cauliflower-like FeS_2 anchored into graphene foam as free-standing anode for high-performance lithium-ion batteries,” Carbon N. Y., vol. 114, pp. 111–116, 2017.

[22]L. Fan et al., “Promising Dual-Doped Graphene Aerogel/SnS_2 Nanocrystal Building High Performance Sodium Ion Batteries,” ACS Appl. Mater. Interfaces, vol. 10, no. 3, pp. 2637–2648, 2018.

[23]Y. Zhang et al., “Carbon coated amorphous bimetallic sulfide hollow nanocubes towards advanced sodium ion battery anode,” Carbon N. Y., vol. 150, pp. 378–387, 2019.

[24]J. Ren, Y. Zhou, H. Wu, F. Xie, C. Xu, and D. Lin, “Sulfur-encapsulated in heteroatom-doped hierarchical porous carbon derived from goat hair for high performance lithium–sulfur batteries,” J. Energy Chem., vol. 30, pp. 121–131, Mar. 2019.

[25]Y. Li et al., “Sulfur-nitrogen doped multi walled carbon nanotubes composite as a cathode material for lithium sulfur batteries,” Int. J. Hydrogen Energy, vol. 39, no. 28, pp. 16073–16080, 2014.

[26]Y. Wang et al., “Tin sulfide nanoparticles embedded in sulfur and nitrogen dual-doped mesoporous carbon fibers as high-performance anodes with battery-capacitive sodium storage,” Energy Storage Mater., vol. 18, no. August 2018, pp. 366–374, 2019.

[27]X. Ren et al., “MoS_2/sulfur and nitrogen co-doped reduced graphene oxide nanocomposite for enhanced electrocatalytic hydrogen evolution,” Int. J. Hydrogen Energy, vol. 41, no. 2, pp. 916–923, 2016.

[28]S. Mohebbi, S. Mikaeily, and A. R. J. Azar, “Cauliflower-like tin sulphide nanoparticles: An amazing material for adsorption of methylene blue dye,” Micro Nano Lett., vol. 10, no. 4, pp. 220–223, 2015.

[29]B. Yang et al., “Structural Phase Transition from Tin (IV) Sulfide to Tin (II) Sulfide and the enhanced Performance by Introducing Graphene in Dye-sensitized Solar Cells,” Electrochim. Acta, vol. 176, pp. 797–803, 2015.

[30]J. Pei et al., “Three-dimensional nitrogen and sulfur co-doped holey-reduced graphene oxide frameworks anchored with MoO_2 nanodots for advanced rechargeable lithium-ion batteries,” Nanotechnology, vol. 29, no. 29, p. 295404, Jul. 2018.

[31]S. Li et al., “Stannous sulfide/multi-walled carbon nanotube hybrids as high-performance anode materials of lithium-ion batteries,” Electrochim. Acta, vol. 136, pp. 355–362, 2014.

[32]E. Groppo, F. Bonino, F. Cesano, A. Damin, and M. Manzoli, CHAPTER 4: Raman, IR and INS Characterization of Functionalized Carbon Materials, vol. 2018-Janua, no. 31. 2018.

[33]M. Gurubhaskar, N. Thota, M. Raghavender, Y. P. V. Subbaiah, G. H. Chandra, and K. T. R. Reddy, “A Facile and TGA Free Hydrothermal Synthesis of SnS Nanoparticles,” Nano, vol. 12, no. 10, pp. 1–10, 2017.

[34]A. Misra, P. K. Tyagi, M. K. Singh, and D. S. Misra, “FTIR studies of nitrogen doped carbon nanotubes,” Diam. Relat. Mater., vol. 15, no. 2–3, pp. 385–388, 2006.

[35]B. H. Baby, A. E. G., and B. M. D., “The formation of orthorhombic SnS nanorods using CTAB in solvothermal method with its phase stability, optical and electrical properties,” Mater. Res. Bull., vol. 128, p. 110883, 2020.

[36]Y. Liu et al., “Amorphous SnS nanosheets/graphene oxide hybrid with efficient dielectric loss to improve the high-frequency electromagnetic wave absorption properties,” Appl. Surf. Sci., vol. 486, no. April, pp. 344–353, 2019.

[37]D. J. Kim et al., “Diffusion behavior of sodium ions in $Na_{0.44}MnO_2$ in aqueous and non-aqueous electrolytes,” J. Power Sources, vol. 244, pp. 758–763, 2013.

[38]J. Xia et al., “Free-standing SnS/C nanofiber anodes for ultralong cycle-life lithium-ion batteries and sodium-ion batteries,” Energy Storage Mater., vol. 17, pp. 1–11, 2019.

[39]J. Liang, L. Zhang, D. XiLi, and J. Kang, “Rational design of hollow tubular SnO_2@TiO_2 nanocomposites as anode of sodium ion batteries,” Electrochim. Acta, vol. 341, p. 136030, 2020.

[40]D. Zhou, Y. Liu, W. L. Song, X. Li, L. Z. Fan, and Y. Deng, “Three-dimensional porous carbon-coated graphene composite as high-stable and long-life anode for sodium-ion batteries,” Chem. Eng. J., vol. 316, pp. 645–654, 2017.

[41]R. Zhan, L. Hu, J. Han, C. Dai, J. Jiang, and M. Xu, “Exploration of $Mn_{0.5}Ti_2(PO_4)_3$@rgo composite as anode electrode for Na-ion battery,” J. Mater. Sci. Mater. Electron., vol. 29, no. 5, pp. 4250–4255, 2018.

[42]J. R. Rodriguez, Z. Qi, H. Wang, M. Y. Shalaginov, M. Kang, and K. A. Richardson, “$Ge_2Sb_2Se_5$ Glass as High-Capacity Promising Lithium-ion Battery Anode,” Nano Energy, p. 104326, 2019.

[43]F. Han, W. C. Li, C. Lei, B. He, K. Oshida, and A. H. Lu, “Selective formation of carbon-coated, metastable amorphous $ZnSnO_3$ nanocubes containing mesopores for use as high-capacity lithium-ion battery,” Small, vol. 10, no. 13, pp. 2637–2644, 2014.

[44]X. Li et al., “Tin Oxide with Controlled Morphology and Crystallinity by Atomic Layer Deposition onto Graphene Nanosheets for Enhanced Lithium Storage,” pp. 1647–1654, 2012.

[45]B. Qin et al., “Exploring SnS nanoparticles interpenetrated with high concentration nitrogen-doped-carbon as anodes for sodium ion batteries,” Electrochim. Acta, vol. 296, pp. 806–813, 2019.

[46]Y. Zhang et al., “Heterostructured SnS/TiO_2@C hollow nanospheres for superior lithium and sodium storage,” Nanoscale, vol. 11, no. 27, pp. 12846–12852, 2019.

[47]S. H. Choi, Y. Jang, Y. J. Choi, and Y. N. Ko, “Facile synthesis of macroporus SnS microspheres as a potential anode material for enhanced sodium ion batteries,” J. Ind. Eng. Chem., vol. 80, pp. 130–135, 2019.

[48]J. Ai et al., “Pomegranate-inspired SnS/ZnS@C heterostructural nanocubes towards high-performance sodium ion battery,” Appl. Surf. Sci., vol. 496, no. August, p. 143631, 2019.

[49]S. S. Zhang, K. Xu, and T. R. Jow, “Electrochemical impedance study on the low temperature of Li-ion batteries,” Electrochim. Acta, vol. 49, no. 7, pp. 1057–1061, 2004.

[50]N. R. Srinivasan, S. Mitra, and R. Bandyopadhyaya, “Improved electrochemical performance of SnO_2-mesoporous carbon hybrid as a negative electrode for lithium ion battery applications,” Phys. Chem. Chem. Phys., vol. 16, no. 14, pp. 6630–6640, 2014.

[51]Y. Zhang et al., “Hierarchical assembly and superior lithium/sodium storage properties of a flowerlike C/SnS@C nanocomposite,” Electrochim. Acta, vol. 296, pp. 891–900, 2019.

[52]Y. Chen et al., “Enhanced electrochemical performance of SnS nanoparticles / CNTs composite as anode material for sodium-ion battery,” Chinese Chem. Lett., vol. 29, no. 1, pp. 187–190, 2018.

[53]S. Zhang, H. Zhao, M. Wang, Z. Li, and J. Mi, “Low crystallinity SnS encapsulated in CNTs decorated and S-doped carbon fibers as excellent anode material for sodium-ion batteries,” Electrochim. Acta., vol. 279, pp. 1–9, 2019.